Topological Currents in Dense Matter

by

Arthur James Charbonneau

Bachelor of Science, Thompson Rivers University, 2004
Master of Science, University of British Columbia, 2007

A THESIS SUBMITTED IN PARTIAL FULFILMENT OF
THE REQUIREMENTS FOR THE DEGREE OF

Doctor of Philosophy

in

The Faculty of Graduate Studies

(Physics)

The University Of British Columbia

(Vancouver)

July 2011

Abstract

This thesis introduces the idea of a topological current that flows in regions with large magnetic fields, dense matter, and parity violation. We propose that such a current exists in the cores of neutron stars and may be responsible for the large proper motion (kicks) observed in some pulsars. This current is similar to the charge separation effect and chiral magnetic effect that may be responsible for parity ($\mathscr{P}$) and charge conjugation-parity ($\mathscr{C}\mathscr{P}$) violation observed at the Relativistic Heavy Ion Collider (RHIC).

We start by deriving the topological current two ways. The first is a macroscopic derivation where we appeal to an anomaly induced by the presence of a fictitious axial field. The second method is microscopic, in which we consider how the modes of the Dirac equation in a magnetic field and chemical potential contribute to the current. We then discuss in great detail the elements necessary for a topological current to exist in a dense star.

Our concern then rests with calculating the magnitude of topological currents in the many phases of matter thought to exist in dense stars. We choose four representative processes to investigate: nuclear matter, hyperons, kaon condensates, and strange quark matter. We then suppose that this current may somehow transfer its momentum out of the star, either by being physically ejected or by emitting radiation, causing a kick. We also discuss how the current may induce magnetic helicity and a toroidal magnetic field in the core of the star.

We end by discussing the topological current in terms of the AdS/CFT correspondence, a powerful tool that allows one to obtain results from strongly coupled field theories by transferring the problem to the language of a weakly coupled gravitational theory. We introduce a toy model to how one might introduce topological currents into the AdS/CFT framework.

Preface

A version of Subsection 2.2.2 and Chapters 3, 4, and 6 has been published. J. Charbonneau and A. R. Zhitnitsky, *Topological Currents in Neutron Stars: Kicks, Precession,Toroidal Fields, and Magnetic Helicity*. JCAP08(2010)010. [arXiv: 0903.4450]. I completed the calculations, the first draft, revisions, and editing, as well as being the principal during the review process. Dr. Ariel Zhitnitsky contributed edits and revisions to the manuscript as well as collaborating to develop the central ideas in the paper.

The results of Chapters 3, 4, and 6 appear in J. Charbonneau, *Observational Consequences of Topological Currents in Neutron Stars*, prepared for the proceedings of the Lake Louise Winter Institute: Fundamental Interactions (LLWI 2009) [arXiv:0904.4268].

A version of Chapter 5 has been published. J. Charbonneau, K. Hoffman and J. Heyl, *Large Pulsar Kicks from Topological Currents*. MNRAS:Letters 404 (2010) L119. [arXiv:0912.3822]. I collaborated with two astronomers in the department, Dr. Jeremy Heyl and his PhD student Kelsey Hoffman. I did the calculations, initial draft, and edits of the paper and was the principal in the review process. Dr. Heyl and Ms. Hoffman contributed to the editing and refined the paper with their knowledge of astronomy.

The results of Chapter 5 appear in J. Charbonneau, *The Axial Anomaly and Large Pulsar Kicks*, prepared for the proceedings of proceedings of Lake Louise Winter Institute: Celebrating 25 Years (LLWI 2010) [arXiv:1005.3851].

A version of Chapter 7 has been published. L. Brits and J. Charbonneau, *A Constraint-Based Approach to the Chiral Magnetic Effect*. Phys. Rev. D 83, 126013 (2011). [arXiv:1009.4230]. While I proposed the idea for the paper to Mr. Brits, a PhD student in the string theory group, this was a very close collaboration with both authors simultaneously contributing to calculations and edits through the use of an on-line wiki. I was the principal in the review process and responsible for the revisions and corrections.

A version of the introduction to the AdS/CFT correspondence in Section 2.3 appears in a collaboration at the 6th Summer School on Particles, Fields and Strings. N. Ambrosetti, J. Charbonneau, and S. Weinfurtner, *The fluid/gravity correspondence*. (2008) [arXiv:0810.2631].

Contents

List of Figures

Acknowledgements

I thank my supervisor Eric Zhitnitsky for his mentorship over this long and at times difficult journey. He introduced me to the rich world of field theory and gave me the freedom to explore it. He has an ability to recognize people's inherent strengths and foster them. His guidance and support are truly valued and his frankness and humour made every step enjoyable.

I thank Roland Stull for providing me with the opportunity that allowed the first steps of this journey to occur. He hired me over the phone, a bolt from the blue, and gave me a co-op job when my small department's co-op program was in its infancy. I credit this job and his references for opening many doors. I also thank Andrea Damascelli for letting me fill a Summer working in his lab.

I thank Kelsey Hoffman, Jeremy Heyl, Lionel Brits, Silke Weinfurtner and Nicola Ambrosetti for enjoyable collaborations on papers and I thank my committee members Jeremy Heyl, Ingrid Stairs and Gordon Semenoff for their guidance and help through the years.

I thank George Hicks, Kory Stevens, Matthew Hasselfield, Kyle Lawson, Jean-Francois Caron, Lionel Brits and Brian Oswell for their conversations, distractions, and humour.

I thank my parents David and Mathilda for being wise and strong and supporting me unconditionally, and I thank Brent and Lynda for providing a home away from home.

I thank my wife Alyssa for her love and her willingness to share this with me.

Dedication

To violets with wind above them.
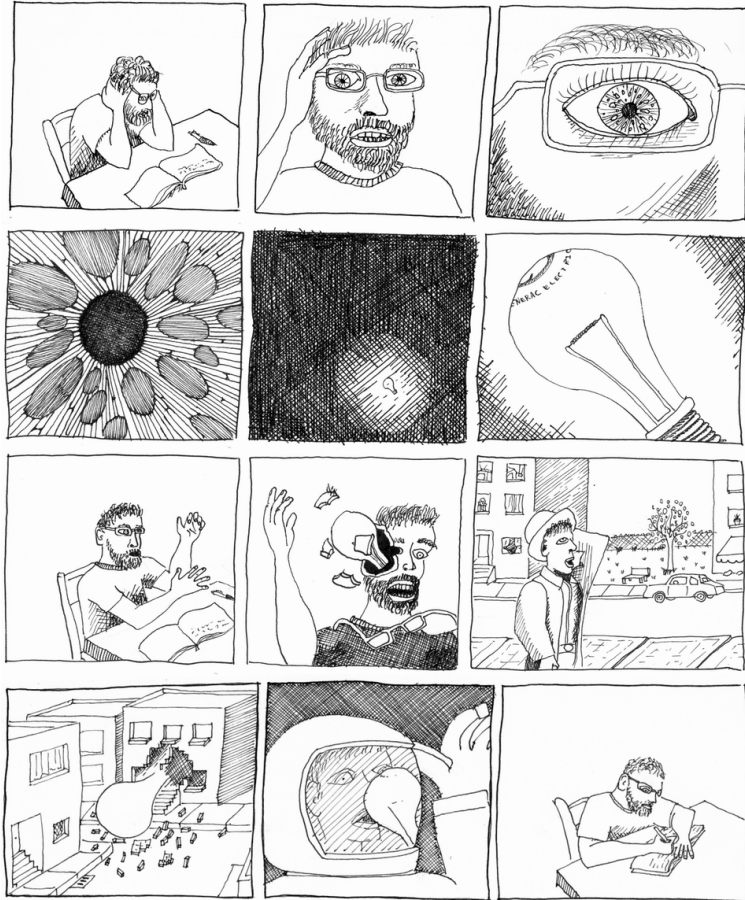
The Dawning.

Who is the third who walks always beside you?
When I count, there are only you and I together
But when I look ahead up the white road
There is always another one walking beside you
Gliding wrapt in a brown mantle, hooded
I do not know whether a man or a woman
But who is that on the other side of you?

T.S. Eliot, The Waste Land (1922)

—What're you chewin' over?
—Dream I had once. I was walkin' in the woods, I don't know why. Wind came
   up and blew me hat off.
—And you chased it, right? You ran and ran, finally caught up to it and you
   picked it up. But it wasn't a hat anymore and it changed into something
   else, something wonderful.
—Nah, it stayed a hat and no, I didn't chase it. Nothing more foolish than a
   man chasin' his hat.

Verna and Tom Reagan, Miller's Crossing (1990)

It takes a lot of lights to make a city, doesn't it?

Joyce Harwood, The Blue Dalia (1946)

Chapter 1

Introduction

In this thesis we will introduce a new kind of current in which the potential is not the standard electric potential but one that arises from the chirality of the particles involved. We will refer to these currents as topological currents and they take the form

$$J_{\mathrm{A}} = (\mu_l + \mu_r)\frac{e\Phi}{(2\pi)^2}, \qquad (1.1)$$

$$J_{\mathrm{V}} = (\mu_l - \mu_r)\frac{e\Phi}{(2\pi)^2}, \qquad (1.2)$$

where μ_r and μ_l are the chemical potential of the right and left-handed Dirac fermions and Φ is the magnetic flux. We are particularly interested in the vector current as it can couple to charge. For the vector current to appear there must be a chiral chemical potential, a difference in the number of left-handed and right-handed fermions, present in the system. The natural places for the current to exist are those where parity symmetry is violated, where processes act differently on left-handed and right-handed fermions. We will focus on parity violation in the Standard Model, particularly the weak interaction. The weak interaction plays a crucial part in the equilibrium processes in neutron stars and we will spend much of the thesis establishing the role these currents play in neutron stars. These currents may also appear in heavy ion collisions such as those performed at the Relativistic Heavy Ion Collider. It is thought that the temperatures of these collisions may cause transitions in the QCD vacuum that induce parity in the system. The last part of this thesis will discuss the nature of these currents in strongly coupled theories. We will start with a short history.

The first example[1] of such a current was studied by Alekseev, Cheianov, and Fröhlich [4] in the context of universal transport properties, namely conductance, in condensed matter systems in equilibrium. They consider a system in which there exist two commuting conserved charges, Q_L and Q_R, that correspond to particles

---

[1]Non-dissipating topological currents were introduced in a series of papers by Vilenkin [1–3], that were lost to the community until very recently (shortly before the author's defence), in which macroscopic parity violation is discussed.

of left and right-handed chirality. These charges are conjugate to the left and right-handed chemical potentials μ_L and μ_R. From this model they derive a universal transport equation that they apply to one-dimensional fermion systems and three-dimensional Dirac fermions coupled to an electromagnetic field, the latter which resulted in the equation (1.2) above. The derivation of the topological current relied on inserting a Chern-Simons term to ensure that the currents were still conserved. Even in the context of transport phenomenon the chiral anomaly plays an important role. The two important conclusions from this paper are that a non-zero topological current implies that massless modes exist in the system and that this current can exist without spontaneous symmetry breaking.

The topic went dormant until Son and Zhitnitsky [5], unaware of [4], discussed anomalies in dense matter. They derive the axial current in (1.1) by starting with the chiral anomaly. They considered an effective field theory that has two $U(1)$ fields. One is the standard electromagnetic field and the other is a fictitious field that has the baryon chemical potential as a zeroth component. They also assume the existence of a Nambu-Goldstone boson as the result of some spontaneous symmetry breaking. From this an axial baryon current can be defined and the standard triangle anomaly can be written in terms of the divergence of this current. With this they were able formulate an effective Lagrangian for the Nambu-Goldstone boson that could be used to compute the axial topological current.

The microscopic understanding of topological currents came with the work of Metlitski and Zhitnitsky [6, 7]. Though they still focused on the axial current they were able to use a simple model of Dirac fermions along with index theorems to specifically identify the zero modes that carried the current. This method removed the necessity of the Nambu-Goldstone boson required in [5] and refine the effective Lagrangian approach. With these techniques they had arrived at identical conclusions as [4], but now had a wealth of techniques for working at non-zero temperature and mass, and for understanding the current in dense nuclear matter.

The focus of study then turned to applications. Neutron stars are an ideal environment for these currents to exist. They are degenerate objects with large magnetic fields which have equilibrium conditions dictated by the weak interactions. Charbonneau and Zhitnitsky [8] studied the effects topological vector currents (1.2) would have on the superconducting vortex structure. For this they considered a topological vector current that runs along along the superconducting vortex. It was shown that a sufficient current could change the vortex structure in the star from type-II to type-I.

Topological vector currents (1.2) continued to be studied in neutron stars by Charbonneau and Zhitnitsky [9] who refined the conditions for their existence and calculated the magnitude for these currents for various phases of matter. The application of topological currents to many problems in neutron stars, including mag-

netic helicity and kicks, were also discussed. The kick model was further refined by Charbonneau, Hoffman, and Heyl [10] and introduced as a possible origin for large pulsar kicks.

Concurrent to these studies of topological currents in dense stars, two terrestrial phenomena associated with topological currents were introduced that sparked real interest in the field. Using the techniques of [6, 7] Kharzeev and Zhitnitsky introduced the charge separation effect [11] and Fukushima, Kharzeev, and Warringa introduced the chiral magnetic effect [12]. These observable effects allowed for topological currents to be potentially observed through $\mathscr{P}$ and $\mathscr{CP}$ violating effects at the Relativistic Heavy Ion Collider (RHIC). It was supposed that the collisions involved in RHIC could generate bubbles of non-zero θ angle or topological transitions in the QCD vacuum. The actual observation of $\mathscr{P}$ and $\mathscr{CP}$ violation in QCD at RHIC [13–17] generated even more excitement leading to a large number of papers being published on the topic.

With the topological current throughly defined in quantum field theory efforts were made to incorporate it into the holographic description of the QCD. The initial attempts by Bergman, Lifschytz, and Lippert [18] using the Sakai-Sigumoto model of holographic QCD easily reproduced the axial (1.1) and vector (1.2) topological currents. This success was short lived. In an effort to reproduce the results of [18] while introducing the appropriate form of the covariant anomaly, which has a conserved vector current in the presence of the chiral anomaly, Rebhan, Schmitt, and Stricker [19] found that the vector topological current is cancelled by counterterms. This opened a debate, that still continues, as to whether or not holographic QCD actually contains the appropriate anomaly to create a topological current. Gorsky, Kopnin, and Zayakin [20] quickly addressed this by using the pseudoscalar sector of the soft-wall model and current algebras to introduce the vector current, but failed to reproduce the correct axial current.

The fundamental problem was that in the holographic dictionary the chemical potentials responsible for the vector currents were being associated with charges that were not actually conserved. The question became how to introduce the chemical potential properly. Rubakov [21] addressed this by defining the charge such that it was conserved. Gynther, Landsteiner, Pena-Benitez, and Rebhan [22] and Brits and Charbonneau [23] addressed the problem through the discussion of nontrivial, unphysical, boundary conditions.

As this is my thesis (Charbonneau) we will focus on the contributions from the papers [9, 10, 23]. These papers span a wide range of topics—field theory, astrophysics, string theory—but they all focus on aspects of the topological vector current (1.2).

A Detailed Layout of the Thesis

Given the range of topics discussed, we will start by reviewing three seemingly disjoint topics: quantum anomalies, dense stars, and string theory. It is our goal that the intersection of these three topic will become apparent as we discuss the origins and observational consequences of topological currents in the bulk of the thesis.

Our review of quantum anomalies in section 2.1 will focus on the origin of the anomaly in quantum field theory. We will first derive it diagrammatically and then discuss how it arises naturally using path integrals. We will also discuss how the anomaly is related to index theorems. This should establish how anomalies fit into a discussion on field theory and topological currents.

In section 2.2 we will give a basic introduction to the astrophysics of neutron stars and quark stars. The physics of dense stars is incredibly rich. Our introduction will first attempt to establish dense stars as observable objects with a discussion on pulsars and pulsar emission mechanisms. We will see how many of the fundamental properties of dense stars can be obtained from these. We will then give an overview of the composition of a dense star, focusing on the possible states of matter they may contain and the processes that exist in these states. This will establish dense stars as a suitable environment for topological currents to exist. This will also provide the groundwork for discussing how topological currents may be used to describe kicks, the focus of Chapter 5.

The discussion in section 2.3 will turn to an aspect of string theory known as the AdS/CFT correspondence. We will introduce the AdS/CFT correspondence as a tool and illustrate its usefulness by doing a calculation of the shear viscosity entropy ratio. This will hopefully illustrate the power of the technique and will prepare the reader for the calculation of topological currents using AdS/CFT later in Chapter 7.

With the review taken care of we can discuss the original work contained in the thesis. In Chapter 3 we will explain how topological currents arise in dense matter. This mirrors the discussion contained in the first part of Charbonneau and Zhitnitsky [9]. We will first explicitly derive the topological vector current (1.2). We will then discuss the elements required for the current to exist in dense matter and devise an expression of their magnitude in dense stars. We will particularly focus on why the current is not washed out due to QED interactions. Our goal is to present a quantitative analysis of the conditions when parity violation ($\mu_r \neq \mu_l$) occurs in dense stars and a persistent, topological current is induced. It is well known that the weak interactions (where parity is strongly violated) play a dominant role in neutron star physics. Producing the asymmetry $\mu_r \neq \mu_l$ for a given process is common in the bulk of neutron stars, but we are interested in

coherent parity violating effects when the asymmetry appears in macroscopically large regions.

Chapter 4 is the direct application of the ideas in Chapter 3 to the various possible forms of matter found in dense stars. This was the focus of the second half of Charbonneau and Zhitnitsky [9]. Our consideration in the primary process that occurs to create electrons in each phase. We will discuss the current that arises from the direct urca process, the modified Urca process, kaon scattering, and the quark Urca process. These are also the primary processes responsible for cooling star through neutrino emission. The calculations to find the magnitude of the current are very close to that of neutrino luminosity, but different enough that some computation effort is required.

We introduce the idea of topological kicks in Chapter 5 as a mechanism for generating large pulsar kicks. Topological kicks were first suggested in Charbonneau and Zhitnitsky [9] and described in detail by Charbonneau, Hoffman, and Heyl [10]. If non-dissipating vector currents are induced they can transfer momentum by either escaping the star or radiating photons. The mechanism is similar to neutrino emission in that we are ejecting a particle from the star, but there are some key differences. Neutrino emission is automatically asymmetric with respect to the direction of the magnetic field $\vec{B}$; however, most neutrino-based kick mechanisms have difficulty delivering the produced asymmetry to the surface of the star. Only when it can reach the surface can the asymmetry push the star. In most neutrino based mechanisms the star must be very hot ($T > 1$ MeV) for neutrinos to be energetic enough to transfer sufficient momentum and the kick occurs in a matter of seconds. But at such high temperatures the neutrinos cannot escape the star without interacting and washing out the asymmetry. The topological kick continues to work even when temperature drops well below $T \ll 1$ MeV because it is the chemical potential $(\mu_l - \mu_r) \neq 0$, not the temperature, that drives the kick.

In Chapter 6 we also suggest that a current running along the magnetic flux (the poloidal field) may be the source of the toroidal magnetic field and the finite magnetic helicity thought to be required in a neutron star [24–27]. The magnetic helicity, $\mathscr{H} \equiv \int d^3x \vec{A} \cdot \vec{B}$, that arises from the linking of toroidal and poloidal magnetic fields is a topological invariant and is a $\mathscr{P}$-odd effect that must be generated though parity violation. Our method of generating a toroidal field naturally produces magnetic helicity without requiring arguments to temporarily break the topological invariance of the magnetic helicity. Many attempts to generate magnetic helicity rely on instabilities in the magnetic field caused by the star's rotation. Such correlations $\langle \vec{B} \cdot \vec{\Omega} \rangle$ are $\mathscr{P}$-even, and though they may generate toroidal fields, they cannot be responsible for magnetic helicity. We will also briefly discuss how the current may change the superconductivity in the star from type-II to type-I.

In Chapter 7 we make a departure from direct applications of the current and

discuss its existence in holographic models of QCD. The discussion will follow that introduced by Brits and Charbonneau [23]. The existence of topological currents in holographic models is important in showing that topological currents exist at the strong coupling limit of QCD, and thus would be observed in the strongly coupled quark-gluon plasma though to result from collisions at RHIC. We will introduce a constraint based paradigm of looking the topological current by investigating how the current arises from non-trivial boundary conditions in the field theory description. Previous attempts to produce topological currents in holographic QCD have redefined the axial charge to be conserved, but this is somewhat unsatisfying. We take a bottom up approach, which is to say we are trying to reverse engineer the holography, and try to determine what kind of boundary conditions on the string theory side act as a constraint to force the axial charge to be conserved on the QCD side. We illustrate the concept with the simplest of holographic QCD models.

Chapter 2

Background Material

This chapter contains the material for understanding the original work contained in the other chapters. We will start with a review on quantum anomalies. Understanding anomalies is central in understanding why topological currents exist in dense matter and why there was trouble finding them in holographic QCD. We will then establish a simple consistent model for dense stars that will be used throughout the paper to show why topological currents exist in dense stars, what their magnitude must be, and how they can be used to provide kicks to pulsars. We finish with a review of the AdS/CFT correspondence, which we will use to show how currents can appear in the strong coupling limit of QCD.

2.1 The Axial Anomaly

It is well known that quantum anomalies have important implications for low-energy physics. Anomalies reveal intricate relationships between topological objects such as vortices, domain walls, Nambu-Goldstone bosons, and gauge fields and often result in very unusual physics. A particularly relevant example is the superconducting cosmic string on which an electric current flows without dissipation and carries momentum [28]. The effects of anomalies are well established and are reviewed in [29].

More recently the role of anomalies in QCD has been studied at finite baryon density [5–7] and similar phenomena have been studied in condensed matter systems [4, 30, 31]. Since the original paper [5] many other applications of anomalies in dense QCD have been considered: an analysis of the axion physics and microscopic derivation of anomalies [6]; studying the vortex structure due to the anomalies currents in neutron stars (type-I versus type-II superconductivity) [8]; the charge separation effect at the relativistic heavy ion collider (RHIC) [11, 32]; magnetism of nuclear and quark matter [33]; anomaly mediated neutrino-photon interactions at finite baryon density [34]; the chiral magnetic effect at RHIC [12] and many others.

The study of the axial anomaly started with Steinberger's [35] calculation of the $\pi \to 2\gamma$ decay using triangle diagrams and the recently developed subtrac-

tion method used to renormalize quantum electrodynamics. With some help from Schwinger [36] these calculations using triangle diagrams became the standard. The real issue came some years later with the introduction of the partial conservation of the axial current (PCAC) and current algebras (where fields form Lie algebras based on classical symmetries) were introduced to explain pion decays. The idea behind PCAC was that the charged pion field was proportional to the divergence of the axial current. This lead to a number of very successful calculations of the charged pion decay rates. But, Sutherland and Veltman showed that if current algebras hold then the rate for π_0 decay should be extremely small, nearly zero. This conclusion contradicted experimental results that showed that the decay did indeed occur.

The next development came when Bell and Jackiw [37] investigated a truncated σ-model that contained a proton, neutral pion, and a scalar meson. This model has PCAC attributes, in that the divergence of the axial current is proportional to a field, and seems to obey the assumptions made by Sutherland and Veltman to show the failure of the current algebras. As would be expected for a PCAC model, Bell and Jackiw were able show that the $\pi \to 2\gamma$ amplitude vanishes as the mass of the pion goes to zero. But they came across a paradox. In calculating the decay to the lowest order in perturbation theory, which is a triangle diagram, they found that the amplitude does not vanish as the mass goes to zero. This is a hint that there is something very special contained within these triangle diagrams. Bell and Jackiw remedied this paradox by attempting to restore the PCAC results by introducing a regulator field that cancels the contributions from the triangle diagrams as the mass goes to zero. For a massive pion the triangle diagrams contributed, but only in a limited capacity.

The final step came when Adler [38] reinterpreted the paradox of Bell and Jackiw by assuming that is was actually PCAC that was breaking down. He assumed that the triangle diagrams gave a genuine contribution to the divergence of the axial current, rather than one that should be removed. He isolated the part of the triangle diagram responsible for the anomalous non-conservation of the axial current and modified the PCAC statement to include this term, known as the anomaly. Using PCAC and with this correction he showed that the correct value of the pion decay could be achieved. Interestingly enough, this was the value Steinberger and Schwinger originally calculated. Nothing was learned about the decay rate of the pion itself, but important lessons were learned about symmetries and how they break down due to the quantum corrections introduced by perturbation theory.

2.1.1 Ward Identities

Beyond this colloquial introduction to anomalies, the study of anomalies involves a discussion of the Ward identities. Ward identities are statements about the amplitudes of diagrams that reflect the underlying conservation laws that can be found through formal manipulations of the field theory. What Adler, Bell and Jackiw found was that the Ward identities do not hold in perturbation theory. The formal field theory derivation of the Ward identities somehow fails. The failure of the Ward identities indicates a breakdown of gauge invariance, which can cause many problems with a theory. We will look at how the anomalous violation of the Ward identities comes about in perturbation theory and how the anomaly can be properly derived with formal field theory using insights from Fujikawa.

Our first step is to derive the conservation laws that the Ward identities will follow from. We will consider only a simple case involving Dirac fields ψ. The axial and vector currents are defined as

$$j^{\mu 5} = \overline{\psi}\gamma^\mu \gamma^5 \psi, \tag{2.1}$$

$$j^{\mu} = \overline{\psi}\gamma^\mu \psi, \tag{2.2}$$

where we define $\overline{\psi} = \psi^\dagger \gamma^0$. We can find the divergence of the axial current using the Dirac equation,

$$(i\gamma^\mu \partial_\mu - m)\psi = 0, \tag{2.3}$$

$$\overline{\psi}(i\gamma^\mu \overleftarrow{\partial}_\mu - m) = 0 \tag{2.4}$$

such that

$$\partial_\mu j^{\mu 5} = (\partial_\mu \overline{\psi})\gamma^\mu \gamma^5 \psi - \overline{\psi}\gamma^5 \gamma^\mu \partial_\mu \psi, \tag{2.5}$$

$$= i2m\overline{\psi}\gamma^5 \psi, \tag{2.6}$$

$$= i2m j^{05}. \tag{2.7}$$

Similarly, we find the divergence of the vector current to be

$$\partial_\mu j^\mu = 0. \tag{2.8}$$

In the massless limit both of these currents are conserved. The mass unnecessarily complicates the argument and adds nothing to the result so we set the mass to zero in what follows.

These conserved currents lead to Ward identities for vertex interactions. Vertex interactions between matter and gauge fields can be written in terms of these

currents. Consider an arbitrary process involving an external photon with a polarization vector ε_μ^* that has the amplitude

$$iT(q) = iT^\mu(q)\varepsilon_\mu^*(k). \tag{2.9}$$

If there are more external photons we can pull out those polarization vectors as well and add more indices to the amplitude. In QED and QCD the only ones that exist are the vector interactions of the form

$$\int d^4x\, g_v j^\mu W_\mu, \tag{2.10}$$

where W_μ is some kind of gauge field. The theory of the weak interactions also has axial current interactions,

$$\int d^4x\, g_A j^{\mu 5} W_\mu. \tag{2.11}$$

In diagrammatic form these interactions look like Figure 2.1 where the three lines meet at a point. In reality though the vertex has many corrections. The grey circle is used as a place holder that accounts for higher order diagrams that could result in this vertex. Included in these higher order corrections is a fermion triangle that will lead to the triangle anomaly.
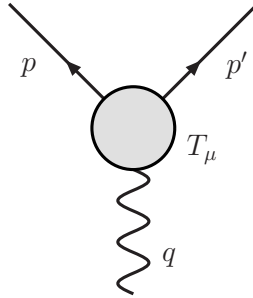
Figure 2.1: A general fermion-gauge boson vertex.

We expect the amplitudes of these vertices to be proportional to a matrix element of these interactions,

$$T^\mu(q) = \int d^4x\, e^{iqx} \langle f | j^{5\mu} | i \rangle, \tag{2.12}$$

where i and f are initial and final particle states. There is a similar expression for the vector current. Contracting the amplitude with a momentum q_μ gives us

$$q_\mu T^\mu = i \int d^4 x\, e^{iqx} \langle f | \partial_\mu j^{5\mu} | i \rangle, \tag{2.13}$$

$$= 0, \tag{2.14}$$

where we remember that the matrix element $\langle f | j^{5\mu} | i \rangle$ vanishes at $x = \pm\infty$ such that the first term from the product rule for derivatives vanishes, as is common for Fourier transforms. The Ward identity holds for a vertex interaction where the current is conserved. The current conservation is a consequence of gauge invariance. The end result is that replacing a polarization vector with a momentum vector causes the matrix element to vanish. Every vertex will have a similar Ward identity that tells us how the current is conserved in the interaction.

2.1.2 Triangle Diagrams and the Anomaly

The Ward identities have many important uses. One is ensuring that non-physical timelike and longitudinal photon polarizations do not contribute to the squared amplitudes used to calculate probabilities in scattering processes. They guarantee that negative norm states can never contribute to physical processes. A breakdown of the Ward identity may allow negative norm states to be considered when evaluating physical processes and threaten the unitarity of the theory. The Ward identities are also used to prove the renormalizability of a theory, ensuring that sensible predictions may be obtained from it.

We are now in a position to discuss the breakdown of the Ward Identities in perturbation theory. For simplicity we will restrict our discussion to anomalies in QED. The discussion of the derivation of the anomaly from the triangle diagrams follows that found in [39–41] We are interested in the matrix element for the axial current to create two photons,

$$\int d^4 x\, e^{-iq\cdot x} \langle p_1, p_2 | j^{5\mu}(x) | 0 \rangle = (2^\pi)^4 \delta^{(4)}(p_1 - p_2 - q) \varepsilon_\rho^*(p_1) \varepsilon_\sigma^*(p_2) T^{\mu\rho\sigma}. \tag{2.15}$$

Expanding the axial vertex shown in Figure 2.1 to fifth order we find a graph that contains a full fermion triangle as seen in Figure 2.2. The graphs are AVV interactions where A= $\gamma^\mu \gamma^5$ and V= γ^μ. There are other contributions at this order and higher come from those with abnormal parity. Examples are AAA triangles, AVVV squares, and AVVVV pentagons and so on. A topic that we will not discuss in this thesis is the role the anomaly plays in renormalization of a theory. The contributions from anomalies to currents that are conserved by gauge symmetries

must completely cancel. It has been shown that the steps taken to cancel the AVV anomaly cancels the contributions from these higher order shapes. In light of this a discussion of the anomaly only needs to consider this simplest graph. The AVV anomaly can also appear as the result of a breakdown in a global symmetry. These anomalies pose no danger to the theory and are the kind we will discuss later in the thesis to derive the current. We should note that the triangle graph shown are the
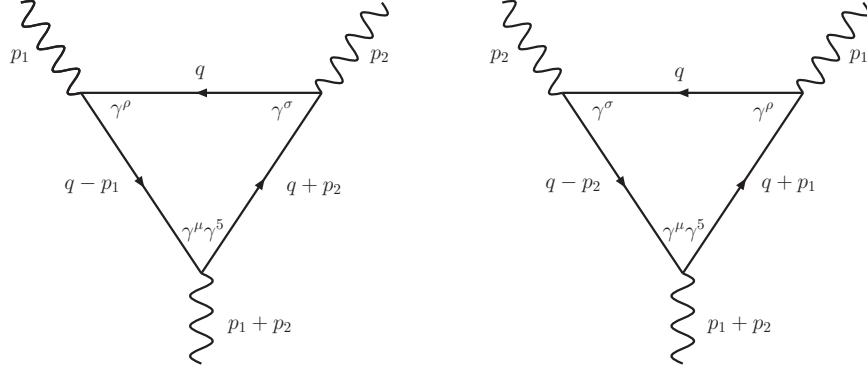
Figure 2.2: The AVV fermion triangles.

only contributions to the anomaly. It has been proved to all orders in perturbation theory that radiative corrections contribute nothing additional [42]. This greatly simplifies the discussion.

We can write the total amplitude as the contribution from both graphs,

$$T^{\mu\rho\sigma}(p_1, p_2) = S^{\mu\rho\sigma}(p_1, p_2) + S^{\mu\sigma\rho}(p_2, p_1). \tag{2.16}$$

Using the Feynman rules we can write down the contribution of just the fermion portion of these graphs when we account for the coupling constants of two external legs,

$$S^{\mu\rho\sigma}(p_1, p_2) = -(-ie)^2 \int \frac{d^4q}{(2\pi)^4} \operatorname{Tr} \left[\gamma^\mu \gamma^5 \frac{i}{\slashed{q} + \slashed{p}_2} \gamma^\sigma \frac{i}{\slashed{q}} \gamma^\rho \frac{i}{\slashed{q} - \slashed{p}_1} \right], \tag{2.17}$$

$$= -ie^2 \int \frac{d^4q}{(2\pi)^4} \frac{\operatorname{Tr} \left[\gamma^\mu \gamma^5 (\slashed{q} + \slashed{p}_2) \gamma^\sigma \slashed{q} \gamma^\rho (\slashed{q} - \slashed{p}_1) \right]}{(q + p_2)^2 (q - p_1)^2 q^2}. \tag{2.18}$$

The amplitude $S_{\mu\rho\sigma}(p_1, p_2)$ contains the information for the currents at each vertex. Using this with the formal arguments earlier, where we replace polarization

vectors for external photons with momentum vectors, one might expect that each vertex conserves current independently, leading to the following Ward identities,

$$(p_1 + p_2)^\mu T_{\mu\rho\sigma} = 0 \quad \text{axial vertex,} \tag{2.19}$$

$$p_1^\rho T_{\mu\rho\sigma} = 0 \quad \text{vector vertex,} \tag{2.20}$$

$$p_2^\sigma T_{\mu\rho\sigma} = 0 \quad \text{vector vertex.} \tag{2.21}$$

We will calculate the Ward identities explicitly and show that the axial and vector Ward identities can never be satisfied simultaneously, only one or the other. We will evaluate the integrals based on symmetry arguments found in Ryder and Frampton, but we will take care to account for any divergences that appear. We will only concern ourselves with one of the two amplitudes that make up $T^{\mu\rho\sigma}$ as both calculations are nearly identical.

Evaluating the axial Ward identity explicitly tells us calculate the integral

$$(p_1 + p_2)_\mu S^{\mu\rho\sigma} = -ie^2 \int \frac{d^4q}{(2\pi)^4} \frac{\text{Tr}\left[(\not{p}_1 + \not{p}_2)\gamma^5(\not{q} + \not{p}_2)\gamma^\sigma \not{q} \gamma^\rho(\not{q} - \not{p}_1)\right]}{(q+p_2)^2(q-p_1)^2q^2}. \tag{2.22}$$

It is obvious that

$$(\not{p}_1 + \not{p}_2)\gamma^5 = -(\not{q} - \not{p}_1)\gamma^5 - \gamma^5(\not{q} + \not{p}_2), \tag{2.23}$$

which can be used to rewrite the integral as

$$
\begin{aligned}
(p_1 + p_2)_\mu S^{\mu\rho\sigma} =& ie^2 \int \frac{d^4q}{(2\pi)^4} \frac{\text{Tr}\left[(\not{q} - \not{p}_1)\gamma^5(\not{q} + \not{p}_2)\gamma^\sigma \not{q} \gamma^\rho(\not{q} - \not{p}_1)\right]}{(q+p_2)^2(q-p_1)^2q^2} \\
&+ ie^2 \int \frac{d^4q}{(2\pi)^4} \frac{\text{Tr}\left[\gamma^5(\not{q} + \not{p}_2)(\not{q} + \not{p}_2)\gamma^\sigma \not{q} \gamma^\rho(\not{q} - \not{p}_1)\right]}{(q+p_2)^2(q-p_1)^2q^2}, \\
=& ie^2 \int \frac{d^4q}{(2\pi)^4} \frac{\text{Tr}\left[\gamma^5(\not{q} + \not{p}_2)\gamma^\sigma \not{q} \gamma^\rho\right]}{(q+p_2)^2q^2} \\
&+ ie^2 \int \frac{d^4q}{(2\pi)^4} \frac{\text{Tr}\left[\gamma^5\gamma^\sigma \not{q} \gamma^\rho(\not{q} - \not{p}_1)\right]}{(q-p_1)^2q^2}.
\end{aligned} \tag{2.24, 2.25}
$$

We now make the observation that $S_{\mu\rho\sigma}$ is a rank 3 pseudotensor. This can be seen by switching indices in equation (2.17) and using the gamma matrix commutation relationships. Contracting one of the indices with a momentum turns it unto a rank 2 pseudotensor. Both of the integrals in equation (2.25) depend on

only one four-momentum. No rank 2 pseudotensor exists that depends on just one four-momentum, so the integrals must vanish. A rough argument for this is by considering what you can contract with four-vectors (or pseudovectors). The only two two objects we have are the metric $\eta_{\mu\nu}$ and the rank 4 Levi-Civita $\varepsilon_{\mu\nu\rho\sigma}$. Given that we want to make a rank 2 pseudotensor with single four-vector dependence our options are to contract the four-vector with the Levi-Civita. We now have to contract another index on the Levi-Civita to make a rank two object, but there is nothing left other than another copy of the four-vector, which upon contracting would makes the object vanish. The vanishing of these integrals seems to confirm the axial Ward identity, but the vector Ward identities still to be confirmed.

Both of the vector ward identities are nearly identical so we will only consider

$$p_{1\rho}S^{\mu\rho\sigma} = -ie^2 \int \frac{d^4q}{(2\pi)^4} \frac{\text{Tr}\left[\gamma^\mu\gamma^5(\slashed{q}+\slashed{p}_2)\gamma^\sigma\slashed{q}\slashed{p}_1(\slashed{q}-\slashed{p}_1)\right]}{(q+p_2)^2(q-p_1)^2q^2}. \tag{2.26}$$

We now shift variables,

$$q'_\mu = (q+p_2)_\mu, \tag{2.27}$$

but we have to be careful because the integral is superficially linearly divergent (7 powers of q in the numerator and 6 in the denominator or D=4L-). We can determine how much the integral changes by looking at the expansion,

$$\int d^4q\, F(q) = \int d^4q'\, F(q'-p_2), \tag{2.28}$$

$$= \int d^4q'\, F(q') + \int d^4q'\, \left.\frac{\partial}{\partial p_2}F(q'-p_2)\right|_{p_2=0} p_2 + ..., \tag{2.29}$$

$$= \int d^4q'\, F(q') + \int d^4q'\, \left.\frac{\partial}{\partial q}F(q)\frac{\partial q}{\partial p_2}\right|_{p_2=0} p_2 + ..., \tag{2.30}$$

$$= \int d^4q'\, F(q') - p_2^\nu \int d^4q\, \frac{\partial}{\partial q^\nu}F(q) + ... \tag{2.31}$$

If F is linearly divergent then the second term in this expansion will be finite and non-vanishing. With this we can account for the shift of variables in the divergent part of our integral. The divergent term in the integral is

$$(p_{1\rho}S^{\mu\rho\sigma})^{\text{div}} = -ie^2 \int \frac{d^4q}{(2\pi)^4} \frac{\text{Tr}\left[\gamma^\mu\gamma^5\slashed{q}\gamma^\sigma\slashed{q}\slashed{p}_1\slashed{q}\right]}{q^6}. \tag{2.32}$$

Equation (2.28) says that a change of variables results in the total integral picking up an addition term as a result of the linearly divergent part of the integral.

Performing the shift of variables (2.27) results in the integral

$$p_{1\rho}S^{\mu\rho\sigma} = p_{1\rho}S'^{\mu\rho\sigma} - p_2^\nu \frac{\partial}{\partial q^\nu}(p_{1\rho}S^{\mu\rho\sigma})^{\mathrm{div}}, \tag{2.33}$$

$$= -ie^2 \int \frac{d^4q'}{(2\pi)^4} \frac{\mathrm{Tr}\left[\gamma^\mu\gamma^5\slashed{q}'\gamma^\sigma(\slashed{q}'-\slashed{p}_2)\slashed{p}_1(\slashed{q}'-\slashed{p}_1-\slashed{p}_2)\right]}{q'^2(q'-p_1-p_2)^2(q'-p_2)^2}$$

$$+ ie^2 p_2^\nu \int \frac{d^4q}{(2\pi)^4} \frac{\partial}{\partial q^\nu} \frac{\mathrm{Tr}\left[\gamma^\mu\gamma^5\slashed{q}\gamma^\sigma\slashed{q}\slashed{p}_1\slashed{q}\right]}{q^6}. \tag{2.34}$$

We can modify the first term through the manipulation

$$\slashed{p}_1 = (\slashed{q}'-\slashed{p}_2) - (\slashed{q}'-\slashed{p}_1-\slashed{p}_2) \tag{2.35}$$

to get

$$p_{1\rho}S^{\mu\rho\sigma} = -ie^2 \int \frac{d^4q'}{(2\pi)^4} \frac{\mathrm{Tr}\left[\gamma^\mu\gamma^5\slashed{q}'\gamma^\sigma(\slashed{q}'-\slashed{p}_2)(\slashed{q}'-\slashed{p}_1-\slashed{p}_2)\right]}{q'^2(q'-p_1-p_2)^2}$$

$$+ ie^2 \int \frac{d^4q'}{(2\pi)^4} \frac{\mathrm{Tr}\left[\gamma^\mu\gamma^5\slashed{q}'\gamma^\sigma(\slashed{q}'-\slashed{p}_2)(\slashed{q}'-\slashed{p}_1-\slashed{p}_2)\right]}{q'^2(q'-p_2)^2}$$

$$+ ie^2 p_2^\nu \int \frac{d^4q}{(2\pi)^4} \frac{\partial}{\partial q^\nu} \frac{\mathrm{Tr}\left[\gamma^\mu\gamma^5\slashed{q}\gamma^\sigma\slashed{q}\slashed{p}_1\slashed{q}\right]}{q^6}. \tag{2.36}$$

The first two terms of this integral are subject to the same symmetry argument discussed earlier to show that the integrals in equation (2.25) vanish. Only the last term remains to be evaluated,

$$p_{1\rho}S^{\mu\rho\sigma} = ie^2 p_2^\nu \int \frac{d^4q}{(2\pi)^4} \frac{\partial}{\partial q^\nu} \frac{\mathrm{Tr}\left[\gamma^\mu\gamma^5\slashed{q}\gamma^\sigma\slashed{q}\slashed{p}_1\slashed{q}\right]}{q^6}. \tag{2.37}$$

The trace can be evaluated using the identity

$$\mathrm{Tr}[\gamma^5\gamma^\rho\gamma^\lambda\gamma^\sigma\gamma^\kappa\gamma^\tau\gamma^\mu] = -4i\varepsilon^{\kappa\tau\mu\alpha}(\delta_\alpha^{\ \rho}g^{\lambda\sigma} - \delta_\alpha^{\ \lambda}g^{\rho\sigma} + \delta_\alpha^{\ \sigma}g^{\rho\lambda}) \tag{2.38}$$

$$+ 4i\varepsilon^{\rho\lambda\sigma\alpha}(\delta_\alpha^{\ \kappa}g^{\tau\mu} - \delta_\alpha^{\ \tau}g^{\kappa\mu} + \delta_\alpha^{\ \mu}g^{\kappa\tau}), \tag{2.39}$$

which allows us to evaluate

$$\mathrm{Tr}\left[\gamma^5\slashed{q}\gamma^\sigma\slashed{q}\slashed{p}_1\slashed{q}\gamma^\mu\right] = -4i\varepsilon^{\rho\sigma\mu\alpha}p_{1\rho}q_\alpha q^2. \tag{2.40}$$

Using this and Wick rotating the integral using $q^0 = iq^0$ yields,

$$p_{1\rho} S^{\mu\rho\sigma} = ie^2 4\varepsilon^{\rho\sigma\mu\alpha} p_{1\rho} p_2^\nu \int \frac{d^4q}{(2\pi)^4} \frac{\partial}{\partial q^\nu} \frac{q_\alpha}{q^4}. \tag{2.41}$$

To evaluate this integral we first notice that if $\nu \neq \alpha$ it vanishes due to it being odd in q. When $\alpha = \nu$ we can rewrite the integral as a divergence,

$$p_{1\rho} S^{\mu\rho\sigma} = ie^2 4\varepsilon^{\rho\sigma\mu\nu} p_{1\rho} p_2^\nu \int \frac{d^4q}{(2\pi)^4} \frac{\partial}{\partial q^\alpha} \frac{q^\alpha}{4q^4}. \tag{2.42}$$

This allows us to use Green's Theorem to rewrite the integral as a surface term,

$$p_{1\rho} S^{\mu\rho\sigma} = ie^2 \varepsilon^{\rho\sigma\mu\nu} p_{1\rho} p_{2\nu} \oint \frac{(d^3q)_\alpha}{(2\pi)^4} \frac{q^\alpha}{q^4}, \tag{2.43}$$

$$= ie^2 \varepsilon^{\rho\sigma\mu\nu} p_{1\rho} p_{2\nu} \lim_{q \to \infty} \int \frac{q_\alpha}{q} q^3 \frac{d\Omega_3}{(2\pi)^4} \frac{q^\alpha}{q^4}, \tag{2.44}$$

$$= ie^2 \frac{1}{8\pi^2} \varepsilon^{\rho\sigma\mu\nu} p_{1\rho} p_{2\nu}. \tag{2.45}$$

A similar calculation can be done for $p_2^\sigma S_{\mu\rho\sigma}$ using the shift $q'' = q - p_2$ and we arrive at our result,

$$p_{1\rho} S^{\mu\rho\sigma} = ie^2 \frac{1}{8\pi^2} \varepsilon^{\rho\sigma\mu\nu} p_{1\rho} p_{2\nu}, \tag{2.46}$$

$$p_2^\sigma S_{\mu\rho\sigma} = -ie^2 \frac{1}{8\pi^2} \varepsilon^{\rho\sigma\mu\nu} p_{2\sigma} p_{1\nu}. \tag{2.47}$$

The vector Ward identities (2.19) that we naively calculated using formal field theory manipulations are wrong. The triangle anomaly has introduced a correction that appears to cause the vector current to pick up a divergence. This is a disaster if left alone as it toys with charge conservation. In order to fix this we must introduce counter-terms by insisting that the vector current be conserved. This has the effect of moving the offending terms from the vector Ward identities to the axial Ward identities. Non-conservation of the axial charge, though unpleasant, is something we can live with. The way we add the counter-terms is to redefine the amplitude for the triangle graph such that equation (2.16) now reads

$$T'^{\mu\rho\sigma}(p_1, p_2) = S^{\mu\rho\sigma}(p_1, p_2) + S^{\mu\sigma\rho}(p_2, p_1) + \frac{ie^2}{4\pi^2} \varepsilon^{\mu\rho\sigma\nu}(p_1 - p_2)_\nu. \tag{2.48}$$

The Ward identities (2.19) now become

$$(p_1 + p_2)_\mu T'^{\mu\rho\sigma} = \frac{i}{2\pi^2} \varepsilon^{\mu\rho\sigma\nu} p_{2\mu} p_{1\nu} \qquad \text{axial vertex,} \tag{2.49}$$

$$p_{1\rho} T'^{\mu\rho\sigma} = 0 \qquad \text{vector vertex,} \tag{2.50}$$

$$p_{2\sigma} T'^{\mu\rho\sigma} = 0 \qquad \text{vector vertex.} \tag{2.51}$$

No method of regularization can avoid this term. Even dimensional regularization, which ensures that the vector Ward identities are valid, fails because γ^5 is an intrinsically four-dimensional object and the manipulations required to deal with that lead to an additional contribution. We can use the axial Ward identity to calculate the divergence of the axial current. From equation (2.15) we can see that

$$\langle p_1, p_2 | \partial_\mu j^{5\mu}(0) | 0 \rangle = \varepsilon_\rho^*(p_1) \varepsilon_\sigma^*(p_2) i(p_1 + p_2)_\mu T^{\mu\rho\sigma}, \tag{2.52}$$

$$= \frac{1}{2\pi^2} \varepsilon^{\mu\rho\sigma\nu} \varepsilon_\rho^*(p_1) \varepsilon_\sigma^*(p_2) (i p_{2\mu})(i p_{1\nu}), \tag{2.53}$$

$$= -\frac{e^2}{16\pi^2} \langle p_1, p_2 | \varepsilon^{\mu\rho\nu\sigma} F_{\mu\rho} F_{\nu\sigma}(0) | 0 \rangle, . \tag{2.54}$$

This gives us the equation for the anomaly,

$$\partial_\mu j^{5\mu} = -\frac{e^2}{16\pi^2} \varepsilon^{\mu\rho\nu\sigma} F_{\mu\rho} F_{\nu\sigma}. \tag{2.55}$$

The triangle diagram has added a correction to the divergence of the axial current. But why? Our formal field theory derivation of the divergence failed to find this. To see why we will look at Fujikawa's derivation of the axial anomaly using a path integral approach.

2.1.3 Fujikawa's Explanation

Fujikawa's approach to deriving the anomaly gives a vivid picture of where the anomaly comes from. We will see that contributions from quantum mechanics will directly interfere with the classical symmetries of the theory. The account given here is complied from discussions found in [40, 43, 44]. Consider the functional integral for fermions with the Dirac operator $D_\mu = \partial_\mu + ieA_\mu(x)$ in the massless limit,

$$Z = \int \mathscr{D}\psi \mathscr{D}\overline{\psi} \, \exp\left[i \int d^4x \overline{\psi}(i\slashed{D})\psi\right], \tag{2.56}$$

with the global chiral transformation

$$\psi(x) \to \psi'(x) = (1 + i\alpha(x)\gamma^5)\psi(x), \tag{2.57}$$

$$\overline{\psi}(x) \to \overline{\psi}'(x) = \overline{\psi}(x)(1 + i\alpha(x)\gamma^5). \tag{2.58}$$

Performing this transformation on the Lagrangian yields

$$\int d^4x\,\overline{\psi}'(i\displaystyle{\not}D)\psi' = \int d^4x\left[\overline{\psi}(1+i\alpha(x)\gamma^5)(i\displaystyle{\not}D)(1+i\alpha(x)\gamma^5)\psi\right], \tag{2.59}$$

$$= \int d^4x\left[\overline{\psi}(i\displaystyle{\not}D)\psi - \alpha(x)\overline{\psi}\gamma^5\displaystyle{\not}D\psi - \overline{\psi}\displaystyle{\not}D\alpha(x)\gamma^5\psi\right], \tag{2.60}$$

$$= \int d^4x\left[\overline{\psi}(i\displaystyle{\not}D)\psi - \alpha(x)\overline{\psi}\gamma^5\displaystyle{\not}D\psi + \alpha(x)\overline{\psi}\gamma^5\displaystyle{\not}D\psi\right. \tag{2.61}$$

$$\left. - \partial_\mu\alpha(x)\overline{\psi}\gamma^\mu\gamma^5\psi\right], \tag{2.62}$$

$$= \int d^4x\left[\overline{\psi}(i\displaystyle{\not}D)\psi + \alpha(x)\partial_\mu(\overline{\psi}\gamma^\mu\gamma^5\psi)\right]. \tag{2.63}$$

We see that a global chiral transformation, with constant α, is a symmetry of the Lagrangian. Contributions from the chiral transformations can only come from terms that contain derivatives of $\alpha(x)$, which can be rearranged to show that a variation with respect to $\alpha(x)$ results in the conservation of the chiral current. This reproduces the formal result (2.5) where the axial current is conserved with massless particles.

The Lagrangian is not the only part that changes with the transformation. We must consider how this transformation affects the measure of the path integral. To see how the functional measure is affected we write the fermions in terms of a complete set of eigenstates of $\displaystyle{\not}D$. We define the left and right eigenvectors of $\displaystyle{\not}D$ by

$$(i\displaystyle{\not}D)\phi_m = \lambda_m\phi_m \quad \phi_m^\dagger(i\displaystyle{\not}D) = \lambda_m\phi^\dagger, \tag{2.64}$$

$$\int d^4x\,\phi_m(x)\phi_n^\dagger(x) = \delta_{mn}, \tag{2.65}$$

$$\sum_n \phi_n\phi_n^\dagger = 1, \tag{2.66}$$

$$\lambda_m^2 = k^2 = (k^0)^2 - (\mathbf{k})^2. \tag{2.67}$$

In order to precisely define the path integral we use these to expand the fermions in a complete basis and change from the x-representation to the m-representation,

$$\psi = \sum_m a_m\phi_m(x) = \sum_m \langle x|m\rangle a_m \quad \overline{\psi} = \sum_m \hat{a}_m\phi_m^\dagger(x) = \sum_m \langle m|x\rangle\hat{a}_m, \tag{2.68}$$

where a and $\hat{a}$ are independent Grassmann coefficients that multiply the eigenvectors of $\displaystyle{\not}D$ to enforce anti-commutation relations. Now we define the functional

measure in terms of these such that

$$\mathscr{D}\psi\mathscr{D}\overline{\psi} = [\det\langle m|x\rangle \det\langle x|m\rangle]^{-1} \prod_m da_m \prod_n d\hat{a}_n, \qquad (2.69)$$

$$= \left[\det \int dx^4 \langle m|x\rangle \langle x|n\rangle\right]^{-1} \prod_m da_m d\hat{a}_m, \qquad (2.70)$$

$$= [\det \delta_{mn}]^{-1} \prod_m da_m d\hat{a}_m, \qquad (2.71)$$

$$= \prod_m da_m d\hat{a}_m, \qquad (2.72)$$

where the normalization constant of the states is set to unity and we used the orthonormal eigenvector expansion under the integral in the measure to make the eigenstates disappear. Under the transformation the expansion becomes

$$\psi'(x) = \sum_n a'_n \phi_n(x) = \sum_n a_n(1 + i\alpha(x)\gamma^5)\phi_n(x). \qquad (2.73)$$

We can manipulate this further using the orthonormality condition,

$$\sum_n a'_n \phi_n(x) = \sum_n \sum_m \delta_{mn} a_m(1 + i\alpha(x)\gamma^5)\phi_n(x), \qquad (2.74)$$

$$= \sum_n \sum_m \int d^4x\, \phi_m(x)\phi_m^\dagger(x) a_m(1 + i\alpha(x)\gamma^5)\phi_n(x), \qquad (2.75)$$

which implies that

$$a'_n = \sum_m \int d^4x\, \phi_m^\dagger(1 + i\alpha(x)\gamma^5)\phi_n a_m, \qquad (2.76)$$

$$= \sum_m C_{m,n} a_m. \qquad (2.77)$$

The measure then changes like

$$\prod_n da'_n = \det[C_{m,n}]^{-1} \prod_n da, \qquad (2.78)$$

where the inverse determinant is the Jacobian of the transformation. The determinant appears as a inverse because of the nature of Grassmannian calculus.

We now evaluate the determinant in the Jacobian,

$$\det[C_{m,n}]^{-1} = \exp(-\text{Tr} \ln C_{m,n}), \tag{2.79}$$

$$= \exp\left(-\text{Tr} \ln\left[\delta_{mn} + \int d^4x \, \phi_m^\dagger i\alpha(x)\gamma^5\phi_n\right]\right), \tag{2.80}$$

$$= \exp\left(-i\,\text{tr}\sum_n \int d^4x \, \phi_n^\dagger \alpha(x)\gamma^5\phi_n\right), \tag{2.81}$$

$$= \exp\left(-i \int d^4x \, \alpha(x)A(x)\right), \tag{2.82}$$

where

$$A(x) = \text{tr}\sum_n \phi_n^\dagger(x)\gamma^5\phi_n(x). \tag{2.83}$$

Note that we used uppercase Tr to indicate the full trace over indices and operators and lowercase tr to indicate just the operator trace. The Jacobian for the other part of the functional measure gives a similar factor. This means that the measure transforms as

$$\mathscr{D}\psi'\mathscr{D}\overline{\psi}' = \mathscr{D}\psi\mathscr{D}\overline{\psi}\exp\left(-2i \int d^4x \, \alpha(x)A(x)\right). \tag{2.84}$$

So after a local chiral rotation our function integral becomes

$$Z = \int \mathscr{D}\psi\mathscr{D}\overline{\psi}\exp\left[i \int d^4x \left(\overline{\psi}(i\slashed{\partial})\psi + \alpha(x)\left\{\partial_\mu j^{\mu 5} - 2A(x)\right\}\right)\right], \tag{2.85}$$

where we used $j^{\mu 5} = \overline{\psi}\gamma^\mu\gamma^5\psi$. Forcing this to vanish gives us the form of the anomaly

$$\partial_\mu j^{\mu 5} = 2A(x). \tag{2.86}$$

All that is left is to calculate $A(x)$. Naively it appears that this is zero given that $\text{tr}[\gamma^5] = 0$, but $A(x)$ must be properly regularized first by cutting off the large eigenvalues $|\lambda_n| > M$. We do this by introducing the regulator

$$A(x) = \lim_{M\to\infty} \text{tr}\sum_n \phi_n^\dagger(x)\gamma^5\phi_n(x)e^{\lambda_n^2/M^2}, \tag{2.87}$$

$$= \lim_{M\to\infty} \text{tr}\sum_n \phi_n^\dagger(x)\gamma^5 e^{(i\slashed{\partial})^2/M^2}\phi_n(x). \tag{2.88}$$

Notice that the sign of the regulator is correct. Upon Wick rotation (2.64) tells us that the eigenvalues squared will be negative. The Dirac operator can be be written as

$$(i\not{D})^2 = -D^2 + e\frac{i}{4}[\gamma^\mu, \gamma^\nu]F_{\mu\nu}. \tag{2.89}$$

We want to expand the exponential that contains this operator. With the γ^5 present the first order of the expansion that will not vanish under a trace must contain at least four Dirac matrices. The second order is the lowest order that meets this requirement. We get

$$A(x) = \lim_{M\to\infty} \text{tr} \sum_n \phi_n^\dagger(x)\mathscr{A} e^{-\partial^2/M^2}\phi_n(x), \tag{2.90}$$

$$\mathscr{A} = \left[\gamma^5 \frac{1}{2!}\left(e\frac{i}{4M^2}[\gamma^\mu, \gamma^\nu]F_{\mu\nu}\right)^2\right]. \tag{2.91}$$

We can expand the eigenfunctions in plane waves, noting that $-\partial^2 = k^2$, to get

$$A(x) = \lim_{M\to\infty} \text{tr} \sum_n \int \frac{d^4k'}{(2\pi)^4}\frac{d^4k}{(2\pi)^4}\, \phi_n^\dagger(k)e^{ikx}\mathscr{A}\, e^{k^2/M^2}\phi_n(k')e^{-ik'x}. \tag{2.92}$$

We are still in Minkowski space so this integral will converge upon a Wick rotation. Using the cyclic property of the trace and the completeness relation for our orthonormal basis we can get rid of the eigenfunctions and leave a delta function,

$$A(x) = \lim_{M\to\infty} \text{tr} \int \frac{d^4k'}{(2\pi)^4}\frac{d^4k}{(2\pi)^4}\,(2\pi)^4\delta(k-k')\,e^{ikx}\mathscr{A}\, e^{k^2/M^2}e^{-ik'x}. \tag{2.93}$$

We then Wick rotate and complete the integral,

$$A(x) = \lim_{M\to\infty} \text{tr} \int \frac{d^4k}{(2\pi)^4}\, e^{ikx}\mathscr{A}\, e^{k^2/M^2}e^{-ikx}, \tag{2.94}$$

$$= \lim_{M\to\infty} \text{tr}\, i \int \frac{d^4k_\text{E}}{(2\pi)^4}\,\mathscr{A}\, e^{-k_\text{E}^2/M^2}, \tag{2.95}$$

$$= \lim_{M\to\infty} i\frac{M^4}{16\pi^2}\text{tr}\,\mathscr{A}, \tag{2.96}$$

$$= \lim_{M\to\infty} i\frac{M^4}{16\pi^2}\text{tr}\left[\gamma^5 \frac{1}{2!}\left(e\frac{i}{4M^2}[\gamma^\mu, \gamma^\nu]F_{\mu\nu}\right)^2\right], \tag{2.97}$$

$$= \lim_{M\to\infty} -i\frac{e^2}{4\cdot 32\pi^2}\text{tr}\left[\gamma^5\gamma^\mu\gamma^\nu\gamma^\rho\gamma^\sigma F_{\mu\nu}F_{\rho\sigma}\right], \tag{2.98}$$

$$= -\frac{e^2}{32\pi^2}\varepsilon^{\mu\nu\rho\sigma}F_{\mu\nu}F_{\rho\sigma}. \tag{2.99}$$

We can then plug this into equation (2.86) to get

$$\partial_\mu j^{\mu 5} = -\frac{e^2}{16\pi^2} \varepsilon^{\mu\nu\rho\sigma} F_{\mu\nu} F_{\rho\sigma}.$$

(2.100)

We have arrived at the exact same axial anomaly as we did when calculating the contribution from the triangle diagrams. But here it is clear where the correction comes from. What would be a classical conservation law is ruined by quantum corrections from the measure of the path integral.

2.1.4 Connection with the Atiyah-Singer Index Theorem

Anomalies are very closely related to Atiyah-Singer index theorem, the statement that the analytic index of an operator is the same as its topological index. In fact we unwittingly calculated the index of the Dirac operator while calculating the contribution of the anomaly to the divergence of the axial current. We will also see that the index theorem plays and integral result in deriving one of the central results of this thesis. We follow the discussion from [43, 44].

The index of the operator a is given by the relationship

$$\text{index(a)} = \dim \ker a - \dim \ker a^\dagger,$$

(2.101)

where dim ker is the dimension of the kernel of the operator. The dimension of the kernel can be found by counting the number of normalizable states u_n of the operator that satisfy the equation

$$a u_n = 0.$$

(2.102)

We can move this discussion into move familiar territory by calculating the index of the standard creation and annihilation operators used to quantize the harmonic oscillator. For the creation and annihilation we count the states that vanish when a and $a^\dagger$ is acted on them. For the annihilation operator a the only such state that exists is the ground state $|0\rangle$. For all other states the annihilation operator just lowers the number state by one. For the creation operator $a^\dagger$ no such state exists. The kernel of a and $a^\dagger$ are

$$\ker a = \{|0\rangle\} \quad \ker a^\dagger = \{\}.$$

(2.103)

The dimension of the kernel is the number of states in the set. The index for the operator that quantizes the harmonic oscillator is

$$\dim \ker a - \dim \ker a^\dagger = 1.$$

(2.104)

The index counts the number of zero eigenvalue states.

We can now talk about our incidental calculation of the index of the Dirac operator during our calculation of the anomaly. First consider the integral of over all space of the operator in equation (2.83),

$$\int d^4x A(x) = \int \mathrm{tr} \sum_n \phi_n^\dagger(x) \gamma^5 \phi_n(x) d^4x. \qquad (2.105)$$

Using the relations $\displaystyle{\not{D}} \phi_n = \lambda_n \phi_n$ and $\displaystyle{\not{D}} \gamma^5 \phi_n = -\lambda_n \gamma^5 \phi_n$, derived using $\displaystyle{\not{D}} \gamma^5 + \gamma^5 {\not{D}} = 0$, we can simplify the operator above. Starting with the surface term we find that

$$\int {\not{D}}(\phi_n^\dagger \gamma^5 \phi_n) d^4x = 0, \qquad (2.106)$$

$$\Rightarrow \int ({\not{D}}\phi_n^\dagger)\gamma^5 \phi_n + \phi_n^\dagger({\not{D}}\gamma^5 \phi_n) d^4x = 0, \qquad (2.107)$$

$$\Rightarrow -2\lambda_n \int (\phi_n^\dagger \gamma^5 \phi_n) d^4x = 0, \qquad (2.108)$$

which tells us that $\int (\phi_n^\dagger \gamma^5 \phi_n) d^4x = 0$ when $\lambda_n \neq 0$. The only modes of (2.105) that survive are those with zero eigenvalue. These modes can be split up into positive and negative chirality states. This results in the relation

$$\int d^4x \, \mathrm{tr} \sum_n \phi_n^\dagger(x) \gamma^5 \phi_n(x) = N_R - N_L, \qquad (2.109)$$

where N_R and N_L are the number of positive and negative chirality states given by $\gamma^5 \phi_n = \pm \phi_n$ that have a zero eigenvalue λ_n. We have calculated the index of the Dirac operator.

Using a regulator we also calculated (2.83) explicitly to get equation (2.94). Integrating (2.94) over all space gives us a topological quantity known as the Pontryagin index or winding number,

$$\nu = -\int d^4x \, \mathrm{tr} \frac{e^2}{32\pi^2} \varepsilon^{\mu\nu\rho\sigma} F_{\mu\nu} F_{\rho\sigma}. \qquad (2.110)$$

Having calculated (2.83) in two different ways we can equate (2.109) and (2.110) to arrive at the relationship

$$N_R - N_L = \nu, \qquad (2.111)$$

which is the Atiyah-Singer index theorem. The technique used here to derive the anomaly and index theorem can easily be extended to all even dimensions. This intimate relationship between the index theorem and the two-dimensional anomaly will be exploited later when calculating topological currents in dense matter.

2.2 Dense Stars

The average neutron star has a mass of 1.35 $M_\odot$ [45] contained in a radius of only 10 km giving it the immense density of 10^{15} g/cm^3. They are also cold objects, in the sense that their Fermi temperature is well above their actual temperature, and they have huge magnetic fields that range from $10^{12} - 10^{15}$ G. The study of neutron stars began with the proposal of the nucleus star by Landau in 1932 [46]. Later in 1934, after the discovery of the neutron, Baade and Zwicky [47] suggested that a neutron star is the result of a supernovae in which the iron core of a massive star exceeds the Chandrasekhar limit, at which the star is so massive that the gravitational forces of the star exceed the electron degeneracy pressure causing the star to collapse. This prompted theorists to investigate such objects. A few years later the famous Tolman-Oppenheiner-Volkoff equations [48, 49] were derived and a basic equation of state was formulated that bounded the mass of a neutron star. The field developed slowly as others refined the equation of state, discussed the possibility of superfluidity in the core, and developed neutrino cooling models. It was not unit the discovery of pulsars by Bell and Hewish [50] and the identification by Pacini [51] and Gold [52] of these radio pulsars as neutron stars that genuine interest in these objects developed. Since then over 2000 objects have been identified as pulsars [53].

The name pulsar comes from the periodic pulses of radiation these stars emit. Figure 2.3 illustrates the standard picture of the neutron star where the rotational axis and the magnetic axis are misaligned. As a result of this misalignment the radio emission caused by charged particles being accelerated and beamed by the magnetic field swings around like the beam of a lighthouse causing us on earth to see a pulse. We will discuss some properties of this emission in Section 2.2.

First we will focus on the direct consequences of a large, misaligned, rotating magnetic dipole. This material is common in many textbooks but Lorimer and Kramer [54] and Ghosh [55] are particularly good references. In this discussion we will try to emphasize how using a simple model many basic properties can be derived just by knowing the pulsar timing data.

A magnetic dipole with moment $|\mathbf{m}|$ inclined an angle θ from the spin axis rotating at an angular velocity Ω will emit radiation at a rate

$$\dot{E} = \frac{2}{3c^3}|\mathbf{m}|^2\Omega^4\sin(\theta)^2, \qquad (2.112)$$

which causes the star to gradually rotate slower and slower. We can quantify how the star slows due to such mechanisms by associating this dipole radiation to the change in the star's rotational kinetic energy $\frac{\partial}{\partial t}(\text{KE}) = \frac{\partial}{\partial t}(I\Omega^2/2) = I\Omega\dot{\Omega} = \dot{E}$, where I is the moment of inertia. This yields the *braking equation* for dipole radi-
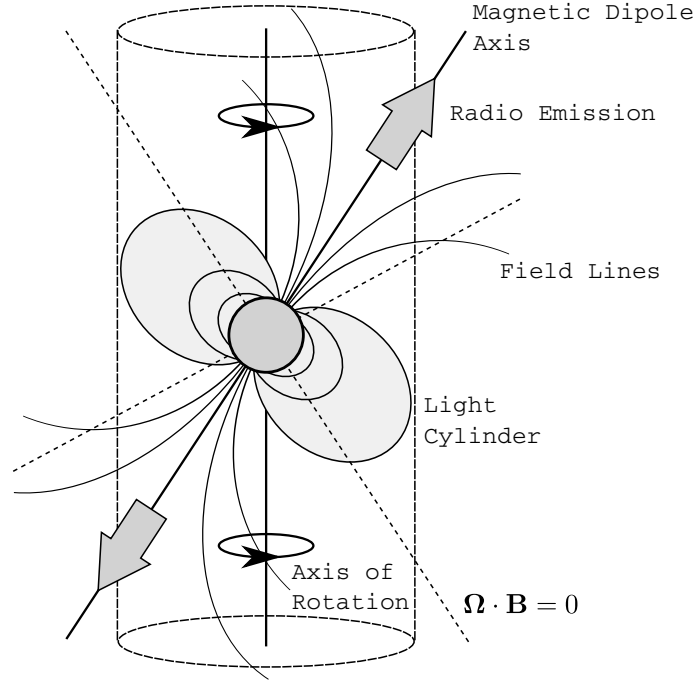
Figure 2.3: This shows the emision structure of a neutron star. Due to the rotation of the star, charged particles are accelerated along magnetic field lines and emit synchrotron radiation in a radio beam. The light cylinder is the point at which the speed of light prevents charged particles from corotating with the magnetic field. The axis of rotation and magnetic field axis are misaligned which causes the radio beam to circle like a lighthouse producing what we observe as pulses of radiation.

ation,

$$\dot{\Omega} = -K\Omega^3, \quad K = \frac{2}{3c^3 I}|\mathbf{m}|^2 \sin(\theta)^2, \quad (2.113)$$

where K is assumed to be constant. In order to compare with observations this braking equation can be generalized to

$$\dot{\Omega} = -K\Omega^n, \quad (2.114)$$

where n is called the *braking index*. This generalization accounts for other possible braking mechanisms. For instance, an observed braking index of $n = 3$ corresponds with pure dipole braking, whereas a deviation from this number would indicate another mechanism that dissipates rotational energy. By taking the derivative of Equation (2.114) with respect to time and substituting it back in to remove K we

find that $n = \ddot{\Omega}\Omega/\dot{\Omega}^2$, which allows us to measure the braking index for given stars based on the timing data, though determining the second derivative can be difficult. Measurements of the braking index show numbers ranging from $n = 1.4$ to $n = 2.9$ [56], indicating that dipole radiation is not always the dominant braking mechanism.

The braking equation can be used to estimate the *characteristic age* of the star. If $n \neq 1$ equation (2.114) can be integrated to yield the characteristic time,

$$\tau = -\frac{\Omega}{(n-1)\dot{\Omega}} \left[1 - \left(\frac{\Omega}{\Omega_0} \right)^{n-1} \right], \tag{2.115}$$

where Ω_0 is the angular velocity at birth and we used (2.114) again to remove K. By assuming that the pulsar was spinning much faster at birth than it is now $\Omega_0 \gg \Omega$ an estimate of the age of the star can be obtained,

$$\tau \approx -\frac{\Omega}{(n-1)\dot{\Omega}} = \frac{P}{(n-1)\dot{P}}, \tag{2.116}$$

where we used $P = \frac{2\pi}{\Omega}$ to write the characteristic age in a more standard form in terms of the spin period P. By assuming pure dipole braking $n = 3$ one can very roughly estimate the ages of pulsars. For example, through historical records we know that the Crab pulsar emerged from a supernova event in 1054 AD, giving it an age of approximately 950 years. The characteristic age is determined to be about $\tau = 1250$ years. A good estimate, but not particularly close.

Young neutron stars have been observed to have rapid increases in their period of rotation of the order $\Delta P/P \sim 10^{-6}$. These rapid changes are called glitches and though they are an interesting subject in their own right, we will only mention that they helped motivate the standard model in which a neutron star has a solid crust and a liquid interior.

The timing data can also be used to estimate the surface magnetic field of star. By rearranging Equation (2.113) and using $B \sim |\mathbf{m}|/r^3$ we write the magnetic field at the surface of the star as

$$B_{\mathrm{s}} = B(r = R) = \left(\frac{3c^3}{8\pi^2} \frac{I}{R^6 \sin\theta} P\dot{P} \right)^{1/2}, \tag{2.117}$$

$$= 10^{12} \, \mathrm{G} \left(\frac{\dot{P}}{10^{-15}} \right)^{1/2} \left(\frac{P}{\mathrm{s}} \right)^{1/2}, \tag{2.118}$$

where we took $\theta = \pi$, $I = 10^{45} \, \mathrm{g \, cm^2}$, and $R = 10$ km. This estimate assumes pure dipole braking and provides an order of magnitude, or characteristic value, for the surface magnetic field of pulsars.

2.2.1 The Magnetosphere and Pulsar Emission

We will present a very simple model of how the emission of a neutron star is structured in which we assume the magnetic field axis and the axis of rotation are perfectly aligned. Though not realistic this will allow us to focus on the key features of emission. It is believed that the magnetic axis and rotational axis are fairly close to each other and it is the hope that the physics of such a system would not differ much from our description. An especially strong review of pulsar emission is given by Lyne and Graham-Smith [57].

The physics outside a neutron star is dominated by the magnetic field. Even near the surface of the star the gravitational forces on an electron are orders of magnitude smaller than the induced electrostatic forces. For instance, the ratio is

$$\frac{F_{\mathrm{G}}}{F_{\mathrm{EM}}} = \left(\frac{GMm}{r^2}\right)\left(\frac{c}{e\Omega rB}\right) \sim 10^{-12} \tag{2.119}$$

for an electron near the surface of the Crab pulsar [57]. These forces lead to the star being surrounded by a dense plasma. The interaction between the magnetic field of the star and the plasma that surrounds the star is responsible for the radio emission we detect from the star. A very general picture of the emission mechanism starts with the plasma being forced to corotate with the neutron star. Charged particles run the along magnetic field lines and emit curvature or synchrotron radiation linearly polarized in the plane of curvature. The emission forms a coherent beam that we detect as pulses. From how the polarization of the beam changes as the pulse passes through detectors it is possible to determine the axis of rotation of the pulsar.

The argument for the magnetosphere that we discuss here was introduced by Goldreich and Julian [58]. The basic physics arises by assuming that the interior of the neutron star is a very good conductor. Because of this, a force free environment in created where an electric field is induced to balance the forces created by the magnetic field sweeping through space,

$$\mathbf{E} + \frac{(\Omega \times \mathbf{r})}{c} \times \mathbf{B} = 0. \tag{2.120}$$

Let us assume for a moment that the star is surrounded by a vacuum instead of a plasma. By solving Laplace's equation we can determine the electric potential induced by the rotating magnetic field as

$$\Phi(r,\theta) = \frac{B_{\mathrm{s}}\Omega R^5}{6cr^3}(3\cos^2\theta - 1). \tag{2.121}$$

The surface charge for such a configuration results in a electric field near the surface,

$$E_{\parallel} = \left.\frac{\mathbf{E}\cdot\mathbf{B}}{B}\right|_{r=R} = -\frac{\Omega B_{\rm s} R}{c}\cos^3\theta. \tag{2.122}$$

As mentioned, the presence of this field causes particles on the surface of the star experience electrostatic forces 10 orders of magnitude larger than gravitational forces for typical neutron star parameter. A vacuum solution outside the star is unstable to these forces and charged are pulled from the surface such that the star is surrounded by a dense plasma.

We now assume that the star is surrounded by a dense plasma called the magnetoshere. This plasma experiences the same $\mathbf{E}\times\mathbf{B}$ field as the interior of the star and is forced to corotate. This corotation continues up to a distance away from the star where the particles would have to move faster than the speed of light to continue corotating with the star. This boundary is a called the light cylinder. The magnetosphere is seen as an extension of the neutron star and forms a region where

$$\mathbf{E}\cdot\mathbf{B} = 0. \tag{2.123}$$

The magnetic field lines are then electric equipotentials. Because of this force free environment, particles that move in the magnetosphere move along the magnetic field lines, which is often described as sliding. The plasma in the magnetosphere arranges itself into a force free configuration that results in a charge distribution given by

$$\rho_e(r,\theta) = \frac{1}{4\pi}\nabla\cdot\mathbf{E} = -\frac{\Omega\cdot\mathbf{B}}{2\pi c} = -\frac{B_{\rm s}\Omega R^3}{4\pi c r^3}(3\cos^2\theta - 1). \tag{2.124}$$

The charge distribution flips signs at $\Omega\cdot\mathbf{B} = 0$, which for our simple model where the magnetic dipole axis and the rotation axis are aligned occurs at $\sec\theta = \sqrt{3}$. This results in a charge distribution where electrons populate the regions near the poles of the star and protons populate the regions near the equator. If the axes are anti-aligned then protons populate the poles and electrons populate the equator. Dividing by the electric charge we get the *Goldreich-Julian density*

$$n_{\rm GJ} \simeq 7\times 10^{10}\ {\rm cm}^{-3}\left(\frac{P}{s}\right)^{-1/2}\left(\frac{\dot{P}}{10^{-15}}\right)^{1/2}, \tag{2.125}$$

which is the maximum value for the charge at the pole, $r = R$ and $\theta = 0$.

Beyond this division of charge, the magnetosphere is broken into two regions divided by whether or not the magnetic field lines close within the light cylinder.
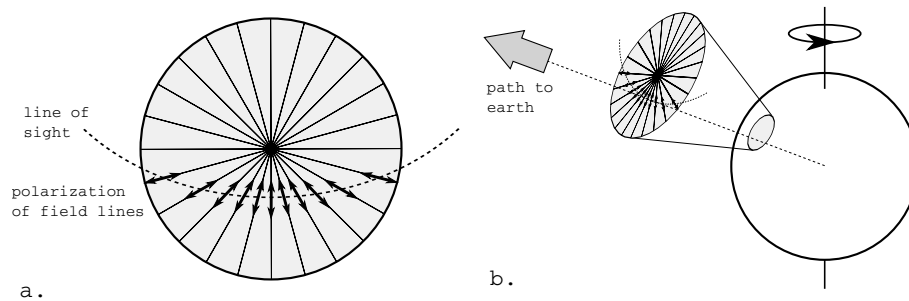
Figure 2.4: The pulse we see from earth traces a line through the polarization of the magnetic field. From how this angle shifts we can infer which infer the rotation vector of the star.

Within these closed field lines, indicated by the light grey in Figure 2.3, the plasma is static. The forces inside this region are completely cancelled by the configuration. The region with open field lines is dynamic. Particles are allowed to escape. Other than the thermal emission that comes from the pulsar, all emission is thought to come from this dynamic portion of the magnetosphere.

The dynamic region where charge is allowed to leave is repopulated by charge ripped from the surface of the star by the electric field at the surface (2.122). Accelerated by this force these particles slide along the magnetic field lines. While following the curve of these field lines the electrons emit radiation through curvature radiation or synchrotron radiation. The structure of the emitting regions is beyond the scope of this review. The observation to be taken from this is that both curvature and synchrotron radiation are linearly polarized in the plane of curvature, though some more complicated radiation mechanism have polarization orthogonal to this. Looking along the axis of the magnetic dipole the polarization forms a pattern similar to the spokes of a bicycle wheel as seen in Figure 2.4.

The model that describes how the polarization changes as the pulse passes through the detector of earth is called the rotating vector model [59]. By knowing how the polarization sweeps across the detector we can infer the direction of the axis of rotation of the star and the angle between the magnetic axis and the rotational axis. This is providing one has good enough data to constrain the measurement of the angle between the spin axis and the magnetic field axis. It is often difficult to sample enough polarization longitudes (measurements during the pulse) to get a well defined polarization sweep.

2.2.2 Inside a Neutron Star

To investigate the internal structure further we are required to look at the nature of nuclear matter at high densities and low temperatures. Neutron stars have the distinction of being extremely cold in terms of statistical mechanical, which points to the possibility that the nuclear matter in the core is a condensate. The challenge in studying neutron stars is trying to come up with a picture that describes all these phenomena.

The primary composition of nuclear matter in a neutron star is constantly being debated [60, 61]. The density of the neutron star lies in a critical area of the QCD phase diagram where many states exist close together. Figure 2.5 outlines the layered structure that is thought to appear as the density increases from that of neutron drip ρ_{ND} near the surface, where neutron rich nuclei start to release free neutrons, to beyond nuclear saturation ρ_0 in the centre, where the density surpasses that of nucleons in heavy atomic nuclei. The most basic division in the layered structure of the star is between the solid crust and the liquid core. The crust contains the density transition from the outer crust, consisting of degenerate electrons and ions, though neutron drip densities to the inner crust where there are free neutrons, electrons, and neutron rich nuclei. As the density increases the outer core is reached, where the neutrons, protons, and electrons are completely free. At the inner core densities are well above nuclear saturation and starts to impinge opon the plethora of possible phases in dense matter. There are many popular scenarios: hyperons, pion and kaon condensates, and pure quark matter. We should note that a recent measurement of a 2 solar mass pulsar [62] favours stiff (incompressible) equations of state which favours nuclear matter and rules out, for that star, many exotic equations of state with hyperons, condensates, and free quark matter.

The core of the star is what we are most interested in for the work of this thesis. We will ignore questions about the equation of state of a neutron star and instead consider many different states. For readers interested in the equation of state a good review can be found in [60]. We will also quickly review the superfluidity and superconductivity in the star and how this affects the magnetic field.

Basic Weak Processes

Fundamentally a neutron star is made of neutrons with small, equal fractions of protons and electrons. In more exotic models hyperons may appear along with pion and kaon condensates. In an effort to simplify the discussion we will constrain ourselves to four fundamental interactions that describe the majority of cases in dense stars. The neutrinos produced during these weak interactions can escape the star, providing the temperature is low enough, and are responsible for cooling the
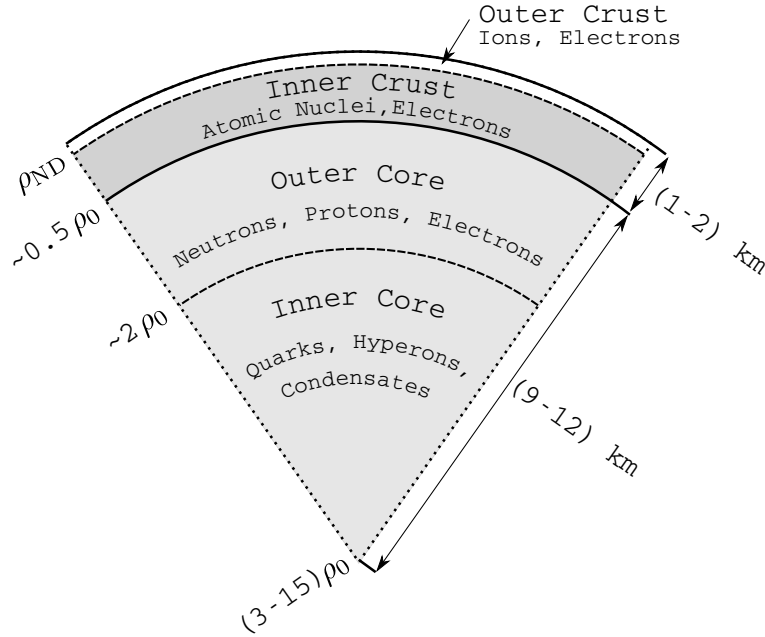
Figure 2.5: The layered structure of the neutrons star broken into four parts. The crust, shown in dark grey and white, is a solid structure. The core, shown in light grey, is a liquid. The transitions are marked by the density at which they occur, where ρ_0 is the nuclear saturation density and ρ_{ND} is the nuclear drip density. This figure is modelled after Figure 1.2 of [60]

star. We will discuss a simple model of cooling in Chapter 5.

The first two processes are quite closely related—the direct and modified Urca processes,

$$e^- + P\left(+\,\overline{\nu}_e\right) \quad \leftrightarrow \quad N\left(+\,\nu_e\right), \tag{2.126}$$

$$e^- + P + N'\left(+\,\overline{\nu}_e\right) \quad \leftrightarrow \quad N' + N\left(+\,\nu_e\right), \tag{2.127}$$
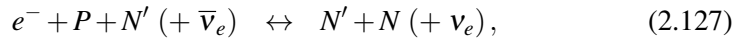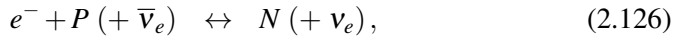
where the neutrinos in parenthesis only appear in the final state of the interaction. Both of these processes obey the beta equilibrium condition $\mu_e + \mu_P = \mu_N$. The neutrinos created in these processes only interact with matter through the weak force, which is so weak that the star is transparent to the neutrinos. They leave the star and do not contribute to the equilibrium condition.

The first of these interactions, the direct Urca Process, should be the dominant process in normal nuclear matter but it is heavily suppressed because the particles are unable to conserve momentum while remaining on their Fermi surfaces. It is

possible for the direct process to conserve momentum if the proton fraction in the star is above 1/9 [63], which could occur with the appearance of hyperons [64]. In these cases the direct Urca process dominates. The modified Urca process is able to conserve momentum using an additional external nucleon. This was the process used in the first neutrino emission calculations [65]. This is thought to be the dominant electron producing process in normal nuclear matter, but it is very slow. The presence of exotic particles introduces processes that create and destroy electrons quicker.

As the density of matter increases it is likely that kaon [66] and pion condensates will appear. We will restrict the discussion to kaon condensates, which appear at much more reasonable densities, $3n_0$, than pion condensates, $300n_0$, but the phenomenology of dealing with the two condensates is almost identical. Electrons are still created and destroyed by the previous interactions, but at a much slower rate than an electron decaying[1] into a kaon and neutrino in the presence of nucleons,

$$e^- + N \left(+ \overline{\nu}_e\right) \quad \leftrightarrow \quad \langle K \rangle^- + N \left(+ \nu_e\right). \tag{2.128}$$

This interaction and its inverse process add another equilibrium condition, $\mu_e = \mu_K$, on top of the previously mentioned beta equilibrium.

The previous three interactions encompass the creation of electrons in almost all possible neutron star interiors [61]. The last interaction we consider is the primary source of electrons in quark stars [67]. It may be possible that the star is so dense that the quarks state extends right to the surface of the star and that the layered structure we outlined for neutron stars does not exist. The direct Urca process for quarks are

$$e^- + u \left(+ \overline{\nu}_e\right) \quad \leftrightarrow \quad d \left(+ \nu_e\right), \tag{2.129}$$

$$e^- + u \left(+ \overline{\nu}_e\right) \quad \leftrightarrow \quad s \left(+ \nu_e\right). \tag{2.130}$$

Unlike in normal nuclear matter there is no trouble conserving momentum in quark matter. The direct process occurs unsuppressed and there is no need to discuss a modified process.

Simple Models for Dense Matter

We will review the features of neutron matter that are required for the rest of the paper. Most importantly we will summarize the short reviews found in [67–70]

---

[1]Throughout this work the term *electron decay* means the transforming of an electron into a neutrino as a result of interactions with surrounding hadrons. This process is often called *electron capture.*

and state the values used in the rest of the paper. The simplest model is the non-interacting gas model where the ground state of the neutron star, $T = 0$, is a mixture of neutrons, protons, and electrons that is electrically neutral. The baryon density is on the order of nuclear density $n_0 = 0.17$ fm^{-3}, which leads to the nucleons and electrons being highly degenerate.

The particles achieve equilibrium though the Urca processes (2.126). The neutrinos produced in these reactions only react weakly in the star and easily leave it at low temperatures. Because of this neutrinos are often assumed to be non-degenerate and the chemical potentials in the star satisfy

$$\mu_e + \mu_P = \mu_N. \tag{2.131}$$

Charge neutrality implies that $n_e = n_P$, which because $n_i \propto k_i^3$ implies that the Fermi momenta of the electrons and protons are equal, $k_e = k_P$. This restriction has two important effects. The electrons are relativistic and the protons are non-relativistic implying that the chemical potential of the proton is much smaller that of the electron. This further implies that the density of neutrons is much higher than the electrons and protons, thus a neutron star. Assuming that the density of the neutrons is that of nuclear matter then

$$k_N = (3\pi^2 n_N)^{1/3} \approx 340 \, (n/n_0)^{1/3} \text{ MeV}. \tag{2.132}$$

Equating the electron and neutron chemical potentials yields

$$k_e \approx \frac{k_N^2}{2m_N} \approx 62 \, (n/n_0)^{2/3} \text{ MeV}. \tag{2.133}$$

In reality there is a correction to the non-interacting model due to the proton being more bound than the electron. It is common in literature to assume a value of

$$k_e \approx 100 \, (n/n_0)^{2/3} \text{ MeV}, \tag{2.134}$$

which is the value we will use through out the paper.

As the density of the star raises above $3n_0$ there is the possibility that K^- condensates will appear [66]. As the density of the nuclear matter increases, the density of the electrons increases to a point where it becomes advantageous to decay into negatively charged kaons though the process (2.128). The system reaches equilibrium through the inverse process. These processes add an additional equilibrium condition,

$$\mu_e = \mu_K. \tag{2.135}$$

Though negatively charged pions are lighter than kaons, they are unlikely to appear until much higher densities due strong interactions in the dense medium increasing the pion's effective mass [64].

At around the same density as kaons appear, light hyperons and muons may appear [64]. The existence of hadrons lowers the neutron density, which lowers the ratio of neutrons to protons, making it possible for the direct Urca process to proceed unsuppressed, and opens up processes such as $\Lambda \to e^- + P + \overline{\nu}_e$, which are also not kinematically suppressed. These processes occur at about the same rate as the direct Urca processes, so we will take the direct Urca process as a reasonable substitute for them. The rate can then be adjusted by an integer factor to compensate for additional processes. The appearance of muons has no effect of our calculations as they are too heavy to couple to the current.

When the density gets high enough it is possible that the quarks deconfine—the hadrons break down into their constituent quarks. The chemical potential for the quarks in the star range from 300-500 MeV [71]. Because of this we will consider only the existence of light quarks in the star, which attain equilibrium through the quark Urca processes (2.129). The equilibrium conditions are

$$
\begin{aligned}
\mu_u + \mu_e &= \mu_d, & (2.136) \\
\mu_u + \mu_e &= \mu_s, & (2.137)
\end{aligned}
$$

where, as in earlier cases, the neutrinos are not trapped and are not degenerate. The quark matter must also be electrically neutral,

$$
Q/e = \frac{2}{3}n_u - \frac{1}{3}n_d - \frac{1}{3}n_s - n_e = 0. \tag{2.138}
$$

The simplest models assume that the quark masses are all zero, thus their Fermi momenta are equal to their Fermi energies, and the predicted electron density is zero. This, however, is not adequate as leptons do exist in the star. Room for the electrons comes from the large mass of the strange quark. Though the up and down quarks are relatively light, $m_u \sim m_d \sim 5 - 10$ MeV, the strange quark mass is actually quite large, $m_s \sim 100 - 300$ MeV. The lower bound of the strange quark mass is given by its current mass, whereas the constituent mass can be higher due to the relatively low density of the dense star. Because of this large mass the strange quark is nonrelativistic meaning there will be fewer of them and electrons must be present to conserve charge. For this paper will will follow [67] by assuming that the quarks are massless, $k_u \sim k_s \sim k_d \sim k_q$, where

$$
k_q = (\pi^2 n_b)^{1/3} \sim 235 \left(\frac{n_b}{n_0}\right)^{1/3} \text{MeV}, \tag{2.139}
$$

where n_b is the baryon number density. For typical densities in the core of the neutron star the Fermi momentum is $k_q \sim 400$ MeV. We can approximate the electron Fermi momentum using the fraction of electrons to baryons, $Y_e = n_e/n_b$, which yields

$$k_e = (3Y_e)^{1/3}k_q. \tag{2.140}$$

The electron fraction Y_e has a complex relation between the mass of the strange quark, the gluon coupling constant and the density of matter. The most sensitive dependence is the sixth power of the strange quark mass, which as discussed can vary by a factor of two. The highest values are $Y_e = 0.01$ [67], whereas a free quark estimate is $Y_e \lesssim 10^{-4}$ [72]. With interactions and a relatively low strange quark mass the typical value for the electron fraction is $Y_e \lesssim 10^{-3}$ [60].

Superfluidity and Superconductivity

Being fermions, and subject to the Pauli exclusion principle, neutrons and protons can only condense by forming pairs known as Cooper pairs. The wave function of a Cooper pair is described as $\psi_{s_1,s_2}(\mathbf{R},\mathbf{r})$, where s_1, s_2 are the spin projections of each particle and R and r are the centre of mass coordinate and orbital coordinates respectively.

Cooper pairs orbit on the order of $r \sim 100$ fm, which seems small, but is large compared to the average distance of neutrons in the star. A Cooper pair is not actually a pair of particles in the traditional sense, but is a pair in momentum space. This pairing of fermions now makes a bosonic state which is no longer subject to the Pauli exclusion principle. It is now possible for a number of Cooper pairs to occupy the same energy state with a gap, Δ, in the energy spectrum. This ordering is called a condensate and it occurs when the system has dropped below some critical temperature T_c which changes depending on the particular baryon species. For a Cooper pair this means that the amplitude of its wave function is coherent over macroscopic distances and a large number of neutron pairs are described by identical wave functions. The appearance of the energy gap is responsible for the properties of the superfluid. Particle states now require a minimum energy to excite and interact. Because it is a Fermi surface phenomenon superfluidity has little affect of the equation of state, masses, and radii of the stars.

While there is no direct evidence that the core of a neutron star contains superfluid neutrons and superconducting protons, there are some compelling observations that point to a superfluid core. The first is the phenomena of glitches, sudden increases in pulsar spin rate, that may be caused by a large number of superfluid vortices simultaneously unpinning and transferring their momentum to the solid
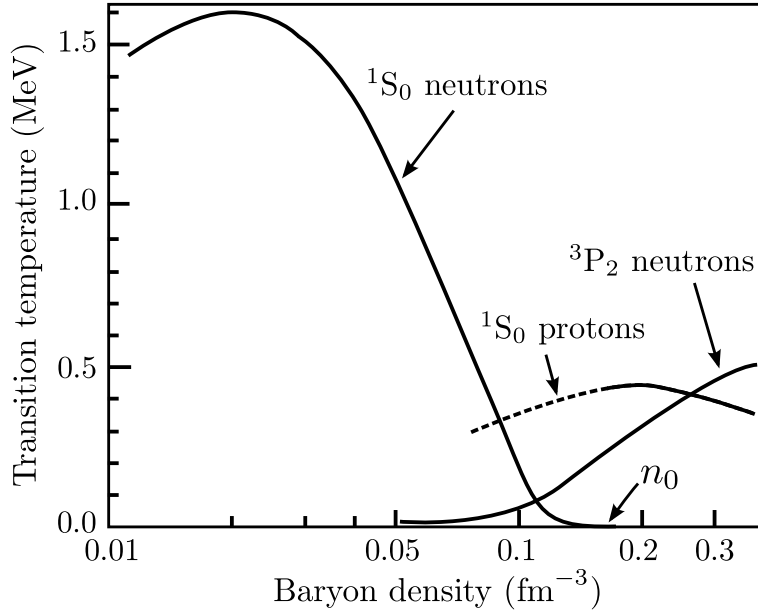
Figure 2.6: The superfluid transition temperature as a function of baryon density for the dominant pairing state in protons and neutrons. The dashed line indicates an extrapolation. This figure is modelled after Fig. 2 in [80].

crust of the star [73]. The second is the observation that Cassiopeia A is in a cooling regime that can be described by the star's core transitioning into a superfluid state [74, 75]. Additionally, a good argument for superfluid cores can be made based on experiments conducted on Earth and predictions from the BCS theory of superconductors. Naively one can use the fact that neutron stars are very cold, having a temperature $T \sim 10^9$ K $\ll T_{\text{fermi}} \sim 10^{12}$ K, and that the transition temperature for nuclear matter to condense here on Earth is $T_c \sim 10^{-3} T_{\text{fermi}}$ [76]. For a more accurate number we can look at the strength of the possible pairing states of nuclear matter.

For fermions to form Cooper pairs, and in turn make a condensate, it is necessary for there to exist an attractive force between them, no matter how small [77]. Much work has been done studying the nucleon-nucleon interactions which form Cooper pairs. The interactions can be determined by looking at the phase shifts of free neutron scattering, which were discussed in the context of neutron star interiors in [78]. As shown in Fig. 2.6 this data can be used to determine what the dominant pairing interactions are at a given density. For neutrons at lower

densities, where the momenta are lower, it is favourable to form zero angular momentum spin-singlet $S = 0$ states $^1S_0$. At higher densities, and consequently higher momenta, the $L = 0$ angular momentum $S = 1$ spin-triplet state $^3P_2$ is favoured. For protons it is thought that the $^1S_0$ state dominates at all pairings [76, 79–81].

Though the strength of the interaction is not important in the formation of a Cooper pair, it does give an indicator of the critical temperature of the nuclear matter. Fig. 2.6 shows transition temperatures $T_c \gtrsim 0.5$ MeV $\approx 5^{10}$ K that are all greater than the temperature the star at most phases of its life. But we should stress that the pairing structure outlined in Fig. 2.6 is a rough outline. The exact details of which pairing states exist in a neutrons star is still unknown. The nature of BCS pairing is that T_c is exponentially proportional to the pairing strength and effective mass of the particles. This makes it difficult to take terrestrial pairing strengths and guesses of the effect nucleon masses to obtain a reliable value for T_c in the star.

There is also a possibility that if quark matter is the dominant state in the star that it may be superconducting. Unlike protons and neutrons the number of flavours and colours of quarks lead to many possible pairing states. In a compact star there are up, down, and strange quarks that each have three colours leading to a 9×9 colour-flavour matrix of possible pairings. A comprehensive review can be found in [82]. The most symmetric paring configuration is where all three colours and flavours contribute. This is called the colour-flavour locked (CFL) phase and is thought do be favoured at high densities. At lower densities the strange mass starts to stress CFL pairing and the 2SC phase, where two quark flavours of two colours pair, may be dominant.

The presence of superfluidity can greatly affect the weak processes discussed earlier [81]. The extreme degeneracy of the baryons only allows those near the Fermi surface to participate in interactions. The strong interaction introduces an attractive force between nucleons resting near the Fermi surface. When the star has cools below the critical temperature T_c a gap Δ appears in the energy spectrum. The ground state of the system reorganizes itself such that no particle can have an energy between $E_F + \Delta$ and $E_F - \Delta$. If the pairing interaction is strong enough this gap suppresses interactions involving these nucleons and can render them inactive. This has the effect of shutting off the Urca processes. At high densities such as those in the core of the star and at temperatures near the critical temperature the star is in a state were Cooper pairs are continually being formed and broken. This process can contribute the to cooling of the star and is the focus of the results in [74, 75] where it is believed that the increased cooling seen in Cassiopeia A is caused by the onset of a superfluid phase. In Chapter 4 we will calculate the current using the standard processes without taking into account the affects of pairing. As we discuss in the next section we are interested in calculating the magnitude of the current in regions of the star where the magnetic field has destroyed the superfluid

proton state. We are also interested in calculating the currents in the core of the star where the pairing is less likely to affect the interactions. Later when discussing kick models we will be concerned with the time right after the stars birth where the temperatures are very hot and superfluids are unlikely to form.

Structure of the Magnetic Field in a Neutron Star

In this thesis we will introduce the idea of a topological current that flows along magnetic flux lines. Magnetic flux structure inside a neutron star is non-trivial. In estimating the magnitude of the topological current in Section 3.2 we will simplify this by considering what would happen if the flux were uniformly and continuously spread throughout the star. The magnitude of the current in the entire star depends only on the amount of flux, not its structure. The total current leaving the star would be the same if some complex structure were present. Bunching flux lines would simply mean there are smaller regions with stronger magnetic fields. However, it is important to be aware of this non-trivial structure as it will be considered later in Chapter 6 when we discuss applications of the current.

As discussed the protons are likely superconducting and the neutrons form a superfluid. The magnetic field is large enough that it is favourable for the flux to penetrate the superconductor, destroying the superconducting state in a small region, rather than being completely expelled. The Meissner effect forces the flux to bundle into into either type-II vortices or type-I domains, which is often called the intermediate state. It is generally believed that the protons form a type-II superconductor. The Landau-Ginzburg parameter $\kappa = \lambda/\xi$ determines the type of superconductivity. Typically in a neutron star the London penetration depth is $\lambda \sim 120$ fm and the coherence length of the proton superconductor is $\xi \sim 30$ fm. This creates a ratio $\kappa > 1/\sqrt{2}$, which indicates type-II superconductivity. For a type-II superconductor the magnetic field will penetrate the star by destroying narrow regions of superconductivity that each carry a single quantum of flux, $\Phi_0 = 2\pi/q = 2 \cdot 10^{-7}$ $G\,cm^2$. But there are problems with this picture [83, 84]. It is possible that the system behaves as type-I superconductor even though the Landau-Ginzburg parameter would suggest type-II behaviour [8]. The argument in [8] relies on the electromagnetic interaction between current carrying vortices rather than altering the value of the Landau-Ginzburg parameter κ.

If the intermediate state is realized in neutron stars the magnetic field distribution will be again non-uniform, but the structure would be quite different. The intermediate state is characterized by alternating domains of superconducting and normal matter where the superconducting domains exhibit the Meissner effect, while the normal domains carry the required magnetic flux. The pattern of these domains is strongly related to the geometry of the problem, see [8] for details.

While precise calculations are required for understanding of the magnetic structure in this case one can give the following estimation for typical size of a domain as suggested in [8, 85],

$$a \sim 10\sqrt{R\lambda}\,, \tag{2.141}$$

where R is a typical external size identified with a neutron star core ($R \sim 10$ km), while λ is a typical microscopical scale of the problem. Numerically $a \sim 10^{-1}$ cm, which implies that a typical domain can accommodate about 10^4 neutron vortices separated by a distance 10^{-3} cm. While the field distribution for the intermediate state and the type-II superconductor are very different one should anticipate that the ratio of normal to superconducting regions are the same.

Regardless of the flux structure, there are two regions of the neutron star to consider—those with magnetic flux and those without. The total units of quantum flux can be estimated as

$$N_{\mathrm{v}} \sim \frac{\pi R^2 B}{\Phi_0} \sim 10^{31} B_{12}, \quad B_{12} \equiv \left(\frac{B}{10^{12}G}\right). \tag{2.142}$$

The region that a single unit of flux occupies has a radius equal to the London penetration depth of the field $\lambda \sim 100$ fm. This is multiplied by the number of vortices N_{v} to get the total area. If we take a slice of the neutron star perpendicular to the magnetic field we find that the ratio of the area occupied by flux tubes is much smaller than the area occupied by the void,

$$\frac{A_{\mathrm{vortices}}}{A_{\mathrm{star}}} \simeq \frac{N_{\mathrm{v}} \pi \lambda^2}{\pi R^2} \simeq \frac{\pi \lambda^2 B}{\Phi_0} \simeq 10^{-3} \cdot B_{12}\,. \tag{2.143}$$

This suppression essentially reflects the difference between typical magnetic field $B \sim 10^{12}$ G and the critical magnetic field $B_{\mathrm{c1}} \sim 10^{15}$ G when the superconductivity is destroyed.

2.2.3 Pulsar Kicks

Various studies have found that pulsars general travel through space between $100-1000$ km/s while their progenitors, normal stars, travel around 30 km/s [86]. This discrepancy indicates that at some time during the pulsar's birth energy was asymmetry imparted to push it up to speed. This asymmetric push is known as a kick.

There have been many attempts to determine the velocity distribution of pulsars. It is difficult to determine space velocities because we only see the proper motion of the pulsar, the angular path it traces through the sky. The analysis of [87] favours a bimodal velocity distribution with peaks at $90 \mathrm{\ km s^{-1}}$ and $500 \mathrm{\ km s^{-1}}$ with 15% of pulsars travelling at speeds greater than $1000 \mathrm{\ km s^{-1}}$. Alternatively

[88] and [89] both predict a single peaked distribution with an average velocity of $\sim 400\,\mathrm{km\,s}^{-1}$.

The origin of these kicks is still uncertain. One of the ambiguities in constraining kick models is that there are very few correlations between the kicks and neutron star properties. For example, the kick direction is currently uncorrelated with the period or magnetic dipole strength, two of the main observational properties of the pulsar. But there does seem to be a correlation between the spin of the pulsar and the direction of the kick. One method of determining the spin axis comes from modelling pulsar wind tori that appear in Chandra X-ray data [90]. By accurately modelling the torus formed around a spinning pulsar it is possible to infer the spin axis. Another method is to use the rotating vector model discussed in the introduction. Knowing the polarization of the radiation in the pulse and by measuring how it sweeps across the sensor it is to determine the spin axis of the star [91]. Both of these studies indicate that the spin axis and kick direction are aligned.

The rotating vector model discussed earlier can be used to determine the angle between the kick direction and the spin. The model does not always hold perfectly because the polarization does not always align with the plane of curvature of the magnetic field, but sometimes orthogonally. Though accounted for in [91], we will discuss the study done in [92], which more directly focuses on this issue. As shown in Figure 2.4 the line of sight, spin axis, and magnetic axis all rest in the same plane are all aligned at the centre of the pulse. The polarization angle at this point will be parallel, for regular emission, or perpendicular, for orthogonal polarization. They pick measurements where the error in pulsar proper motion is under 15 degrees and the polarization is under 20 degrees. They calculate the difference in these two and discard those results with error larger than 25 degrees. After starting with a data set of 233 [88] they are left with 24 pulsars. The plotted distribution of the polarization minus the proper motion is peaked at 0 and 90 degrees. Assuming that some pulsars prefer to emit orthogonal polarization and some normal, they conclude that the spin axis and kick direction are very closely aligned.

Though there have been many attempts to explain kicks each mechanism has its own problems [93]. The mechanisms fall into three basic categories: hydrodynamic kicks, neutrino kicks. Hydrodynamic kicks occur due to asymmetric buildups of mass in the star during supernova. This asymmetry causes an off-centre explosion that can kick the star. The original models could not kick the star to velocities much higher than 100 km/s. Recent models that include neutrino luminosities to drive the explosions have been more successful [94, 95] in reaching the higher velocities observed. These models require maximum asymmetry due to instabilities and neutrino energy to be artificially introduced and fail to intrinsically predict the alignment of the spin and kick. Despite this they are appealing because

they take advantage of the immense energy of the supernova, which we know exist.

Neutrino kicks arise because of the asymmetry in neutrino emission created by the existence of a single spin state in the lowest Landau level of the electron. Because they only interact weakly neutrinos easily leave the star. The left-handedness of the neutrino conspires with the electron stuck in the lowest Landau level to force some neutrinos to leave the star in a preferred direction casing a kick. We will discuss these models in detail when we introduce the idea of topological kicks in Chapter 5. The main problem with neutrino kicks is that they require temperatures so high that the bulk of the star becomes opaque to the neutrino and it cannot escape. To remedy this many models consider neutrinos only being emitted from a thin shell on the surface of the star. Unfortunately, these models require very large surface magnetic fields ($\sim 10^1 5$ G) to get a large enough asymmetry. These models however do predict the spin-kick correlation quite naturally.

The third category, electrodynamic kicks [96, 97], are less studied but deserve mention. The off axis rotating dipole responsible for spin braking can emit radiation that very gradually imparts an acceleration along the pulsar's spin axis. This effect naturally produces the spin-kick correlation, but requires sustained spin periods less than 2 ms and an initial spin period of less than 1ms to produce substantial kicks. Pulsar birth spins are much greater than 1 ms, likely ruling this mechanism out.

In Chapter 5 we will introduce the idea of topological kicks where we use the topological kicks introduced in this thesis to generate the asymmetry required to kick the star. Topological kicks get their energy from the chemical potential rather than the temperature and avoid many of the problems that plague neutrino kicks.

2.3 The AdS/CFT Correspondence

A hologram is a two-dimensional object that, when light hits it just the right way, can produce a three-dimensional image. All the information for the extra dimension of the image is encoded in the two-dimensional object. It has been proposed by Thorn, 't Hooft, and Susskind that a similar connection exists between gravity and quantum mechanics. More precisely, they state that a description of physics in our universe with gravity in three spatial dimensions has an equivalent theoretical description in two dimensions in which the laws are different and there is no gravity.

The insight gained from these investigations is that the physics in a volume of space can be alternatively, and completely, described by a different theory that exists at lower dimensions on the boundary of that volume. As a crude example imagine our universe was the fruit of an orange. Holography states that the laws that govern the universe, the fruit, can be described by considering a theory that lives on the boundary of the universe, on the peel of the orange. It looks nothing like the theory that governs our universe, yet we can use it to derive similar conclusions about our universe. We will discuss the most striking example of this holographic principle, the conjecture of the AdS/CFT correspondence.

The AdS/CFT correspondence conjectures a connection similar in spirit to those discussed above, but it is between 10-dimensional string theories and 4-dimensional gauge theories. Two such theories are said to be dual to each other. The first AdS/CFT correspondence was introduced by Maldacena [98], but since then many models have been proposed. We are particularly interested in dual models in which one of the dual theories approximates the world we live in and the other theory is easy to solve. These models have a parameter space such that string theory can be effectively described by a familiar theory of gravity and the gauge theory can be effectively described by hydrodynamics. These are known as fluid/gravity correspondences and they will we the focus of our discussion.

There is a symbiotic relationship between these theories and the insight gained is rooted in the fact that they are dual to each other via the AdS/CFT correspondence. Their respective coupling constants scale inversely to each other, meaning that doing perturbative calculations in the weak coupling limit of one theory can give us non-perturbative results in the strong coupling limit of the other. This is provided we have the dictionary between the two theories that give us a map between objects in both theories.

The fluid/gravity correspondence provides us with an exceptionally powerful tool for calculations and provides an interesting connection between two seemingly disconnected fields. It is analogous to a giant Laplace transform for field theories where, when confronted with a difficult problem, we can switch to a space where

the calculations can be carried out, then the results are translated back into the language of the original problem.

The goal of this section is to introduce the AdS/CFT correspondence by showing how it can be used to explore the universal properties of matter. The eventual aim of such a program is to do calculations in the strongly coupled regimes of quantum chromodynamics (QCD), relevant to describe for example the quark-gluon plasma produced in relativistic heavy ions collisions. Using gravity at weak coupling to calculate hydrodynamic properties has been successful in yielding the shear viscosity to entropy density ratio of the strongly coupled quark-gluon plasma created in RHIC collisions [99],

$$\frac{\eta}{s} = \frac{1}{4\pi}. \tag{2.144}$$

The key to doing this calculation was the observation that the long distance dynamics of any interacting quantum field theory near thermal equilibrium is well described by a relativistic fluid equation. In this introduction we will discuss what the AdS/CFT correspondence is in a more technical terms and show how it can be used to calculate dynamic properties of gauge fields [100].

2.3.1 Motivation for Studying the Correspondence

The motivation for studying the fluid/gravity correspondence is the observation of a quark-gluon plasma at the Relativistic Heavy Ion Collider (RHIC) Brookhaven. The plasma is created by smashing gold nuclei into each other at velocities with a gamma factor of about 100. In this collision the individual protons and neutrons that make up the gold ion break into their constituent quarks creating a hot soup of particles made of quarks and gluons. These quarks quickly rejoin in a spray of mesons and hadrons that are observed in particle detectors. At extremely high temperatures QCD enters a new phase in which the quarks and gluons become a free gas. But at the temperatures accessible by RHIC the quarks a gluons are still strongly coupled and the plasma they form is difficult to describe theoretically because perturbative techniques do not work.

This strongly coupled quark-gluon plasma is modelled as a relativistic hydrodynamic system. The shape of the plasma that appears after a collision has to do with how squarely the gold ions hit each other. Consider the plane perpendicular to the collision axis where the ions are essentially circles. A head-on collision would create perfectly circular region filled with plasma. An off-centre collision would create an almond shaped plasma (imagine the intersection of two circles in a Venn diagram). By studying how the particles form from the plasma of the off-centre collisions it is possible to study the elliptic flow of this almond shaped plasma as

it dissipated and infer hydrodynamic properties of the plasma. These properties generally fall into two categories, static and dynamic.

The static properties are those concerned with the system in thermal equilibrium, such as the entropy density, and are handled well using lattice QCD. The dynamic properties of the system, such as shear viscosity, must be treated are not handled well using lattice QCD. Dynamic properties require the use of a Minkowski formalism, rather than the Euclidean formalism inherent to lattice QCD.

2.3.2 Argument for the Correspondence

The AdS/CFT correspondence we will discuss is the classic example between type IIB string theory on $AdS_5 \times S^5$, a 10-dimensional theory of gravity, and $\mathcal{N} = 4$ supersymmetric Yang–Mills (SYM), a 4-dimensional gauge theory. As we are interested in the correspondence as a tool we will focus calculations using the theory rather than the origin of the theory. We will give a short introduction here, but those readers interested in a comprehensive review should read [101]. This is different than the simple AdS/CFT correspondence we will develop in Chapter 7, but it should acquaint the reader rather well with the basic concept.

Crucial to the understanding of the correspondence is the identification of two very similar objects, Dp-branes and p-branes. The first formulations of string theory considered only excitations of string-like objects. A string can be open with loose ends wiggling at the speed of light, or closed, where the excitations are periodic. A renaissance occurred when it was realized that there existed membrane-like objects with spatial dimension p that open strings could end upon with Dirichlet boundary conditions, thus the moniker Dp-brane. A D0-branes is a single point, a D1-brane is a line, and so on. The D-brane is also a source for closed strings to propagate from.

The massless modes of the open strings that end on D-branes describe the oscillations of the brane and the gauge field that lives on it. The boson degrees of freedom of the Dp-brane can be described with a $p+1$-form gauge potential. An example is a D0-brane, a point particle, can be described by a one form gauge potential, which one might recognize as something similar to electromagnetism. As shown in figure 2.7, if there are N coincident Dp-branes a string has N places to start and end upon. It turns out that the low energy dynamics of such strings is described by a $U(N)$ gauge theory. These $p+1$-form gauge fields have $p+2$-form field strengths. In the presence of D-branes these field strengths contribute to the stress energy tensor, which curves the geometry of the spacetime. This is associated with closed string modes.

The other object we must consider is the p-brane. Initially p-branes were introduced as solitonic solutions to supergravity, the merger of supersymmetry and
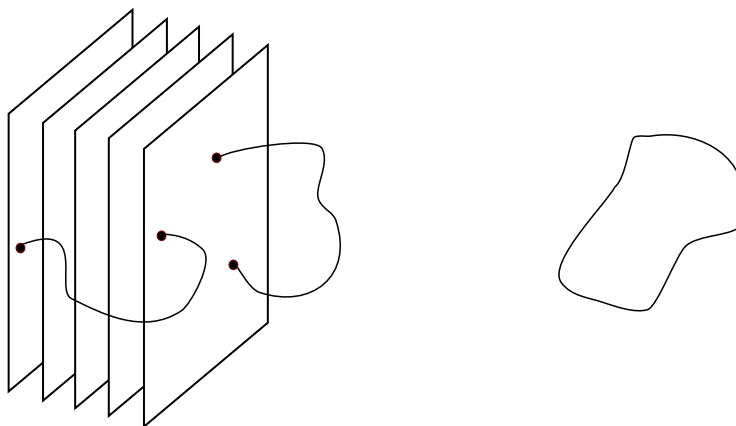
Figure 2.7: A stack of *N* D-branes with open strings attached to them. The ends of the open strings are confined to the D-branes. Away from the D-branes is a closed string drifting in spacetime.

general relativity. Supergravity is also the low energy limit of string theory. The *p*-brane solutions often have horizons where the singularities are not just points, but could be extended objects like lines. The solutions are often called black *p*-branes. It was found that a certain set of these solutions, called extremal solutions, are actually equivalent to the low energy limit of D-branes in string theory.

We are now at least conceptually prepared to discuss the correspondence that arises from 10-dimensional type IIB string theories. The II implies that the theory contains only closed string configurations. Open strings must be attached to D-branes. The B indicates that the theory contains $p =$ odd solutions and is a chiral theory. Consider the string theory formed by stacking *N* D3-branes on top of each other. Such a system can be thought of in two ways, one as a quantum field theory and one as a gravitational theory that curves space. On the field theory side there are two parameters—the number of colours *N* (i.e., the rank of the gauge group $SU(N)$) and the gauge coupling *g*. When the number of colours is large perturbation theory is controlled by the 't Hooft coupling $\lambda = g^2 N$. On the string theory side the parameters are the string coupling g_s, the string length $\ell_s = \sqrt{\alpha'}$, and the radius *R* of the AdS_5 space, which is proportional to $N^{1/4}$, where *N* is also the number of branes.

D-Branes as Gravity

We will start by considering the gravity side. A single Dp-brane has a mass

$$M_{D3} = \frac{1}{(2\pi)^3 \ell_s^4 g_s}, \tag{2.145}$$

which is inversely proportional to the string coupling. It is a non-perturbative object in the weak coupling limit. Vice-versa, at strong coupling Dp-branes become light and a large number, of order $N \sim 1/g_s$, are required to have a sizeable gravitational effect. The Dp-brane is also charged under a $(p+1)$-form potential with a charge Q equal to its tension resulting in the BPS bound being saturated.[2] In a supersymmetric theory saturation of the bound means that half of the supersymmetry is preserved and the other half is broken. Most importantly, it means that the configuration is stable. In our case this implies that we can stack an arbitrary number of Dp-branes and the configuration will remain stable. The mass of a black hole scales as $M \sim N^2 \sim 1/g_s^2$ so stacking N branes creates a background with a black brane equivalent of a black hole.

We can now look at these stacked D-branes from the low energy limit, which is a supergravity. The object we are interested in is a D3-brane, which is a $3+1$-dimensional plane in a $9+1$-dimensional space. We start by looking at the p-brane solution. The solution to the equations of motion of type IIB supergravity for a black 3-brane [102, 103] is the metric

$$ds^2 = H^{-1/2} \left(-f dt^2 + dx^2 + dy^2 + dz^2 \right) + H^{1/2} \left(f^{-1} dr^2 + r^2 \, d\Omega_5^2 \right) \tag{2.146}$$

where

$$H(r) = 1 + R^4/r^4 \quad \text{and} \quad f(r) = 1 - r_0^4/r^4, \tag{2.147}$$

and the Ramond–Ramond 5-form

$$F_{(5)} = -\frac{4R^2}{H^2 r^5} (R^4 + r_0^4)^{1/2} (1 + *) dt \wedge dx \wedge dy \wedge dz \wedge dr. \tag{2.148}$$

The Ramond–Ramond 5-form, $F_{(5)}$, is self dual and couples to the D3-brane, and the dilaton field Φ is constant. Since $g_s = e^\Phi$ we are free to choose any value for the string coupling. Note that we have chosen a solution that has an event horizon at r_0 and thus a black hole (black brane). The extremal solution when this becomes equivalent to a D3-brane is given by setting $r_0 = 0$. By comparing the low energy limit of the string theory with general relativity it is possible to rewrite the string parameters in terms of gravity parameters $16\pi G = (2\pi)^7 g_s^2 \ell_s^8$.

---

[2]The BPS bound is in general $M \geq Q$.
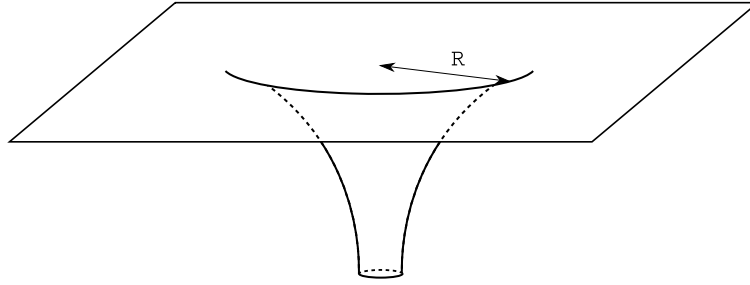
Figure 2.8: This is a representation of ds/dr, the radial part of extremal p-brane geometry (2.146), multiplied by -1 for aesthetics. The throat geometry at $r \ll R$ and the flat spacetime at $r \gg R$ are apparent.

An important aspect of our discussion is the asymptotic behaviour of the metric (2.146) as shown in Fig. 2.8. The radius of curvature defines two regions which will be important in the discussion. When $r \ll R$, known as the near horizon limit, the geometry has a funnel-like shape called a throat. Far away form the centre at $r \gg R$ the spacetime becomes flat. That there are these two separate regions, a throat and a flat space with type II supergravity, become important when establishing the correspondence.

The spacetime (2.146) above has an AMD mass, which is a quantity defined similarly to the charge found using Gauss's law in electrodynamics. It reflects the total contribution of the stress-energy to the curvature of the spacetime. The ADM for this spacetime has been calculated to be

$$M_{\mathrm{ADM}} = \frac{2\pi^3}{8\pi G_{10}} R^4 = \frac{R^4}{32\pi^4 g_s^2 \ell_s^8}, \tag{2.149}$$

where we have written M_{ADM} in terms of string parameters for comparison.

The final step is to associate the ADM mass of this black brane (black hole) with the mass obtained from the string tension of N D3-branes, $M_{\mathrm{D3}} = M_{\mathrm{ADM}}$. We get the relation

$$\frac{R^4}{\ell_s^4} = 4\pi N g_s, \tag{2.150}$$

where remember that $\ell_s^2 = \alpha'$. This is the first step in building the AdS/CFT dictionary between gravity variables and field theory variables.

D-Branes as Field Theory

We have considered low energy limit of string theory with N D3-branes. The description from this is that of a supergravity described by solitonic solutions called 3-branes. Another relationship between parameters comes from considering the gauge theory created by open strings attached to Dp-branes. The massless spectrum of the open strings on the Dp-brane is that of the maximally supersymmetric $(p+1)$-dimensional gauge theory with gauge group $SU(N)$ for N stacked branes. In the case of D3-branes the field theory is four-dimensional $\mathcal{N} = 4$ supersymmetric Yang-Mills (SYM), which is a gauge theory that has a gauge field, six real scalar fields, and four Weyl fermions [104]. The supersymmetric charge $\mathcal{N}$ the number of independent supersymmetries and is a indicator of how many superpartners a particle has. The most familiar is $\mathcal{N} = 1$ supersymmetry, which is considered a possible solution to the hierarchy problem in the Standard Model. For our discussion we will only be concerned with the gauge field of the theory. The particle content and supersymmetric aspects will be largely ignored in our discussion.

The effective action of the Dp-brane is the Dirac–Born–Infeld (DBI) action that, when expanded at first order in α', yields the usual Yang-Mills action in the large N limit plus other terms we will ignore,

$$S_{\mathrm{ND3}} \simeq \frac{1}{4\pi g_s} \mathrm{Tr} \int d^4x \left(\frac{1}{2}(F_{\mu\nu})^2 + \text{ dilation and fermion terms} \right). \qquad (2.151)$$

By identifying of the coefficient of the gauge kinetic term as the Yang-Mills action we get the gauge coupling of Yang-Mills in terms of string theory parameters,

$$g^2 = 4\pi g_s. \qquad (2.152)$$

In this picture the D-branes also act as a source of closed strings. These closed strings propagating away from the D-branes form a type IIB supergravity. We have established another way to look at string theory as N D3-branes stacked together to form a gauge theory, which also sources closed string that from a supergravity in a flat background far away from the branes.

Absorption in Two Pictures

We have discussed two pictures of D-branes. In one picture the open strings on the D-branes form a field theory while far away from the brane closed strings form a supergravity. In the other picture an extremal p-brane that is identified as the low energy counterpart to a Dp-brane, forms a black hole. Far away from this black hole the spacetime is flat and contains a supergravity. In fact, it is is the same

supergravity that appears in the both pictures: closed strings propagating in 10-dimensional flat spacetime. This comes about because of the equivalence between *p*-branes and D-branes.

An interesting aspect of these two pictures is that one can calculate the absorption cross section of both the black hole geometry, called the throat, and the N D3-branes from the surrounding 10-dimensional supergravity. We follow the discussion found in [105]. The absorption cross section from the throat geometry is done in a regime where stringy corrections are suppressed such that $R^4/\ell_s^4 = g_{YM}^2 N \gg 1$ and the theory looks like a classical gravity theory. The cross section obtained from this is

$$\sigma_{\text{throat}} = \frac{\pi^4}{8} \omega^3 R^8 \,. \tag{2.153}$$

The cross section from of the stack of D-branes is calculated by using DBI action from earlier and doing perturbative dilaton-photon interactions in the 't Hooft coupling, which implies $\lambda = g_{YM}^2 N \ll 1$. This process gives

$$\sigma_{\text{ND3}} = 2\pi^6 g_s^2 N^2 \ell_s^8 \omega^3 \,. \tag{2.154}$$

Using the string relationships derived earlier it can be shown that these absorption cross sections are identical. Though the details of calculating these cross sections are beyond the scope of this thesis, one aspect is important. Each of these cross sections was calculated in different regimes of the 't Hooft parameter. The supergravity result was calculated in the supergravity approximation at strong 't Hooft coupling The D-brane calculation was done at weak 't Hooft coupling. This curiosity provided the motivation for the conjecture of the duality.

The Decoupling Limit

Maldacena took the similar cross sections as evidence that the theories where linked in some way and proposed the decoupling limit. If one takes the R, $\alpha' \to 0$ while keeping the 't Hooft coupling $\lambda = R^4/\ell_s^4 = 4\pi g_s N = \text{constant}$, the absorption cross sections go to zero $\sigma \to 0$.

Each of our two pictures now has two decoupled theories. From the point of view of the open strings on N D3-branes we have a four-dimensional $\mathcal{N} = 4$ SYM field theory decoupled from closed strings away from the D-branes that form a type IIB supergravity. In the supergravity picture there exists a throat geometry containing a black hole and closed strings that is decoupled from a supergravity in flat space far away from the black hole. In this limit the theory of gravity in the throat becomes

$$ds^2 = \frac{r^2}{R^2}(-dt^2 + dx^2 + dy^2 + dz^2) + \frac{R^2}{r^2} dr^2 + R^2 d\Omega_5^2 \,. \tag{2.155}$$
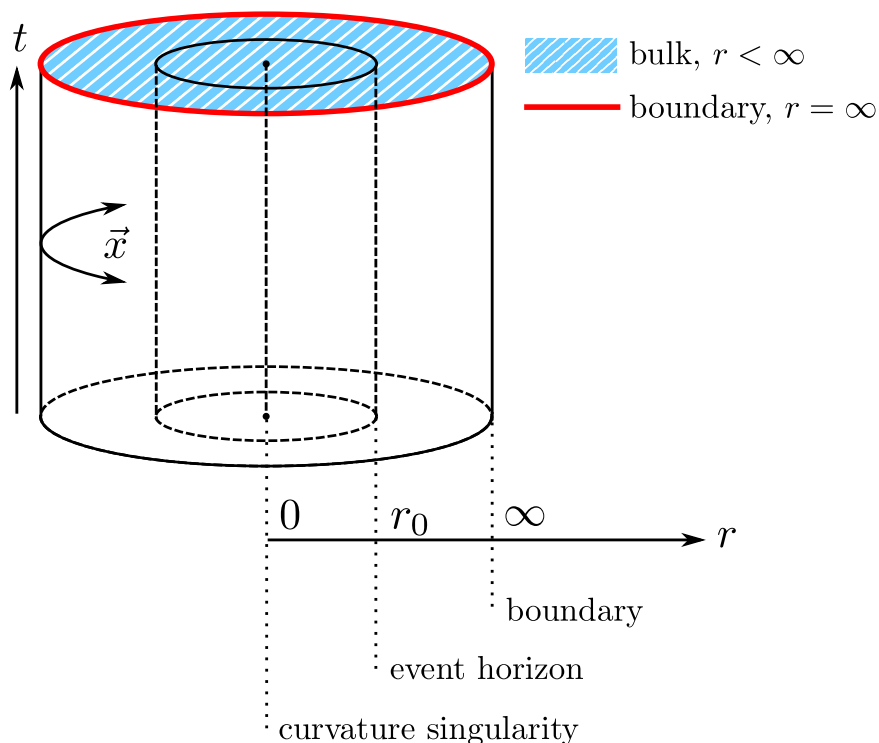
Figure 2.9: An illustration of where $\mathcal{N} = 4$ SYM lives on AdS_5 space. The 4 dimensions of the gauge theory $(t, \mathbf{x})$ live on the boundary of the AdS_5 space at $r = \infty$.

which is the geometry of 5 dimension Anti de-Sitter space crossed with the 5 sphere, $AdS_5 \times S^5$.

The two pictures share a decoupled theory, that of type IIB supergravity. It is natural to identify the other two theories. This leads to the conjecture that four-dimensional $\mathcal{N} = 4$ supersymmetric Yang-Mills is equal to (dual to) five-dimensional AdS_5 spacetime. The first thing that one might notice about such a conjecture is that the two theories have a different number of dimensions. In terms of the correspondence the gauge theory lives on the 4-dimensional boundary, located at $r = \infty$, of the 5-dimensional AdS_5 space. This relationship is illustrated in Figure 2.9. The gravity theory dual to this field theory extends into the bulk of the AdS_5 space where $r < \infty$.

For the gravitational description of string theory to be valid we require for the

Table 2.1: Summary of the corresponding elements that appear in our duality.

	bulk	**boundary**
AdS/CFT	type IIB string theory on asymptotically AdS$_5 \times$S^5	$\mathcal{N} = 4$ SYM on S$^3 \times \mathbb{R}^1$ or with a Poincaré patch $\mathbb{R}^3 \times \mathbb{R}^1$
effective description	Einstein equation with cosmological constant	relativistic fluid dynamics
known static solutions	black hole or black brane in AdS	static configuration of a perfect fluid
perturbation	non-uniformly evolving black branes	dissipative fluid flow

two dimensionless string parameters that

$$\frac{R}{l_s} = \frac{R}{\sqrt{\alpha'}} \gg 1 \quad \text{and} \quad g_s \ll 1, \tag{2.156}$$

where the ratio between the curvature scale for the string background R and the string length l_s to be large (to suppress stringy effects), and simultaneously we assume the string coupling to be small (to further suppress quantum effects).

The equivalent of the gravitational limit in terms of fundamental parameters for the conformal field theory, the 't Hooft coupling λ and the Yang–Mills coupling g, is given by the correspondence

$$\left\{ \frac{R^2}{\ell_s^2}, 4\pi g_s \right\} \quad \rightleftharpoons \quad \left\{ \lambda = g^2 N, g^2 \right\}. \tag{2.157}$$

Therefore the suppression of stringy and quantum effects on the boundary requires that

$$\lambda \gg 1 \quad \text{and} \quad \frac{\lambda}{N} \ll 1, \tag{2.158}$$

and that both $\lambda \to \infty$ and $N \to \infty$. This is the 't Hooft limit with $\lambda \to \infty$. We can see that holding λ constant and varying N causes $4\pi g_s = g^2$ to vary inversely. This is where the advantage gained by the correspondence. In the large N limit, when λ is large, the gauge theory is strongly coupled. At the same time g_s is small and the stringiness is suppressed such that we can use the low energy approximation, type IIB supergravity, to do calculations.

The fundamental ideas behind the conjectured correspondence are outlined in Table 2.1. We will now move on to discuss some of the details of the dictionary between CFT operators on the boundary and field configurations in the bulk.

2.3.3 The Operator-Field Relationship

Now that the conjecture has been established we can see how it might be useful in calculating properties of matter. It would be particularly useful to be able to use the gravity theory to somehow calculate two-point functions in field theory. This requires a relationship between operators and field theory and some object (fields) in the gravity theory. The original operator-field relationship was made using the Euclidean formalism [106, 107]. The gauge-gravity correspondence states that a retarded two-point correlation function in gauge theory can be calculated by taking derivatives of the generating functional of its dual gravity theory. On the gauge side the sources $J(x)$ are coupled with operators $O(x)$. On the gravity side there is a field ϕ that is dual to the operator $O(x)$. The correspondence says that the expectation value of the operator is equated to the value the field on the gravity side takes on the boundary of the theory. Technically this means that the derivatives on the generating functional that are usually taken with respect to the source $J(x)$ and now taken with respect to $\phi_0 = \phi(r = \infty)$.

This idea can be written more formally as

$$Z_{\text{gauge}}[J(x)O(x)] = Z_{\text{gravity}}[\phi]\bigg|_{\phi_0 \to J}, \qquad (2.159)$$

where Z_{gauge} and Z_{gravity} are the partition functions of the dual gauge and gravity theories. Now it is clear that when we find gauge field correlation functions by taking functional derivatives with respect to the sources J that couple to our desired operator, that on the gravity side we actually take these derivatives with respect to the scalar field at the boundary ϕ_0. This is a non-trivial statement, and it is true that there is a one-one mapping between sources J and boundary conditions of the scalar field ϕ_0.

For example, to calculate two-point correlation functions one takes two derivatives of the generating function. The correspondence tells us to take two derivatives of the generating function on the gravity side,

$$G(x-y) = -i\langle TO(x)O(y)\rangle = \frac{\delta^2}{\delta J(x)\delta J(y)}Z_{\text{gravity}}[\phi]\bigg|_{\phi_0 \to J}. \qquad (2.160)$$

Because there are only two derivatives with respect to ϕ_0 we are only required to consider the AdS action up to the quadratic order when looking for two point

functions on the CFT side. After equating the sources and the field at the boundary, J is still set to zero, as in the regular method of finding correlation functions, and any higher terms in the action will vanish.

Discussion of the quark-gluon plasma often requires a Minkowski formalism [99, 108, 109]. It might not be clear why a Minkowski formalism is needed when the Euclidean one is so successful, especially when the Euclidean results can be analytically continued by Wick rotation to get the Minkowski result. The method of Wick rotating only works in systems in thermal equilibrium. The Euclidean method, though generally easier to work with, runs in to a problem when we want to calculate quantities that are slightly out of equilibrium. To calculate non-equilibrium quantities retarded and advanced Green's functions are required. To find these Green's functions it is necessary to take the low frequency limit. In the Euclidean formalism the Euclidean time becomes periodic in the temperature. When the Euclidean Green's function is Wick rotated back to make a retarded or advanced Green's function, only discrete frequencies, the Matsubara frequencies, will survive. The lowest of these frequencies is already $2\pi T$, too large to be useful, so it is necessary to calculate the retarded Green's function directly from a Minkowski formalism. Working in the Minkowski formalism requires a different definition of the Green's function to ensure that the retarded Green's function is imaginary.

2.3.4 Calculating Thermal Properties from Gravity

We will provide a quick sample calculation using the correspondence to give the reader a feel for the technique. We will follow the work done in [99, 100, 108, 109]. To calculate thermal properties it is necessary to look at the non-extremal black 3-brane metric is a solution to the type IIb equations of motion. As discussed, at low energy this has the form

$$ds^2 = H^{-1/2}\left(-hdt^2 + dx^2 + dy^2 + dz^2\right) + H^{1/2}\left(h^{-1}dr^2 + r^2 d\Omega_5^2\right), \quad (2.161)$$

where $H(r) = 1 + R^4/r^4$ and $h(r) = 1 - r_0^4/r^4$. This solution is slightly different that the earlier one in that the event horizon explicitly appears in the metric at $r = r_0$ as a measure of its non-extremalness. As we will determine later a nonzero value for r_0 is associated with the Hawking temperature of the system, which through the correspondence is equal to the temperature of the field theory. A non-extremal 3-brane is dual to a finite temperature field theory. As discussed, for the AdS/CFT correspondence to work we need to take the near horizon limit of this metric, $r \ll R$, which technically amounts to "dropping the 1" in $H(r)$. Dropping the 1 yields

$$ds^2 = \frac{r^2}{R^2}\left(-h(r)dt^2 + dx^2 + dy^2 + dz^2\right) + \frac{R^2}{r^2 h(r)}dr^2 + R^2 d\Omega_5^2. \quad (2.162)$$

As discussed earlier this kind of metric gives rise to actions for the scalar field ϕ of the form

$$S = K \int d^4x dr \sqrt{-g} g^{\mu\nu} \partial_\mu \phi \partial_\nu \phi + \ldots, \qquad (2.163)$$

where the coefficient $K = -\pi^3 R^5/4\kappa_{10}^2$ comes from the normalization of the dilation field. The constant $\kappa_{10} = \sqrt{8\pi G}$ is the ten-dimensional gravitational constant. Using the parameter matching discussed in the introduction it can be rewritten as $\kappa_{10} = 2\pi^2 \sqrt{\pi} R^4/N$. Substituting this in gives $K = N^2/16\pi^2 R^3$.

Entropy Density

Here we can get our first result from the AdS/CFT correspondence. The Hawking temperature is determined by the even nearer horizon behaviour which is found by Taylor expanding around $r^2 h(r)$ around r_0 to find $r^2 h(r) \simeq 4r_0(r - r_0)$. Ignoring the spherical part of the metric and focusing on the t and r part we get

$$ds^2 = -\frac{4r_0}{R^2}(r - r_0)dt^2 + \frac{R^2}{4r_0(r - r_0)}dr^2. \qquad (2.164)$$

We can change coordinates $r = r_0 + \rho^2/r_0$ to make the metric non-singular,

$$ds^2 = \frac{R^2}{r_0}\left(d\rho - \frac{4r_0^2}{R^4}\rho^2 dt^2\right). \qquad (2.165)$$

Performing a Wick rotation $t \to i\tau$ and letting $\theta = 2r_0 R^{-2}\tau$ it's clear that we're dealing with a metric that is proportional to the flat metric expressed in polar coordinates,

$$ds^2 = \frac{R^2}{r_0}(d\rho + \rho^2 d\theta^2). \qquad (2.166)$$

We want to interpret the black hole horizon as a regular origin where locally we are unable to detect any curvature, unlike if we had a conical singularity. To avoid a conical singularity we make it flat near the origin by identifying $\theta = 0$ with $\theta = 2\pi$ such that $\theta \sim \theta + 2\pi$. The Euclidean time τ in thermal field theory is also periodic, but in the inverse temperature $\tau \sim \tau + 1/T$. So, going around the origin once gives us the relation

$$2\pi = \frac{2r_0}{R^2}\frac{1}{T} \Rightarrow T = \frac{r_0}{\pi R^2}, \qquad (2.167)$$

which defines the Hawking temperature. It is the Hawking temperature on the gravity side that we associate with finite temperature in $\mathcal{N} = 4$ $SU(N)$ SYM theory.

Calculating the entropy of the black hole using the Bekenstein-Hawking formula we can find the entropy in $\mathcal{N}=4$ SYM by converting the parameters according to the AdS/CFT prescription outlined in the introduction. The horizon lies at $t =$ constant and $r = r_0$ or $u = 1$. The area of this surface is

$$A = \int d^3x d^5\Omega\sqrt{g}. \qquad (2.168)$$

The determinant of the metric is $\sqrt{g} = r_0^3/R^3$ and the area of the five sphere is $\pi^3 R^5$ and the $V_3 = \int d^3x$ is an infinite spatial volume leaving

$$A = \pi^3 r_0^3 R^2. \qquad (2.169)$$

We can rewrite Newton's constant as

$$G = \frac{\pi^4 R^8}{2N^2}, \qquad (2.170)$$

so the entropy becomes

$$\begin{aligned} S = \frac{A}{4G} &= \frac{\pi^2 V_3 N^2}{2}\left(\frac{r_0}{\pi R^2}\right)^3 \qquad &(2.171)\\ &= \frac{\pi^2}{2}V_3 N^2 T^3, \qquad &(2.172) \end{aligned}$$

where we have used the formula for the Hawking temperature and V_3 is the three-dimensional volume. This result is $3/4$ the value of the entropy density found in the weak coupling regime where the 't Hooft coupling is zero . A difference is to be expected when dealing with a strongly coupled plasma. What is very interesting is that similar deviations are found in lattice QCD calculations. For those interested in further reading I suggest [103] and [110]. This is a static property though and we did not need to use the Minkowski formalism. We still haven't calculated a dynamic property.

Shear Viscosity

To calculate a dynamic property we want to use the Minkowski formalism. We follow the work of [99, 100, 108, 109] To do this we still want to work in the near horizon limit ("dropping the 1"). The first step is to the coordinate change $u = r_0^2/r^2$,

$$ds^2 = \frac{(\pi T R)^2}{u}(-h(u)dt^2 + dx^2 + dy^2 + dz^2) + \frac{R^2}{4u^2 h(u)}du^2 + R^2 d\Omega_5^2, \quad (2.173)$$

where we have used the Hawking temperature to rewrite the metric in terms of thermal quantities. We see that the event horizon occurs at $u = 1$ and spatial infinity, the boundary of the space, occurs at $u = 0$. Based on the Minkowski prescription we want to find low frequency solutions to the equations of motion of this space. This will give us the what we need to calculate the Green's function on the CFT side. As found in Appendix A.1 the equation of motion is

$$\partial_\mu \sqrt{-g}(g^{\mu\nu}\partial_\nu)\phi = 0, \tag{2.174}$$

where μ, ν run over all coordinates.

The AdS/CFT correspondence says that the operators in the CFT side live at the boundary of the gravity theory. To find a solution we need to impose boundary conditions on the gravity side. We use separation of variables to write the solution of the equation of motion with the boundary condition $\phi(k, r = 0) = \phi_0(k)$ as

$$\phi(k, r) = f_k(r)\phi_0(k), \tag{2.175}$$

where $f_k(r)$ is the called the mode function.

To proceed two results are needed. The quark-gluon plasma can be thought of as a relativistic hydrodynamic system. The shear viscosity η is a hydrodynamic property that can be described by the Kubo formula discussed in appendix A.2,

$$\eta = -\lim_{\omega \to 0} \frac{1}{\omega} \text{Im } G^R(k, \omega). \tag{2.176}$$

The second result is the form the Green's function takes in the Minkowski field-operator relationship (2.160). The details from deriving the relationship are given in appendix A.1. The relationship itself is

$$G^R(k) = -2F(k, r)\Big|_{r_B}. \tag{2.177}$$

where,

$$\begin{aligned} F(r,k) &= K\sqrt{-g}g^{rr}f_k^*(r)\partial_r f_k(r) \\ &= F(r,-k)^*, \end{aligned} \tag{2.178}$$

We can now calculate a dynamic quantity of a strongly coupled hydrodynamic system using the AdS/CFT correspondence. Note that we discarded contributions to (2.177) from the horizon $r = r_H$ and we will consistently do so throughout the calculation.

Using the black three-brane metric 2.173 with the equation of motion 2.174 with these boundary conditions we get the mode equation

$$f_k'' - \frac{1+u^2}{uh(u)}f_k' + \frac{\mathfrak{w}^2}{uh(u)^2}f_k - \frac{\mathfrak{k}^2}{uh(u)}f_k = 0, \qquad (2.179)$$

where prime is a derivative with respect to u and we have defined

$$\mathfrak{w} = \frac{\omega}{2\pi T} \text{ and } \mathfrak{k} = \frac{k}{2\pi T}. \qquad (2.180)$$

The mode equation is second order differential equation with a singular point at $u = 1$. When solving such equations the first thing we want to do is find the behaviour of the singularity. If we substitute

$$f_k = (1-u^2)^\alpha H(u) \qquad (2.181)$$

into the mode equation we find that has α has two possible values $\alpha = \pm i\mathfrak{w}/2$. This is unlike the Euclidean case were it only takes one value. We are left with a differential equation for $H(u)$ which is impossible to solve analytically. A power series representation for $H(u)$ in $\mathfrak{w}$ and $\mathfrak{k}^2$ can be found perturbatively,

$$H(u) = 1 + \frac{i\mathfrak{w}}{2}\ln\frac{2u^2}{1+u} + \mathfrak{k}^2\ln\frac{1+u}{2u} + \dots. \qquad (2.182)$$

We will make a low frequency $\omega \ll T$ low momentum $k \ll T$ approximation and disregard everything but the first term, $H(u) \approx 1$.

We now have to make an interesting decision. Our solution for the wave function f_k has two possible values and we must choose which is correct. The two solutions can be written in form more conducive to our argument by doing the coordinate transformation

$$r_* = \frac{\ln(1-u)}{4\pi T}. \qquad (2.183)$$

Restoring the phase $e^{-i\omega t}$ yields

$$e^{-i\omega t}f_k = e^{-i\omega(t+r_*)}, \qquad (2.184)$$
$$e^{-i\omega t}f_k^* = e^{i\omega(t-r_*)}, \qquad (2.185)$$

which take the form of plane wave solutions. The horizon lies lies at $r_* = 0$ of the new coordinate system. The first solution corresponds to a wave moving toward the horizon, an incoming wave, and the second solution is a wave moving away from the horizon. The choice of which solution to discard is simply motivated by the fact that nothing should leave the horizon. This leaves us with one solution,

$$f_k(u) = (1-u^2)^{-i\mathfrak{w}/2}. \qquad (2.186)$$

Changing variables back to $u = r_0^2/r^2$ we get

$$f_k(r) = \left(1 - \frac{r_0^4}{r^4}\right)^{-i\mathfrak{w}/2} = h(r)^{-i\mathfrak{w}/2}. \tag{2.187}$$

Using the incoming wave solution for $f_k(r)$, $-K = N^2/16\pi^2 R^3$, $\sqrt{-g} = r^3/R^3$ for the determinant of the metric, and $g^{rr} = r^2 h(r)/R^2$ we find that

$$K\sqrt{-g}g^{rr} = -\frac{N^2 r^5 h(r)}{16\pi^2 R^8}, \tag{2.188}$$

and the kernel (2.178,A.8) of our action becomes

$$F(r) = -\frac{N^2 r^5 h(r)}{16\pi^2 R^8} f_{-k}(r)\partial_r f_k(r). \tag{2.189}$$

Recognizing that $f_{-k} = f_k^*$ and substituting in the incoming wave solution we find that

$$F(r) = i\mathfrak{w}\frac{\pi N^2}{16T}\left(\frac{r_0}{\pi R^2}\right)^4 \tag{2.190}$$

$$= i\mathfrak{w}\frac{\pi N^2 T^3}{16}. \tag{2.191}$$

We now use the conjectured relationship (2.177), where as discussed we have thrown out the contribution form the horizon, to calculate the Green's function,

$$G^{\mathrm{R}}(k) = -2F(k,r)\bigg|_{r=\infty} \tag{2.192}$$

$$= -i\mathfrak{w}\frac{\pi N^2 T^3}{8}. \tag{2.193}$$

We use the Kubo formula for shear viscosity (2.176) to get

$$\eta = \frac{\pi N^2 T^3}{8}, \tag{2.194}$$

the shear viscosity of $\mathcal{N} = 4$ SYM, where N is the number of colours and T is the temperature.

The Shear Viscosity to Entropy Density Ratio

We have calculated two thermal properties in $\mathcal{N} = 4$ SYM using the AdS/CFT correspondence - the entropy (2.171) and the viscosity (2.194). If we write equation (2.171) in terms of the entropy density $s = S/V_3$ then the entropy and viscosity have, up to a constant, identical forms. The ratio of the two is

$$\frac{\eta}{s} = \frac{1}{4\pi} = \frac{\hbar}{4\pi k_B} \text{ (with dimensionality restored)}. \tag{2.195}$$

This ratio has been shown to be true for all thermal field theories in a regime to be described by gravity duals. Corrections to this have been calculated in [111] for $\mathcal{N} = 4$ SYM and are shown to be positive. It is natural then to conjecture a bound,

$$\frac{\eta}{s} \geq \frac{1}{4\pi}. \tag{2.196}$$

This implies that a fluid with a finite entropy density can never truly reach zero viscosity.

The lower bound is quite small compared to the most substances. For example water has $\eta/s \approx 380/4\pi$. One place to look where the bound should break down is in superfluids. Superfluids flow without dissipation, which implies zero viscosity. However, any superfluid describes by the Landau effective theory actually has a shear viscosity, which is the property being bounded in the conjecture. For superfluid helium the shear viscosity has been measured in a torsion-pendulum experiment and the ratio η/s remains at least 8.8 times larger than the minimum value of $\hbar/4\pi k_B \approx 6.08 \times 10^{-13}$ Ks for all ranges of temperatures and pressures. Numerical models indicate that the shear viscosity quark-gluon plasma at RHIC is very close to, but still above this bound. Further discussion on universality can be found in [112], [100] and [113].

Chapter 3

Topological Currents in Dense Matter

We are now ready to discuss the central ideas of the thesis. The goal of this section is to formally introduce topological vector currents and discuss what is required for these currents to appear in matter. Our motivation comes from the possible application of topological currents to the physics of neutron stars. In previous work it [8] was suggested that the presence of topological currents could cause the formation of a type-I superconductor in the neutron star. We will see that the neutron star is an ideal system for the current. Critical to the topological vector current is the existence of parity violation in the system. The weak interaction, which strongly violates parity, is a natural source for the required asymmetry and is where we focus our attention.

We will start with two derivations, one using the chiral anomaly and one using index theorems, which will illuminate two important aspects of the current. First, boundary conditions of the system are important for manifesting the current in a physical system. Second, the current can be understood on a microscopic level by counting the particles that contribute to the current. We will see that both of these concepts are critical for finding a reasonable estimate for the current in dense matter and how a current would flow in the neutron star. Another aspect of the current illustrated by both of these derivations is that the current has a topological character and that the phenomenon is quite robust. The interior of a neutron star is hostile and we will go through great lengths to describe how the current can survive in the star without being washed out.

In nuclear matter we will assume that electrons are the only reasonable charge carrier because all other charged particles in the star are too heavy. The particles in a neutron star attain equilibrium through the weak interaction, which creates predominantly left-handed particles. This creates an intrinsic difference in the number of left-handed and right-handed electrons. In an infinite system this imbalance would disappear—the average helicity of the electrons would be washed out due to the inverse weak $\mathscr{P}$-violating processes. The key is that the neutron star is a finite system and electrons are removed from the star by the current before they can decay. The asymmetry that created the current is allowed to propagate to the

surface and not get washed out.[1]

This topological current corresponds to the lowest energy state in the thermo-dynamic equilibrium when $\mu_l \neq \mu_r$ is held fixed. In reality there is a tendency for μ_l and μ_r to equilibrate though weak interactions; however, due to the finite size of the system a complete equilibrium cannot be achieved. This is analogous to how neutrinos in cold stars can leave the system without further interactions, but unlike with neutrinos the electron chemical potential does not drop to zero. The induced current only remains non-dissipating when the system is degenerate, $\mu \gg T$. In the star's crust this condition becomes invalid, the current will become dissipative and the trapped electrons will return into the system.

In the following subsections we will discuss the structure and processes of dense matter, formally derive the topological current, and discuss in greater detail how the magnitude of the current can be estimated.

3.1 Topological Vector Currents

The purpose of this section is to explicitly derive the form of the vector current. We will do this two ways: one using the anomaly and one using index theorems. The methods compliment our understanding of the current. The derivation using anomalies approaches the current from a effective field theory point of view using fictitious fields to generate the necessary terms. The index theorem derivation approaches the current from microscopic point of view, counting each mode of the Dirac equation that contributes. Even with these approaches are quite different they are linked by the intimate relationship between anomalies and indexes.

3.1.1 Derivation Using the Axial Anomaly

The first derivation will involve effective action created by considering a fictitious axial field $A^\mu = (\mu_5, 0, 0, 0)$, where $2\mu_5 = \mu_L - \mu_R$ is the axial chemical potential and a regular $U(1)$ vector field V^μ. In subsection 2.1.3 we used the path integral approach to show that the axial current becomes anomalous in the presence of a regular $U(1)$ vector field. We will use the same mechanics to show that the presence of an axial field causes the vector current to become anomalous.

---

[1]Here and in what follows we neglect all QED re-scattering effects, which are much stronger than weak interactions but they are $\mathscr{P}$-even and, therefore, cannot wash out the produced asymmetry. This is discussed in detail in Section 3.2. Because of the large magnetic field the electron only travels in the direction of the magnetic field while the motion in transverse directions confined to Landau levels. The term "mean free path" in this paper implies the weakly interacting $\mathscr{P}$-odd "mean free path" when a produced asymmetry can be washed out.

We consider the same functional integral we did earlier in equation (2.56),

$$Z = \int \mathscr{D}\psi \mathscr{D}\overline{\psi} \, \exp\left[i \int d^4 x \overline{\psi}(i\slashed{D})\psi \right], \tag{3.1}$$

but now we consider a Dirac operator that has both axial and vector fields,

$$D_\mu = \partial_\mu + ie\mathscr{A}_\mu(x), \tag{3.2}$$

$$\mathscr{A}_\mu(x) = V_\mu + \gamma^5 A_\mu. \tag{3.3}$$

We are interested in the vector Noether current, so we apply a global $U(1)$ transformation $\psi(x) \to e^{i\alpha(x)}\psi(x)$. Being a global symmetry an anomaly is not a threat, but is a legitimate part of the theory. This is a symmetry of the Lagrangian so we are left with just terms that are derivatives of α, which can then be written as

$$\int d^4 x \overline{\psi}'(i\slashed{D})\psi' = \int d^4 x \left[\overline{\psi}(i\slashed{D})\psi + \alpha(x)\partial_\mu(\overline{\psi}\gamma^\mu\psi) \right]. \tag{3.4}$$

One arrives at the statement that the vector current is conserved. If the fictitious axial field were set to $A_\mu = 0$ then there would be no quantum corrections to this. But in our derivation we are forcing axial field to be nonzero and there are contributions from the measure of the path integral, just as the axial current gets corrections vector field contributions from the measure.

If we apply the same argument we did for the axial current by considering the contribution of the measure we find the we find that the functional integral becomes

$$Z = \int \mathscr{D}\psi \mathscr{D}\overline{\psi} \exp\left[i \int d^4 x \left(\overline{\psi}(i\slashed{D})\psi + \alpha(x)\left\{ \partial_\mu j^\mu - 2K(x) \right\} \right) \right] \tag{3.5}$$

where we used $j^\mu = \overline{\psi}\gamma^\mu\psi$ and

$$K(x) = \lim_{M\to\infty} \mathrm{tr} \sum_n \phi_n^\dagger(x) e^{(i\slashed{D})^2/M^2} \phi_n(x). \tag{3.6}$$

Note that we have already inserted the regulator. Forcing the $\alpha(x)$ term to vanish gives us the anomaly associated with the vector current in the presence of an axial field,

$$\partial_\mu j^\mu = 2K(x). \tag{3.7}$$

The calculation of $K(x)$ is almost identical to before. The Dirac operator becomes

$$(i\slashed{D})^2 = -D^2 + 2i\left(\frac{i}{4}[\gamma^\mu, \gamma^\nu] \right) D_\mu D_\nu, \tag{3.8}$$

$$= -D^2 + i\left(\frac{i}{4}[\gamma^\mu, \gamma^\nu] \right) (V_{\mu\nu} + \gamma^5 A_{\mu\nu}), \tag{3.9}$$

which we can see has picked up an axial tensor component compared to equation (2.89). The calculation from this point is identical to the case with just the vector field. The critical moment comes when we reach

$$K(x) = -i\frac{1}{4 \cdot 32\pi^2}\text{tr}\left[\gamma^\mu\gamma^\nu\gamma^\rho\gamma^\sigma(V_{\mu\nu} + \gamma^5 A_{\mu\nu})(V_{\rho\sigma} + \gamma^5 A_{\rho\sigma})\right], \qquad (3.10)$$

as compared to (2.94). The only terms that contribute are the mixed terms that contain a single γ^5. The other terms are antisymmetric objects contracted with symmetric ones and thus they vanish. We are left with

$$K = -\frac{1}{16\pi^2}\varepsilon^{\mu\nu\rho\sigma}A_{\mu\nu}V_{\rho\sigma}. \qquad (3.11)$$

The divergence of the vector current is then

$$\partial_\mu j^\mu = -\frac{1}{8\pi^2}\varepsilon^{\mu\nu\rho\sigma}A_{\mu\nu}V_{\rho\sigma}. \qquad (3.12)$$

We have shown that the vector current in the presence of an axial field is anomalous. If we remove the background axial field by setting $A_{\mu\nu} = 0$ we indeed reproduce the canonical conservation of the vector current.

There are many ways we can proceed to get the current from this. One is to appeal to chiral symmetry breaking and invoke a goldstone boson to write an effective Lagrangian. We will instead consider a region in which the axial chemical potential that is the zeroth component of our fictitious field $A_0 = \mu_5$ is confined to a domain R where inside $A_0 = \mu_5$ and outside the domain $A_0 = 0$. This is illustrated in Fig. 3.1[2]. The existence of this domain wall is a characteristic feature of the current that will be the focus of this thesis. To find the current in the real world one must find in what situations these domain walls appear. Note that this is the exact situation we will apply later to finding the current in neutron stars.

Proceeding with our pillbox derivation of the current we assume that the vector charge density is zero and choose $V_{\mu\nu}$ such that there is only background magnetic field $\vec{B}$ and no electric field. The expression for the current (3.12) then takes the form

$$\nabla \cdot \vec{j} = \frac{4}{8\pi^2}\nabla \cdot (A_0\vec{B}), \qquad (3.13)$$

which vanishes inside and outside R. But, integrating over a small pillbox on the boundary of R inside the domain we get

$$\vec{j} \cdot d\vec{S} = \frac{1}{2\pi^2}\mu_5\vec{B} \cdot d\vec{S}. \qquad (3.14)$$

---

[2]This figure is modelled after Fig. 4 in [114].
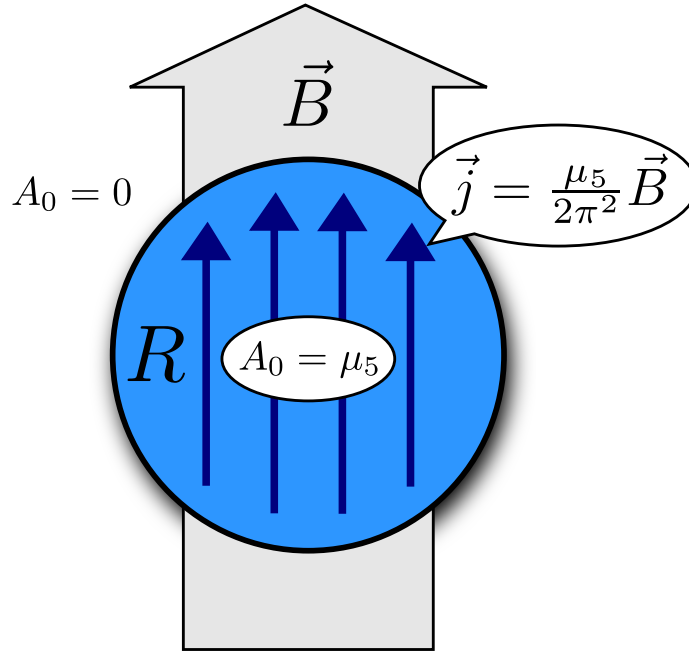
Figure 3.1: Outside the domain R the temporal component of the fictitious axial field A_0 is zero. Inside R we set $A_0 = \mu_5$. The change in A_0 across the boundary of R causes a current to be induced within R that is proportional to the background field $\vec{B}$.

This is the topological vector current running through a surface S inside a region with axial charge μ_5. Using the definition for flux $\Phi = \int \vec{B} \cdot d\vec{S}$, the total current $J = \int \vec{j} \cdot d\vec{S}$, and the axial chemical potential $2\mu_5 = \mu_l - \mu_r$ we find the total current,

$$ J_V = \frac{1}{(2\pi)^2}(\mu_l - \mu_r)\Phi, \tag{3.15} $$

which is the same as that given by 1.2. This concludes our derivation of (1.2) using anomalies directly. We will now derive the same current using the index theorem.

3.1.2 Derivation Using the Index Theorem

We now move to a microscopic derivation of the axial current. The previous derivation shows the intimate connection between the current and anomalies, but is somewhat nebulous with its use of a fictitious axial field. We start by considering the

Lagrangian

$$\mathcal{L} = \overline{\psi}i(\partial_\mu + ieA_\mu)\psi - m\overline{\psi}\psi + \mu\overline{\psi}\gamma^0\psi. \tag{3.16}$$

which describes a single light fermion ψ of mass m with a background electromagnetic field A_μ, at a chemical potential μ. The Dirac Hamiltonian in the presence of a magnetic field is given by

$$H = -i(\partial_i - eA_i)\gamma^0\gamma^i + m\gamma^0. \tag{3.17}$$

We are interested in calculating the expectation value of the vector current $J_v^3 = \int d^2x \langle j_v^3(x) \rangle$ in the presence of a magnetic field pointing z-direction. The current is defined as $j_v^3(x) = \overline{\psi}\gamma^3\psi(x)$, where ψ is a Dirac spinor. Ultimately we are interested in the left and right-handed modes and write the current in the Weyl representation,

$$j_v^3 = \psi_l^\dagger \sigma^3 \psi_l - \psi_r^\dagger \sigma^3 \psi_r. \tag{3.18}$$

The Dirac equation in a magnetic field with potential $\vec{A}$ can be written as

$$-H_r\psi_l + m\psi_r = E\psi_l, \tag{3.19}$$

$$m\psi_l + H_r\psi_r = E\psi_r, \tag{3.20}$$

where $H_r = (-i\partial_i + eA_i)\sigma^i$. This means that $\psi_l = \frac{1}{m}(E - H_r)\psi_r$, which substituting back leads us to

$$(H_r^2 + m^2)\psi_r = E^2\psi_r. \tag{3.21}$$

The eigenvalues of H_r acting on ψ_r are labelled ε, hence the Dirac equation has two solutions that have energies $E_\pm = \pm\sqrt{\varepsilon^2 + m^2}$. The Dirac spinor can be written entirely in terms of the right-handed spinor and its eigenvalues,

$$\psi_\pm = \begin{pmatrix} \psi_l \\ \psi_r \end{pmatrix}_\pm = \frac{1}{[4(m^2+\varepsilon^2)]^{1/4}} \begin{pmatrix} \pm[(m^2+\varepsilon^2)^{1/2} \mp \varepsilon]^{1/2} \\ [(m^2+\varepsilon^2)^{1/2} \pm \varepsilon]^{1/2} \end{pmatrix} \psi_r \tag{3.22}$$

We further break up the operator H_r into transverse and longitudinal components $H_r = p_3\sigma^3 + H_\perp$, where p_3 are momentum eigenstates along the magnetic field, $-i\partial_3\psi_r = p_3\psi_r$, and $H_\perp = (-i\partial_i + eA_i)\sigma_i$ is a transverse operator with eigenstates $|\lambda\rangle$. We take the longitudinal direction to be periodic in L and take the limit $L \to \infty$ later. One can prove that the zero modes of $H_\perp$ are simultaneously eigenstates of H_r with eigenvalue $\varepsilon = p_3\sigma^3$.

The expectation value for the current is found in the usual manner by summing the current over all states weighted by the probability of each state. For fermions the probability is given by the Fermi-Dirac distribution. We consider the possibility

that the densities of left-handed and right-handed modes are different and assign them each their own Dirac distribution, f_l and f_r, which gives an expectation value,

$$
\begin{aligned}
\langle j_v^3(x) \rangle &= \sum_{E_\pm} \left[f_l(E) \, \psi_l^\dagger \sigma^3 \psi_l(x) - f_r(E) \, \psi_r^\dagger \sigma^3 \psi_r(x) \right], \\
&= \sum_{\varepsilon} \left[f_l(E_+) + f_l(E_-) - f_r(E_+) - f_r(E_-) \right] \psi_r^\dagger \sigma^3 \psi_r, \quad (3.23)
\end{aligned}
$$

where we used the spinor definition above and the fact that summing over terms odd in ε vanish. We now integrate to find the total current and find the expectation values of the wavefunction. If we write everything in terms of the eigenstates of $H_\perp$ it can been shown that only the zero modes of λ survive and we are left with

$$
\langle J_v^3 \rangle = \frac{1}{L} \sum_{p_3} \sum_{\lambda=0} \left[f_l(E_+) + f_l(E_-) - f_r(E_+) - f_r(E_-) \right] \langle \lambda | \sigma^3 | \lambda \rangle. \quad (3.24)
$$

Following the standard arguments from [6], the factor $\langle \lambda | \sigma^3 | \lambda \rangle$ counts the difference in transverse zero modes travelling parallel to the magnetic field with positive or negative eigenvalues, N_+ and N_-. Taking $L \to \infty$ and integrating each Dirac distribution gives the number density of 1-dimensional left and right-handed fermions, $n(T,\mu)_l - n(T,\mu)_r$ where,

$$
n(T,\mu)_{l/r} = \int_0^\infty \frac{dp_3}{2\pi} \left[f_{l/r}(E_+) + f_{l/r}(E_-) \right]. \quad (3.25)
$$

Note the integral is only over half the range of p_3 because of the nature of the spectrum for left and right handed particles. With this all taken into account the current can be written as

$$
\langle J_v^3 \rangle = \left[n_l(T,\mu) - n_r(T,\mu) \right] (N_+ - N_-). \quad (3.26)
$$

As we discussed in Section 2.1.4 the difference in the positive and negative modes travelling along the magnetic field is given in physical terms by the index theorem. In Section 2.1.4 we calculated the index of a 4-dimensional operator. Here we use the index of the two-dimensional Dirac operator [6] given by

$$
N_+ - N_- = \frac{e\Phi}{2\pi}, \quad (3.27)
$$

where Φ is the magnetic flux. We see that the topological index counts the units of quantum flux $\Phi_0 = 2\pi/q$ in the system. The current is then

$$
\langle J_v^3 \rangle = (n_l - n_r) \frac{e\Phi}{2\pi}, \quad (3.28)
$$

where $n_r(T, \mu)$ and $n_l(T, \mu)$ are one-dimensional number densities of left and right-handed Dirac fermions. Furthermore, at zero temperature the one-dimensional number density in the massless limit can be written in terms of the chemical potential $n_{l/r}(T = 0, \mu) = \mu_{l/r}/2\pi$ in which case the expression for the current is reduced to

$$\langle J_v^3 \rangle = (\mu_l - \mu_r) \frac{e\Phi}{(2\pi)^2}, \qquad (3.29)$$

In this case it is purely topological.

In the zero temperature, massless case it is easy to see how the current appears through defining separate left and right-handed chemical potentials to reproduce (1.2). In a neutron star it is unclear what exactly these chemical potentials are. We will use a different language to describe the current. Additionally, the systems we are interested in require us to consider massive fermions. With a mass we can only write one chemical potential and the current as we have it (3.28) is zero. The chemical potential that both the left and right-handed modes see is the same and left to its own devices the current is washed out $n_r(T, \mu) = n_l(T, \mu)$.

What is required for the current to be nonzero is some boundary condition. In our case the boundary condition will result in time reversal symmetry being violated. We stressed this in the derivation using the anomaly but have not explicitly introduced one. In the massless case this boundary condition is introduced so seamlessly that one barely notices it. The boundary condition is captured by the fact that we can set the left and right handed chemical potentials to different values, that we somehow have a reserve of each handedness of particle. We have to find a way to introduce left and right-handed particles in such a way that the particle density is not simply a function of the temperature and chemical potential. The density has to be promoted to some more general function involving the processes w occurring in the system $n(T, \mu, w)$ to add new particles.

3.1.3 Interpretation

These currents are simply statements of the motion of left and right-handed particles given their spin alignment in a magnetic field. Formulae (3.23) and (3.28) have a very simple physical meaning: to compute the current one should simply count the difference between left-handed and right-handed modes in the background of a magnetic field, as shown in Figure 3.2. We assume that the modes of the current couple to electrons. The splitting of the Landau levels is $\omega = eB/m$ and Landau levels manifest themselves when $T \ll \omega$. For a magnetic field of $eB \sim 10^{12}$ G ~ 0.1 MeV^2 the splitting normalized to the mass of the electron is $\sim 0.2 \, m_e/m$ MeV. The typical temperature for the neutron star is about 10^9 K ~ 0.01 MeV. So the Landau levels affect the electrons much more than they affect they affect heavier particles,
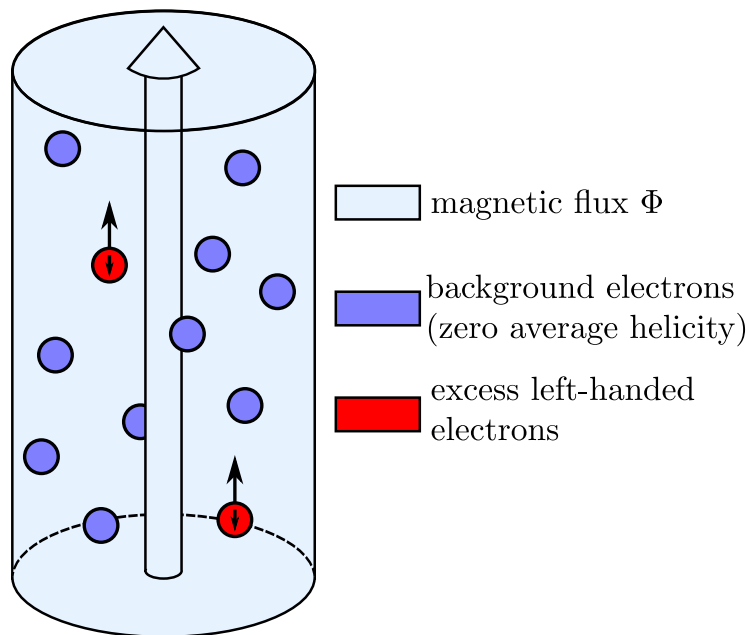
Figure 3.2: A left-handed electron placed inside the magnetic flux in a background of electrons with no average helicity will be pushed out. The current wants to balance the number of left-handed and right-handed particles and acts as a helicity pump.

say protons or even muons. When we do out calculations later we will take into account both the temperature and the chemical potential on the Landau levels of the electron.

The lowest Landau level is the one that breaks the symmetry in the problem and is critical to the formation of the current The single spin state in the lowest Landau level only allows the spin of an electron to anti-align with the field. In the lowest Landau level left-handed zero modes move along the magnetic field and right-handed zero modes move against the magnetic field. An excess of left-handed or right handed modes will couple to electrons and form a current that runs either along the field or against the field. The topological vector current acts as a pump to remove the average helicity and it stops pumping once the average helicity is zero again.

In general the difference in left and right-handed modes is a complicated function of many parameters: magnetic field B, chemical potential μ, temperature T,

and mass of the particle m; but in the chiral limit ($m = 0$) the expression for the current takes the simple form (3.29), has pure topological character, and can be derived from an anomalous effective Lagrangian without referring to the dynamics. The current is expressed in terms of one-dimensional fermi distributions (3.26) and the physics of two other dimensions is determined by Landau levels (the lowest one for $m = T = 0$). When $T \neq 0$ and $m \neq 0$ the current will still be induced, but it will not have a simple topological form (3.29). The relevant formula in this case becomes much more complicated and is determined by the ratios of a number of dimensional parameters mentioned above, see [12] where some limiting cases have been studied.

The current is insensitive to the structure of the magnetic field and will be induced if the magnetic field is confined to magnetic flux tubes or uniformly distributed. The current is simply confined to the regions where the magnetic field is present. Our eventual goal is to derive a form for the current in neutron stars. For our purposes it is not essential whether the magnetic field is represented by magnetic flux tubes, as found in type-II superconductors, or by magnetic domains, the typical structure for the intermediate state[3] argued for in argued for in [8]. The current is strongest in the degenerate regions with $\mu \gg T$ where the background magnetic field is large. When the system becomes a less degenerate (or not degenerate at all) one should expect strong suppression [6, 12]. For numerical estimates of the effect it is convenient to count number of superconducting flux tubes in the entire star and compute the current per unit quantum flux $\Phi_0 = \frac{2\pi}{q} = 2 \cdot 10^{-7} \, \mathrm{G\,cm^2}$, where $q = 2e$ is the charge of the proton Cooper pair.

3.2 Non-dissipating Currents in Dense Stars

There are three requirements for topological vector currents to be present: an imbalance in the number of left and right-handed particles $n_l \neq n_r$, degenerate matter $\mu \gg T$, and the presence of the background magnetic field $B \neq 0$. All of these are present in neutron and quark stars. The weak interactions, which the star attains equilibrium through, violate parity; particles created in this environment are primarily left-handed, see the Appendix for a quantitative estimates. As discussed the interior of the star is dense, $\mu_e = 100$ MeV, and cold, $T = 0.1$ MeV, such that the degeneracy condition $\mu \gg T$ is met, and the star is known to have a huge magnetic field, $B \sim 10^{12}$ G.

All three criteria are met but there is a subtlety to consider. In an infinite system,

---

[3]The intermediate state is characterized by alternating domains of superconducting and normal matter where the superconducting domains exhibit the Meissner effect, while the normal domains carry the required magnetic flux.

a system large enough to allow the electron to decay, any asymmetry in left and right-handed electrons created by the weak interaction would be washed out; the creation and annihilation rates of the left-handed particles are the same. Though many more left-handed electrons are created, they are also destroyed much faster than the right-handed and no asymmetry builds. This is similar to the argument found in [115]—there is no asymmetry in equilibrium in an infinitely large system. Unlike in [115], we are interested in low temperatures where the neutron star is a finite system with respect to the weak interaction—see Figure 3.3. The electron travels to the surface of the star before the inverse process that captures the electron can remove it. Removing the reverse process effectively breaks the time reversal symmetry of the system and the weak interaction can no longer remove the parity introduced into the system. As a result a current forms to remove the parity.

In Section 3.2.1 we will first explain how the current is induced and derive a formula more calculating the magnitude of the current. In Section 3.2.2 we will discuss why the induced current is not washed out by fast quantum electrodynamic (QED) processes, but can only be washed out by slow weak interactions. The reason is the $\mathscr{P}$-odd nature of the phenomenology: an effect induced by $\mathscr{P}$-odd forces, can only be washed out by $\mathscr{P}$-odd forces.

3.2.1 Estimating the Strength of Induced Currents

Directly calculating the current would require careful consideration of the helicity of electrons in regions with flux, where all electrons created are left-handed, and regions without flux, where the helicity can be washed out, and how electrons diffuse from one region to the other. If we assume that the magnetic field is uniformly distributed (as discussed in Section 2.2.2) then every electron created by a $\mathscr{P}$-odd process in the star potentially contributes to the current. As discussed in Section 3.1.3 we can calculate the current by counting the number of left-handed electrons minus the number of right-handed electrons created in the star. Unlike Section 3.1.3 there is now a large Fermi momentum that opens up many Landau levels, but only the lowest Landau level contributes to the current. The current arises because the lowest Landau level has a single spin state, electrons created in that spin state are primarily left-handed, and this helicity state propagates out of the star, preserved through through countless QED interactions, before the inverse weak process can remove it. These helicity states propagating out of the star make up the current.

We explicitly see how both the magnetic field and parity violation are necessary for the current. The spin degeneracy of the lowest Landau level is one, while all other Landau levels have spin degeneracy two. This implies that the produced $\mathscr{P}$-asymmetry in the polarization $\langle \Lambda \rangle = \langle \vec{\sigma} \cdot \vec{P}/|\vec{P}| \rangle$ is not translated into
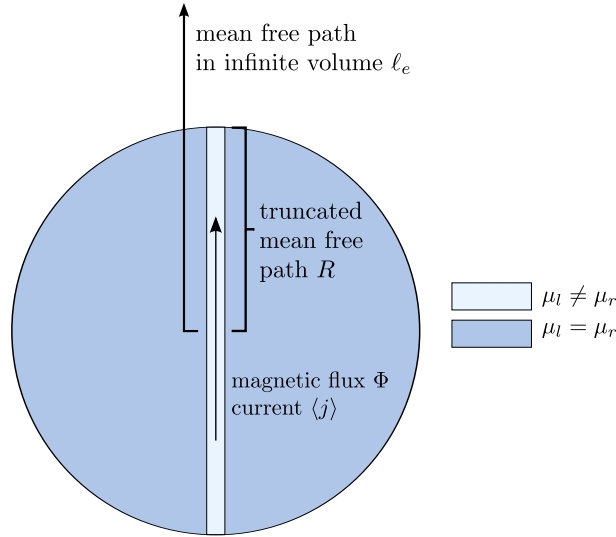
Figure 3.3: The neutron star is a finite system—the mean free path with respect to the weak interaction is much larger than the radius of the neutron star $\ell_{\text{weak}} \gg R$. Electrons leave the system before they can be captured. The current flows because the system is not in equilibrium.

$\mathscr{P}$-asymmetry in the correlation of the momentum and magnetic field $\langle \vec{B} \cdot \vec{P} \rangle$ for all Landau levels except the lowest one. Even though the $\mathscr{P}$-asymmetry is present in the higher levels the spin degeneracy allows particles with the same polarization are allowed to travel in opposite directions, which results in zero current. The single spin degeneracy of the lowest Landau level means that any longitudinal polarization will result in more particles moving one way than the other, thus a current. The correlation between spin and the magnetic field is a $\mathscr{P}$-even effect $\langle \vec{\sigma} \cdot \vec{B} \rangle$ and together with the $\mathscr{P}$-odd correlation between spin and momentum $\langle \vec{\sigma} \cdot \vec{P} \rangle$ it produces the $\mathscr{P}$-odd asymmetry $\langle \vec{B} \cdot \vec{P} \rangle$ we are interested in.

Equation (3.28) tells us how to proceed. If we considered a single unit of quantum flux the current is found by counting the difference in left and right-handed electrons in the lowest Landau level. The occupation of the lowest Landau level is given by the number of electrons that are created during the equilibrium processes. For two units of quantum flux the current is twice as big and so on. The magnitude of the current only depends on the flux. The current through the surface of the star can then be found by counting the difference in rates of left-handed and right-handed electrons created in a magnetic field in the entire volume of the star.

For the entire star this results in a current of the form

$$J_{\mathrm{v}} = P_{\mathrm{asym}}(B,\mu,T) \cdot \frac{w}{\Omega} V_{\mathrm{star}}, \tag{3.30}$$

where w/Ω is the transition rate per unit volume assuming the magnetic field is uniformly distributed, $P_{\mathrm{asym}}(B,\mu,T)$ accounts for both the polarization of electrons created in a magnetic field and the suppression due to Landau levels, and V_{star} is the volume of the region of degeneracy, which we assume is about the same size as the star itself.

The extreme degeneracy of the electrons means that electrons are uniformly distributed throughout the Landau levels. As we will discuss in Section 4.1.2 the number of Landau levels is $n_{\mathrm{max}} = (E_e^2 - m_e^2)B_{\mathrm{c}}/2m_e^2 B$. Each Landau level except the lowest one has a degeneracy of two. Only an electron created in the lowest Landau level will contribute to the current. The ratio of the lowest Landau level to the total number of states is approximately $\sim m_e^2 B/\mu_e^2 B_{\mathrm{c}}$, which is supported by the analysis in [116]. Therefore, we estimate $\mathscr{P}$-odd asymmetry factor as

$$P_{\mathrm{asym}}(\mu_e,T,B) \simeq -\langle \Lambda \rangle \cdot \left(\frac{m_e^2}{\mu_e^2} \frac{B}{B_{\mathrm{c}}} \right) \sim 2 \cdot 10^{-5} \left(\frac{B}{B_{\mathrm{c}}} \right) \left(\frac{n}{n_0} \right)^{-4/3}, \tag{3.31}$$

where the polarization $\langle \Lambda \rangle$ calculated later and is given by (4.55). Numerically we see that a large chemical potential means that the number of states in the lowest Landau level is small compared to the total number of states. We have calculated the average polarization not just for the lowest level, but for electron created in all levels. Because we are looking at an average current in a large system it is likely that polarization states other than those in the lowest landau level are the ones to propagate. What is important is that there are more spin-down states than spin-up states and there is an average polarization. The density dependence in (3.31) reflects that found in a neutron star; in the case of quark stars we use the appropriate electron chemical potential and density dependence described in the background material.

For non-trivial vortex structures it is convenient to determine the current per unit fundamental flux by dividing by the total number of flux tubes. In a type-II structure this would be the current that runs along a single vortex; in a uniformly distributed environment it is simply a convenient normalization,

$$J_{\mathrm{v}} = P_{\mathrm{asym}}(B,\mu,T) \cdot \frac{w}{\Omega} \frac{V_{\mathrm{star}}}{N_{\mathrm{v}}}. \tag{3.32}$$

The current in a type-I domain is found by multiplying (3.32) by the units of flux trapped inside the domain.

The expression for the induced current, (3.30) and (3.32), naively has a different form than previously discussed (3.26), but in fact is precisely the same induced current with the same physical meaning. The separation of transverse and longitudinal degrees of freedom (with respect to magnetic field B_z) that is explicit in (3.26) is hidden now in the formula for $P_{\text{asym}}(B, \mu, T)$ where the Landau levels (transverse degrees of freedom) are treated separately from longitudinal motion. This is explicitly calculated in Section 4.1.3. The longitudinal degrees of freedom in eq. (3.26) are represented at $T = 0$ by the one-dimensional number density $\sim \mu/\pi$, which is the correct expression when the problem is treated as a grand-canonical ensemble with μ_L and μ_R constant due to the infinitely large bath surrounding the system. In our case the neutron star is a finite system at $T \neq 0$ where particles are continuously injected at a rate w. Along with $P_{\text{asym}}(B, \mu, T)$ this describes the resulting asymmetric number density as a function of external parameters T, μ, B. And as they should, both equations (3.26) and (3.30) have units of current: number of particles per unit time.

The topological vector current[4] arises specifically because the system is no longer in equilibrium with respect to the weak interaction and a small asymmetry $(n_L - n_R) \neq 0$ appears. The current is a steady state[5], but constantly requires new polarized electrons to be created in the magnetic field background, then pushed out of the system, into the crust or into space. Because of this steady state the rate w/Ω is calculated when the electron chemical potential is constant.

The electron chemical potential μ_e does not necessarily go to zero as it does for neutrino emission. Only a small fraction of electrons equal to the number in the lowest Landau level actually participate in the current and these will constantly be repopulated by the equilibrium processes in the star. When electrons leave the region of degeneracy, where the non-dissipating current is produced, the current loses its quantum properties and becomes a normal dissipating current capable of transferring momentum, emitting photons, etc. These electrons may get trapped in the crust and diffuse back in, maintaining μ_e.

If the electrons manage to escape, the chemical potential μ_e will slowly decrease over time. As electrons escape the star may become positively charged and start to accrete matter. Eventually, when μ_e becomes sufficiently small, the production of the induced current stops. Later we will introduce the current as a mechanism for produce pulsar kicks. This is precisely the moment when the neutron

---

[4]The axial current will always be induced even when $\mu_l = \mu_r$, but it will not be coupled to the electromagnetic field, and cannot carry the momentum. The physical consequences of this axial topological current might be quite interesting, but shall not be discussed in the present paper.

[5] We assume that the variation of $(\mu_L - \mu_R)$ is adiabatically slow process, with a typical variation time to be much longer than any other time scales of the problem. It allows us to treat the system as being in the equilibrium when $(\mu_L - \mu_R)$ is assumed to be a fixed parameter.

star kick engine stops. As we mentioned previously it is the chemical potential that fuels the kick, not the temperature. The engine stops when chemical equilibrium is achieved, not when the temperature drops which happens much earlier.

3.2.2 $\mathscr{P}$-odd Effects, QED, Polarization and Thermodynamics

An important aspect of the topological current is that it is neither a zero temperature effect nor a chiral effect. It persists as long as parity, an asymmetry in left and right-handed electrons, is present in the system. While topological currents originally were computed at $T = 0$ for exactly massless fermions [5], it was later shown [6] that the effect persists for $T \neq 0, m_e \neq 0$. The lesson learned from these calculations is that the effect is not washed out, even when a nonzero temperature is introduced and an arbitrarily large number of collisions between electrons occur to maintain thermodynamic equilibrium. The crucial point for our mechanism is that $\mathscr{P}$-odd effects are not washed out by fast QED processes.

It is important to remember there are three scales in our problem: the mean free path of quantum electrodynamic processes ℓ_{QED}, the mean free path of weak interactions ℓ_{weak}, and the radius of the neutron star R. For the temperatures we are interested the scales are ordered as $\ell_{\text{weak}} \gg R \gg \ell_{\text{QED}}$. We see that with respect to QED interactions the neutron star is considered to be an infinite system, but with respect to weak interactions it is finite.

Quantum electrodynamic processes cannot wash out polarization even though massive particles introduce processes that can flip helicity, even when these processes occur thermally. The key here is the unitarity of interactions; processes go forwards and backwards at the same rate. Though helicity is lost through these interactions, it is also created. This cancellation due to unitarity is aptly illustrated in [115], where the authors consider the weak interactions inside a star at high temperatures. Just as in [115] we can use thermal equilibrium and unitarity to show how the current propagates.

Consider electron-proton scattering where neither particle is confined to Landau levels. The change in the number of electrons with a given helicity $n^{(e)}(\mathbf{q} \cdot \boldsymbol{\sigma}, t)$ can be written as

$$\frac{\partial}{\partial t} n^{(e)}(\mathbf{q} \cdot \boldsymbol{\sigma}, t) = \sum_{\sigma, \sigma', \mathbf{s}, \mathbf{s}'} \int \frac{d^3 \mathbf{p}}{p_0} \frac{d^3 \mathbf{p}'}{p_0'} \frac{d^3 \mathbf{q}'}{q_0'} \tag{3.33}$$

$$\begin{aligned} &\left[\mathscr{S} \, W(\mathbf{q} \cdot \boldsymbol{\sigma}, \mathbf{p} \cdot \mathbf{s} | \mathbf{q}' \cdot \boldsymbol{\sigma}', \mathbf{p}' \cdot \mathbf{s}') \right. \\ &\left. - \mathscr{S}' \, W(\mathbf{q}' \cdot \boldsymbol{\sigma}', \mathbf{p}' \cdot \mathbf{s}' | \mathbf{q} \cdot \boldsymbol{\sigma}, \mathbf{p} \cdot \mathbf{s}) \right], \end{aligned} \tag{3.34}$$

where $\mathbf{q}$ and $\mathbf{p}$ denote the momentum of the electron and proton, $\boldsymbol{\sigma}$ and $\mathbf{s}$ denote the electron and proton spin, and $W(\mathbf{q}' \cdot \boldsymbol{\sigma}', \mathbf{p}' \cdot \mathbf{s}' | \mathbf{q} \cdot \boldsymbol{\sigma}, \mathbf{p} \cdot \mathbf{s})$ is the probability of scat-

tering $|p(\mathbf{q},\mathbf{s})e(\mathbf{q},\sigma)\rangle \to |p(\mathbf{q'},\mathbf{s'})e(\mathbf{q'},\sigma')\rangle$ per unit time per unit phase volume. These are all the processes that change the helicity of the electron.

There is a statistical factor $\mathscr{S}$ to account for the Fermi distribution of the initial states and the Pauli blocking of the final particles. In the massive limit the chemical potential enters the Lagrangian by a term μN, where the particle number N is the charge associated with the chemical potential. The mass term literally mixes up the left and right spinors in the Lagrangian. One can write this chemical potential in terms of left and right-handed chemical potentials, but because the mass term mixes the helicity only one chemical potential can enter the statistics of the problem. In this case the current is given by equation (3.28) where we calculate the difference in the numbers of left and right-handed electrons. It is common to work in the chiral limit where there is no mass term and it is possible in the Weyl representation to introduce two separate chemical potentials, one for the left-handed and one for the right-handed spinors. There are then two charges that enter the statistics and there are two separate Fermi surfaces. The current could then be determined by looking at the difference in these chemical potentials. But in the chiral limit there are no helicity flipping amplitudes and the imbalance in left and right-handed chemical potentials created by the weak interaction would never be washed out. The purpose of this section is to show that the current does not get washed out when helicity flipping amplitudes exist so we choose the massive limit where the electrons feel only a single chemical potential regardless of their helicity.

With this in mind the statistical factor written explicitly is

$$\mathscr{S} = \frac{1}{1 + e^{-(E(p_e) - \mu_e)/T}} \frac{1}{1 + e^{-(E(p_p) - \mu_p)/T}} \times$$
$$\frac{1}{1 + e^{(E(p'_e) - \mu'_e)/T}} \frac{1}{1 + e^{(E(p'_p) - \mu'_p)/T}}. \tag{3.35}$$

The factor $\mathscr{S'}$ is similar but has the primed and unprimed variables swapped. We have chosen degenerate functions to illustrate that the average polarization of the electrons along a specific direction (in our case along the magnetic field) is constant, and cannot be washed out by QED interactions, see eq. (3.43) below. We have made no assumptions about the initial and final chemical potentials and assume that they are different.

The general statement of thermal equilibrium is

$$\mathscr{S} = \mathscr{S'}, \tag{3.36}$$

Thermal equilibrium is attained with respect to QED interactions because the mean free path is much smaller than the size of the neutron star. This in not the case with the weak interactions, which have a mean free path much larger than that of the

star. This non-equilibrium of the weak interaction generates the parity asymmetry required for the current and is discussed in detail in Section 3.2.1. Given our specific distributions, the statement of thermal equilibrium has two solutions,

$$E(p'_e) - \mu'_e = E(p_e) - \mu_e \quad \text{and} \quad E(p'_p) - \mu'_p = E(p_p) - \mu_p, \tag{3.37}$$

or

$$E(p_e) - \mu_e = E(p'_p) - \mu'_p \quad \text{and} \quad E(p'_e) - \mu'_e = E(p_p) - \mu_p. \tag{3.38}$$

Substituting either of these solutions into the conservation of energy equation for the interaction $E(p_e) + E(p_p) = E(p'_e) + E(p'_p)$ yields

$$\mu_e + \mu_p = \mu'_e + \mu'_p, \tag{3.39}$$

which is the condition for chemical equilibrium. Particles can only scatter from their Fermi surface onto another Fermi surface.

The key element of the argument is the unitarity of the interaction,

$$1 \;=\; \sum_{\sigma', s'} \int \frac{d^3\mathbf{p}' \, d^3\mathbf{q}'}{p'_0 \, q'_0} W(\mathbf{q} \cdot \sigma, \mathbf{p} \cdot \mathbf{s} | \mathbf{q}' \cdot \sigma', \mathbf{p}' \cdot \mathbf{s}') \tag{3.40}$$

$$=\; \sum_{\sigma', s'} \int \frac{d^3\mathbf{p}' \, d^3\mathbf{q}'}{p'_0 \, q'_0} W(\mathbf{q}' \cdot \sigma', \mathbf{p}' \cdot \mathbf{s}' | \mathbf{q} \cdot \sigma, \mathbf{p} \cdot \mathbf{s}), \tag{3.41}$$

This says that every initial state scatters into a final state and that every final state scatters into an initial state.

Using (3.36) the electron and proton distributions can be factored out and using (3.40) we find that the forward and reverse rates cancel each other, causing the right hand side of (3.33) to vanish. We have found that the number of electrons of a given helicity is constant,

$$\frac{\partial}{dt} n^{(e)}(\mathbf{q} \cdot \sigma, t) = 0. \tag{3.42}$$

This is the result of detailed balance, which ensures that there can be no asymmetry in the creation and annihilation rates of particles in thermal equilibrium. Given this spectrum of static solutions, the average polarization of the electrons along a specific direction (in our case along the magnetic field) is constant,

$$\langle \Lambda \rangle = \frac{\int d^3\mathbf{q} \left[n^{(e)}(+|\mathbf{q} \cdot \sigma|) - n^{(e)}(-|\mathbf{q} \cdot \sigma|) \right]}{\int d^3\mathbf{q} \left[n^{(e)}(+|\mathbf{q} \cdot \sigma|) + n^{(e)}(-|\mathbf{q} \cdot \sigma|) \right]} = \text{constant.} \tag{3.43}$$

The physical meaning of equation (3.43) is very simple: if we start with no average polarization, none develops; if we start with an overall polarization, it cannot be washed out. This interaction by interaction proof provides the dirty details for a very simple argument: a system that starts with some kind of parity violation (i.e., different numbers of left and right-handed electrons) cannot have that parity violation removed by QED because QED does not violate parity.

An example of this principle can be found in the experimental set up of a beam of electrons. Consider an unpolarized beam of electrons travelling along the *z*-direction. While there are many electromagnetic interactions, the result (3.43) states that the longitudinal polarization P_z remains zero as time passes. Why does this happen? Consider the collision of two particles in the beam with initial momenta $\vec{k}_1$ and $\vec{k}_2$ and zero total polarization along the *z*-axis. After the collision polarization can be induced in the transverse direction $\vec{P} \cdot \vec{k}_1 \times \vec{k}_2$, but not in the longitudinal directions, $\vec{P} \cdot \vec{k}_1$ or $\vec{P} \cdot \vec{k}_2$, as this would contradict the fundamental parity symmetry of the QED Lagrangian. In particular, suppose $(\vec{k}_1, \vec{k}_2)$ are in the *xz*-plane. The polarization can be only induced in the positive *y*-direction. It is clear that in the thermodynamical equilibrium there will be another pair of particles which produce a polarization in the negative *y*-direction such that total polarization remains zero. This simple example explains what equation (3.43) states: if longitudinal polarization of the beam was initially zero, it will remain zero in spite of the fact that each given process may induce polarization.

So far the discussion has considered only particle-particle QED scattering and not scattering off a background field. It is tempting to think that the helicity flipping amplitudes of an electron scattering off a semi-classical background field will wash out an asymmetry. Such arguments neglect that polarization is given to the background field in the form of operators such as the magnetic helicity $\langle \vec{A} \cdot \vec{B} \rangle$ and higher order operators that are not invariant under $\mathscr{P}$ transformations. These operators are the manifestation of the parity lost by electrons to the background field, and is the parity responsible for creating the toroidal magnetic fields discussed in Chapter 6. There is a point where the background field, which now contains $\mathscr{P}$-odd parity configurations in the form of magnetic helicity, will start to give parity back to the electrons through scattering. This steady state is once again achieved through unitarity and thermal equilibrium. This system of topological currents combined with an E&M field carrying magnetic helicity is complicated and it is not our goal to present a complete description of how these $\mathscr{P}$-odd effects transform from one form to another. This would require us to analyze a system comprising of time dependent Maxwell equations with non-static sources. We explicitly calculate the current when these interactions with the external magnetic field are effectively turned off. However, from the $\mathscr{P}$ invariance of QED we know that $\mathscr{P}$-odd effects will stay even when these interactions with the external magnetic field are turned

on.

This has a physical analogue in beam physics as well. As discussed, a beam with no longitudinal polarization that has only particle-particle QED interactions will remain unpolarized. However, a beam with longitudinal polarization can be created if a magnetic field configuration with nonzero helicity is applied, which is the standard technique used to produce a longitudinally polarized beam. As this polarized beam propagates it cannot lose its polarization due to the internal particle-particle QED interactions. If it did, time reversal symmetry, which is unitarity, would tell us that a beam with no longitudinal polarization could spontaneously polarize due to particle-particle interactions. This is untrue and the polarization stays in the beam. Furthermore, time reversal symmetry applied to the longitudinally polarized beam tells us that when the beam encounters a magnetic field, the field may reconfigure itself to absorb some $\mathscr{P}$-odd magnetic helicity from the beam. This is exactly how the current in a neutron star imparts magnetic helicity to the field. To conclude, the entire $\mathscr{P}$-odd configuration which includes longitudinal electron polarization and magnetic helicity (and higher order $\mathscr{P}$-odd operators) cannot be washed out by QED interactions.

We must also consider that some collective bosonic mode such as heat may destroy the current. To destroy the current these dissipative modes must carry the helicity out of the star faster than the current does. It does not imply that $\mathscr{P}$-odd effects are destroyed. Rather it means that $\mathscr{P}$-odd configurations in principle may leave the system. We can account for these dissipative modes by assuming they are carried out of the star by photons or phonons. The helicity modes that the current carries out of the star are subject to direct walk and leave the star close to the speed of light while a photon is subject to a random walk. The number of steps in a random walk is the square of the number of steps in a direct walk, so it takes much longer for a photon to escape than the current to carry helicity out. Some tiny fraction of the helicity manages to escape this way, but the current remains intact. Thermal cooling of the star is also not the dominant cooling mechanism of the star while the current is active, neutrino emission is. The processes that create the neutrinos are the exact processes responsible for the current. We can quantify when the star is too hot for the current to propagate by finding the temperature where $\ell_e < R$. This means that the current can no longer carrying the helicity out of the system and does not flow. Essentially this violates the conditions formulated above for the current to be induced.

The statement that $\mathscr{P}$-odd effects, if produced, cannot be destroyed or washed out by conventional QED processes is correct for any system, including condensed matter systems. However, there is a crucial difference between our discussion of the current and conventional condensed matter systems, where it is known that the induced spin polarization inevitably relaxes even though QED preserves parity. In

any condensed matter system the relaxation process takes relatively short period of time as the heat can easily leave the system. This heat is actually represented by long wavelength photons (microwaves) that are partly polarized and can easily leave the system. The situation is drastically different for neutron stars or quark stars (due to the very large density) when it takes very long period of time before a photon can reach the surface of the star to have a chance to escape. In principle, the $\mathscr{P}$-odd effects in neutron/quark stars will also inevitably relax when no new polarization is pumped in. However, the time scale for this to happen is much longer than in condensed matter systems. This is analogous to the evolution of the magnetic field in neutron stars trapped in a type I superconductor. It is known that the magnetic field should be expelled from the bulk of type-I superconductors. However, it takes a very long time (much longer than the life time of the universe) before the magnetic field is actually expelled from neutron stars.

Nowhere in the arguments above have we assumed (or implied) that our state is a pure quantum state with definite parity; on the contrary, our arguments are based on thermodynamics and a density matrix formalism where the polarization for a mixed electron state is defined as the sum over all particles $\vec{P} = \sum_n g_n \vec{P}_n$ where g_n is a probability to find the $n-$th particle with polarization $\vec{P}_n$ with normalization $\sum_n g_n = 1$.

For the sake of curiosity there is an example of a strongly interacting, many body system where a $\mathscr{P}$-odd configuration could be produced, but nevertheless is not washed out by very fast strong interactions, which is very similar to the case we consider. Specifically, we have in mind the charge separation effect in heavy ion collisions [11, 32] where $\mathscr{P}$ and $\mathscr{CP}$ odd effects survive in spite of the fact that the system is in thermodynamical equilibrium with respect to strong interactions. There is a simple argument why a $\mathscr{P}$-odd effect is not washed out by the strong interactions: it is an invariance of QCD with respect to $\mathscr{P}$ and $\mathscr{CP}$ symmetries. The analogy between our topological current and the $\mathscr{P}$-odd effect in heavy ion collisions is even deeper than it appears: both effects in fact originate from the same anomaly[11, 32].

3.3   Summary

We first derived the topological vector current in two ways: using anomalies and using index theorems. These two derivations led to understanding two important aspects of the current. First, the current requires a boundary condition to manifest itself. It is the physics of surface terms. This will become even more important when we discuss the current later in terms of holographic QCD. The second aspect

resulted from the formula (3.28),

$$\left\langle \int_S \vec{j}_v \cdot d\vec{S} \right\rangle = (n_l - n_r) \frac{e\Phi}{2\pi} , \tag{3.44}$$

where the current is described by the difference in one-dimensional number densities of left and right-handed particles $n_l - n_r$. The conclusion is that the current is not mysterious. It is simply the result of counting modes in a magnetic field.

We then focused on how this boundary condition arises in dense stars. The key is the finite size of the star and the relatively long life of particles with respect to the weak interaction. This allows left-handed particles to be made inside the star and travel to the surface before they are destroyed. In a more technical sense the finite radius of the star causes the time reversal symmetry of the weak interaction to be destroyed. The system can create left-handed electrons, but is unable to destroy them.

Our simple counting argument lead to the parameterization of the magnitude of the current created in the star along the magnetic field is

$$J_v = P_{\text{asym}}(B, \mu, T) \cdot \frac{w}{\Omega} V_{\text{star}} , \tag{3.45}$$

which is equation (3.30) in the text. This is the current that arises by considering the creation of particles in the lowest Landau level. The quantity $P_{\text{asym}}(B, \mu, T)$ determined in equation (3.31) captures the breaking of parity symmetry by the weak interaction and the lifting of the spin degeneracy in the lowest Landau Level.

Chapter 4

Estimating the Magnitude of the Current

Now that we have established how the current arises in dense stars we will use this new expression (3.32) to calculate the magnitude of the topological vector current in a variety of different phases. We choose four representative phases that capture the behaviour of the the majority of phases thought to exist inside a dense star.

Notation

We use the convention $\hbar = c = k_B = 1$ unless otherwise stated. We will always denote the momentum of particle as p_i, the Fermi momentum as k_i, and the chemical potential as μ_i. When convenience dictates, the subscript i will either be the symbol of the particle or a number, which will be labelled on the Feynman diagram. The three momentum will be bolded $\mathbf{p}_i$, with a magnitude denoted p_i, and the four momentum will have a greek index p^μ.

4.1 Nuclear Matter: The Direct Urca Process

We want to determine the mean free path of the weak interaction of an electron travelling inside a neutron star and the rate at which electrons are created. To do so we will estimate the transition rate following the standard techniques from [65]. Estimating the mean free path allows us to determine whether the helicity built from the weak interaction is washed out or if the asymmetry can escape the star[1]. Similar calculations have been done only for neutrinos as the electron's mean free

---

[1] Here and in what follows we do not assume that an electron physically escapes a star: we use the term "escape" to emphasize that the electron can leave the region of degeneracy without being re-scattered by dense surrounding matter. The fate of the moving electrons when they enter the non-degenerate region $\mu_e \sim T$ from deep degenerate region depends on specific properties of matter with $\mu_e \sim T$. In this region the current becomes dissipating, and the electrons may transfer their energy/momentum to the surrounding dense environment. This subject is beyond the interests of the present work, and shall not be discussed here.

path is assumed to be much shorter due to electromagnetic interactions. However, as we argued above, the electromagnetic interactions do not wash out $\mathscr{P}$-odd asymmetry and the electrons are allowed to propagate due to the non-dissipating, topological vector current. In order to find the mean free path we will consider the direct Urca process, equation (2.126), given by the Feynman diagram in Figure 4.1.
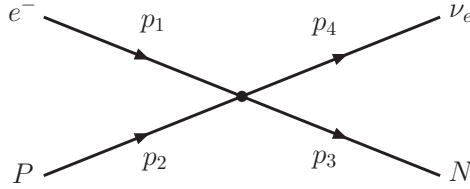
Figure 4.1: The direct Urca process.

Given the order of the diagram this should be to dominant process in normal nuclear matter, but it is not. It is suppressed because the particles taking part are unable to conserve momentum. If all interacting particles lie on their Fermi surface then

$$p_e + p_P - p_N \ll T,\tag{4.1}$$

where T is approximately the energy of the neutrino. In order for the process to conserve momentum the initial electron and proton, or the final neutron, must be far from their Fermi surface in a region with almost no particle occupation. Forcing this inequality to become an equality introduces a suppression of order $\sim e^{-k_N/T}$.

We can calculate the proton fraction required to conserve momentum and allow the direct Urca process to proceed unfettered. In a system well below the Fermi temperature the particles momentum is that of their Fermi momentum. If we ignore the small contribution from neutrinos then the condition for conservation of momentum is $k_e + k_P > k_N$. Charge neutrality forces the proton and electron density to be equal $n_e = n_P$, which means that their fermi momenta are equal resulting in $2k_P > k_N$. The number density for a particle species goes as $n_i \propto k_i^3$, which leaves the inequality as $8n_P > n_N$. We find that momentum is conserved only when the proton fraction is sufficiently large $x_p = n_P/(n_P + n_N) > 1/9$.

The transition rate is given by

$$w = \frac{\Omega^4}{(2\pi)^{12}} \int d^3 p_1 d^3 p_2 d^3 p_3 d^3 p_4 \ \mathscr{S} \ (2\pi)^4 \Omega \ \delta(p_f - p_i) \ |\hat{S}|^2,\tag{4.2}$$

where Ω is the volume of the phase space, the p_i are respectively the electron, proton, neutron, and neutrino momentum, $\mathscr{S}$ is a statistical factor that takes into account the Fermi blocking, and $\hat{S}$ the scattering matrix.

The Fermi blocking factors limit the phase space in which the initial particles can exist and the final particles can be created. Particles that exist at the beginning of the reaction, such as the electron and proton in this case, are given a factor equal to the Fermi distribution,

$$f_i \; = \; \frac{1}{1+e^{-(E_i-\mu_i)/T}}\,, \tag{4.3}$$

which tells us where particles exist. The particles to be created, such as the neutron, are given a factor of one minus the Fermi function,

$$1-f_i \; = \; \frac{1}{1+e^{(E_i-\mu_i)/T}}\,, \tag{4.4}$$

which restricts the phase space that particles can be created in. There is no Fermi blocking term associated with the neutrino because they leave the star without interacting and do not become dense enough to form a Fermi surface. All of these blocking factors make the statistical factor $\mathscr{S}$.

We use the standard four Fermi scattering matrix element

$$|\hat{S}|^2 = \frac{G_F^2}{\Omega^4}(1+3C_A^2)\left[1-\frac{1-C_A^2}{1+3C_A^3}\frac{\mathbf{p}_1\cdot\mathbf{p}_4}{E_1 E_4}\right]\,, \tag{4.5}$$

where $C_A = 1.26$ is the Gamow-Teller coupling and $G_F = 1.17\times 10^{-11}$ MeV^{-2}.

Following [65] we separate the angular and radial integrals such that the transition rate becomes

$$w = \frac{\Omega^5}{(2\pi)^8}|\hat{S}|^2 P Q\,, \tag{4.6}$$

where

$$P \;\; = \;\; \int p_1^2 dp_1\, p_2^2 dp_2\, p_3^2 dp_3\, p_4^2 dp_4\, \mathscr{S}\, \delta(E_f - E_i)\,, \tag{4.7}$$

$$Q \;\; = \;\; \int d\Omega_1\, d\Omega_2\, d\Omega_3\, d\Omega_4\, \delta^{(3)}(\mathbf{p}_f - \mathbf{p}_i)\,. \tag{4.8}$$

We start with the Q integral. The contribution from the momentum of the neutrino is small compared to the rest so we neglect it in the δ-function. This allows us to take an integral over all angles causing the term with angular dependence to vanish. As in [65] the angular integrals become

$$Q = \frac{(4\pi)^5}{2p_1 p_2 p_3}\,, \tag{4.9}$$

which we evaluate in detail in Appendix B. We can now do the *PQ* integral,

$$PQ = \frac{(4\pi)^5}{2} \int p_1 dp_1 \, p_2 dp_2 \, p_3 dp_3 \, p_4^2 dp_4 \, \mathscr{S} \, \delta(E_f - E_i) \,. \tag{4.10}$$

The first step is to change variables from energy to momentum. In doing so we will approximate the energy by the value at the Fermi surface as these are the particles most likely to participate in the interaction. For the proton and neutron, which are nearly non-relativistic, we will approximate the energy by the effective mass, $m_N^* \sim 0.8 m_N$ and $m_P^* \sim 0.8 m_N$ [69]. For the electrons, which are highly relativistic, the chemical potential is equal to the Fermi momentum, $k_e = \mu_e$. These factors can be pulled out of the integral. Doing the transformation yields

$$p_1 dp_1 = \mu_e dE_1 \,, \tag{4.11}$$
$$p_2 dp_1 = m_P^* dE_2 \,, \tag{4.12}$$
$$p_3 dp_1 = m_N^* dE_3 \,, \tag{4.13}$$
$$p_4^2 dp_1 = E_4^2 dE_4 \,. \tag{4.14}$$

Performing the neutrino integral, dE_4, over the δ-function leaves

$$PQ = \frac{(4\pi)^5}{2} \mu_e m_N^* m_P^* \int dE_1 \, dE_2 \, dE_3 \, (E_1 + E_2 - E_3)^2 \, \mathscr{S} \,. \tag{4.15}$$

The next step is to make the integral dimensionless making the substitutions

$$x_1 = (E_1 - \mu_e)/T \,, \tag{4.16}$$
$$x_2 = (E_2 - \mu_P)/T \,, \tag{4.17}$$
$$x_3 = -(E_3 - \mu_N)/T \,, \tag{4.18}$$

such that the statistical factor accounting for the Fermi blocking becomes

$$\mathscr{S} = \prod_{i=1,2,3} \frac{1}{1 + e^{x_i}} \,. \tag{4.19}$$

The Jacobian of these transformations introduces a factor of T for each measure. Also, a factor of T^2 comes from the $(E_1 + E_2 - E_3)^2$ term. The chemical potentials introduced all cancel because of the equilibrium condition $\mu_e + \mu_P - \mu_N = 0$. The substitution also causes $m_N^* \to -m_N^*$ such that we are left with a positive transition rate,

$$PQ = \frac{(4\pi)^3}{2} m_N^* m_P^* \mu_e T^5 I \,. \tag{4.20}$$

where I is an analytic integral evaluated in Appendix B,

$$I = \int_{-\infty}^{\infty} dx_1 \int_{-\infty}^{\infty} dx_2 \int_{-(x_1+x_2)}^{\infty} dx_3 \frac{(x_1+x_2+x_3)^2}{(1+e^{x_1})(1+e^{x_2})(1+e^{x_3})}, \quad (4.21)$$

$$= \frac{3}{4}\left(\pi^2\zeta(3) + 15\zeta(5)\right), \quad (4.22)$$

$$\approx 20.56. \quad (4.23)$$

Putting everything together, and using the numerical estimates from the nuclear matter discussion, the transition rate becomes

$$\frac{w}{\Omega} = 8\pi^5 G_F^2 (1+3C_A^2) m_N^* m_p^* \mu_e T^5 I, \quad (4.24)$$

$$= 1.1 \times 10^{31} \left(\frac{\mu_e}{100 \text{ MeV}}\right)\left(\frac{m_N^*}{m_N}\right)\left(\frac{m_P^*}{m_P}\right)\left(\frac{n}{n_0}\right)^{2/3} (T_9)^5 \text{ s}^{-1} \text{ cm}^{-3}. \quad (4.25)$$

where $T_9 = T/(10^9 \text{ K})$ is the dimensionless, scaled temperature. A typical value for the reduced mass factor is 0.6. The temperature dependence T^5 is consistent with literature—remember that we are calculating the transition rate, not the luminosity. The luminosity contains an additional factor of energy in the integral that contributes an extra factor of T.

4.1.1 Estimate of the Current from Direct Urca

The first step is to ensure that the electron can actually escape the star before it decays via the weak interaction. This involves calculating the mean free path and seeing if it is larger than the radius of the star. In the literature for calculations of this type, such as neutrino luminosity for cooling, Ω is the volume of the neutron star—it is necessary to account for all the transitions that occur in the entire star. Here, we are interested in the decay rate of a single electron, so we will take Ω to be the volume in which a single electron exists, which is the inverse of the electron number density,

$$\Omega_e = \frac{1}{n_e} = \frac{3\pi^2}{\mu_e^3} = 2 \cdot 10^{-37} \left(\frac{n}{n_0}\right)^{-2} \text{ cm}^3. \quad (4.26)$$

Assuming that the electron travels at the speed of light though the protons—due to the non-dissipative nature of the current with respect to the electromagnetic interactions, the mean free path can be found using

$$\ell_e \sim \frac{c}{w} \sim 1.2 \times 10^{11} (T_9)^{-5} \left(\frac{n}{n_0}\right)^{4/3} \text{ km}. \quad (4.27)$$

The typical radius for the neutron star is $R \sim 10$ km. We see that for $T \leq 10^{10}$ K the electrons can easily escape the degenerate region before the P-odd asymmetry gets washed out due to the weak interactions. The counterintuitive density dependence—at higher densities the mean free path is larger—is a natural consequence of Pauli blocking. As the density of the star increases the number of protons increases and we would expect a shorter mean free path, but the number of neutrons increases as well. The suppression due to the higher neutron chemical potential is greater than the enhancement gained by increasing the proton density.

Using (3.32) we are now in a position to estimate the magnitude of the current travelling along a single quantum of flux,

$$J_{\mathrm{v}} = 9.4 \times 10^{-10} \left(\frac{n}{n_0} \right)^{-2/3} (T_9)^5 \ \mathrm{MeV}. \tag{4.28}$$

There is no dependence on the magnetic field because we have normalized per unit of quantum flux. As discussed earlier this reaction is dominant when hyperons appear at $n/n_0 \geq 3$ or when the proton fraction is large $x_p > 1/9$.

From (4.27) we see that is it much easier for an electron to escape a cool star rather than a hot, newly born star, $T \geq 10^{11}$ K. If the star is very hot the electron is not able to keep its asymmetry due to the weak rescattering, as one can see from (4.27). As it cools there will be a critical value where the electrons can escape, but are still created at a large rate, meaning the current is very large (4.28). The current is largest when the star is hot, but not so hot that the electrons are unable to escape the region of degeneracy, $\mu_e \gg T$. This temperature is roughly determined by the condition that the electron mean free path with respect to weak interactions is approximately equal to radius for the neutron star is $R \sim 10$ km. It is expected that this temperature drastically depends on the equation of state and other specific properties of the environment as (4.27) suggests.

4.1.2 The Effect of a Large Magnetic Field on the Transition Rate

We will now argue that the effects of the magnetic field can be safely neglected in calculating the transition rate. Of course, the magnetic field still plays a crucial role in producing the required asymmetry for the current. There has been much consideration of Landau levels on the rates of processes that occur in neutron stars. Landau levels can have drastic effects on the spin of electrons, though these effects are suppressed by the unusually high chemical potentials found in neutron stars. An extremely large magnetic field is needed for these effects to manifest themselves in neutron stars. It must be roughly comparable to the chemical potential $eB \sim \mu_e^2$ in order for substantial changes for the transition rates to occur. Numerically, this corresponds to very large fields $B \sim B_{\mathrm{c}} \mu_e^2 / m_e^2 \sim 10^{17}$G, which are much larger than

the magnetic fields found in typical neutron stars. As a note, magnetic field of 10^{17} G are thought to appear in the off-centre Au-Au collisions at RHIC.

To introduce Landau levels to the earlier calculation we can simply replace the electron dispersion relation with

$$E_e^2 = p_z^2 + m_e^2(1 + 2nb),$$

(4.29)

where n are all natural numbers, but only electrons with a spin antiparallel to the magnetic field are allowed in the lowest, $n = 0$, level and $b = B/B_c$ is the magnetic field normalized to the critical field, $B_c = m_e^2/e = 4.4 \times 10^{13}$ G. The electron phase space becomes

$$\Omega \int \frac{dp_z}{2\pi} \sum_{n=0}^{n_{\max}} \frac{g_n m_e^2 b}{(2\pi)^2},$$

(4.30)

where the term after the sum is the degeneracy per unit area and g_n, equal to 1 for $n = 0$ and 2 otherwise, counts the spin degeneracy. The maximum Landau level occurs for $p_z = 0$ when all the energy goes to putting the electron in the Landau level and none goes into the momentum. This yields

$$n_{\max} = \frac{E_e^2 - m_e^2}{2m_e^2 b}.$$

(4.31)

If the number of Landau levels is very large, $n_{\max} \sim \frac{E_e^2}{2bm_e^2} \gg 1$, which is a common case for a typical neutron star, then the phase space returns to the one we used in the previous Section (4.24). Therefore, for a typical neutron star the transition rate basically remains the same, as the electron phase space essentially unchanged,

$$\Omega \int \frac{dp_z}{(2\pi)^3} \mu_e^2,$$

(4.32)

where we used $E_e \sim \mu_e$ and $\mu_e \gg m_e$. This result is in accordance with our previous rough argument that a very large magnetic field is required to produce any substantial changes.

We want to contrast this generic case with a rare situation when only the lowest Landau level is accessible, $n_{\max} = 0$. This occurs when $eB \sim \mu_e^2 \sim 10^{17}$ G [116]. In this approximation we recover the usual electron dispersion relation, while the available phase volume becomes

$$\Omega \int \frac{dp_z}{(2\pi)^3} m_e^2 b.$$

(4.33)

As before, we move the momentum dependent parts of the phase space outside of the integral by approximating them by their Fermi momenta. The rest of the

integral takes place identically. We can compensate for the magnetic field in our calculation of the transition rate simply by taking

$$\mu_e \to \frac{m_e^2 b}{\mu_e} \, . \tag{4.34}$$

This suppression factor is identical to (3.31) but appears because only one Landau level exists in the system. This is different than in (3.31) where the factor appears because we are only considering the Landau levels that contribute to the current. In fact this transformation can be done to account for the magnetic field for any of the other rates we derive (4.73), (4.85), (5.10). In particular, for the direct Urca case we are left with

$$\frac{w}{\Omega} = \frac{G_F^2}{8\pi^5}(1 + 3C_A^2) m_N^* m_P^* \frac{m_e^2 b}{\mu_e} T^5 I, \tag{4.35}$$

which we can compare to equation (4.24). This expression is valid when $b > \mu_e^2/m_e^2$. This condition has a chance of manifesting itself in magnetars, where huge magnetic fields on the order of $B \sim 10^{16}$ G are thought to exist. Otherwise the Landau levels do not have a significant contribution and the earlier expression is valid.

4.1.3 Calculation of the Helicity $\Lambda(\mu, B, T)$

In order to calculate the average helicity of the electrons, we must consider the creation of an electron through nuclear beta decay in a large magnetic field and chemical potential. There have been many calculations of transition rates in magnetic fields, notably [117, 118], and more recently for both large magnetic fields and chemical potentials [116] and references within. We are looking for a specific property of the weak interaction, the helicity of electrons produced in a large magnetic field and chemical potential. The helicity of a particle is given by $\Lambda = \sigma \cdot \mathbf{p}/|\mathbf{p}|$, where σ are the Pauli matrices and $\mathbf{p}$ is the particle's spatial momentum. The two eigenstates of the helicity operator correspond to the values

$$\mathbf{p} \cdot \boldsymbol{\xi} = \pm |\mathbf{p}| \, , \tag{4.36}$$

where $\boldsymbol{\xi}$ is the rest spin vector of the particle. The expectation value of the helicity can be calculated by looking at the ratio of decay rates Γ with different helicity,

$$\langle \Lambda \rangle = \frac{\Gamma(\mathbf{p} \cdot \boldsymbol{\xi} = |p|) - \Gamma(\mathbf{p} \cdot \boldsymbol{\xi} = -|p|)}{\Gamma(\mathbf{p} \cdot \boldsymbol{\xi} = |p|) + \Gamma(\mathbf{p} \cdot \boldsymbol{\xi} = -|p|)} \, . \tag{4.37}$$

The small scale of the interactions and the immense magnitude of the magnetic field make it necessary to consider the Landau levels the electrons decay into. Detailed analysis of the effect of the Landau levels on interactions while considering the complete electron wave function has concluded that the only significant change is in the energy of the electron,

$$E_e^2 = \mathbf{p}_e^2 + m_e^2(1 + 2nb), n = \begin{cases} 1, 2, \ldots & \text{spin up} \\ 0, 1, 2, \ldots & \text{spin down} \end{cases} \tag{4.38}$$

where $b = B/B_c$ is the ratio of the magnetic field and the critical magnetic field, $B_c = \frac{m_e^2 c^3}{\hbar e} \sim 4.4 \times 10^{13}$ G.

The magnetic field also affects the phase space of the electron. It can only carry linear momentum in the direction of the magnetic field. The magnetic field also causes degeneracy of levels. With this taken in to account the phase space becomes

$$\int \frac{dp_e}{2\pi} \frac{m_e^2 b}{2\pi} . \tag{4.39}$$

We will confine ourselves to calculating the helicity for an electron created through beta decay, one half of the direct Urca processes, Figure 4.1. We sum over everything but the electron spin,

$$\sum |M|^2 \simeq 16 G_F^2 E_N E_P \left[(1 + 3C_A^2) E_\nu (E_e - \mathbf{p}_e \cdot \boldsymbol{\xi}_e) \right. \tag{4.40}$$
$$\left. - (1 - C_A^2) \mathbf{p}_\nu \cdot (\mathbf{p}_e - m_e \mathbf{s}_e) \right] ,$$

where $C_A \simeq 1.26$ is the axial current constant, G_F is the Fermi coupling constant, and the spin is given by

$$\mathbf{s} = \boldsymbol{\xi} + \frac{(\mathbf{p} \cdot \boldsymbol{\xi})\mathbf{p}}{m(m+E)}, \tag{4.41}$$

where $\boldsymbol{\xi}$ is the unit polarization vector.

In order to find the decay rate we use the modified electron phase space. To find the total decay rate it is necessary to sum over the probability of an electron appearing in the each of the Landau levels. The sum truncates where the energy of a Landau level is high enough to be disallowed by conservation of energy. Specifically we let $n_{\max}$ be the largest n that satisfies $E_e^2 > m_e^2(1 + 2nb)$. The total decay rate is the sum of the decay rate of each level,

$$\Gamma = \sum_{n=0}^{n_{\max}} \Gamma_n , \tag{4.42}$$

where

$$n_{\max} = (E_e^2 - m_e^2)/m_e^2 2b . \tag{4.43}$$

The highest Landau level is reached when all of the energy goes into putting the electron in the highest landau level and none into the momentum p_z. We see that increasing the magnetic field decreases the number of levels to which the electron has access. When $b > E_e^2/2m_e^2 - 1/2$ the electron only has access to the lowest Landau level meaning that all the electrons are spin down.

We must also account for the non-zero chemical potentials of the protons, electrons, and neutrons. Because the electron and proton have large chemical potentials their phase spaces are constricted. The presence of a Fermi surface means that only higher energy electrons and protons can be created. This is modelled by multiplying the usual phase space by Fermi blocking terms $1 - f(E)$, where $f(E)$ is the Fermi distribution. With these considerations the decay rate into a single Landau level n is

$$d\Gamma_n = \frac{1}{2E_N} \frac{dp_z}{2E_e 2\pi} \frac{m_e^2 b}{2\pi} \frac{d^3 p_\nu}{2E_\nu (2\pi)^3} \frac{d^3 p_P}{2E_P (2\pi)^3}$$
$$\times |M|^2 (2\pi)^4 \delta^4 (p_N - p_P - p_e - p_\nu)(1 - f_P)(1 - f_e), \qquad (4.44)$$

There are a few quantities that naturally align themselves with the magnetic field. Firstly, all spins are either aligned or anti-aligned so if we choose $\mathbf{B} = (0, 0, B_z)$ then

$$\boldsymbol{\xi}_e = (0, 0, \xi_e) \text{ and } \boldsymbol{\xi}_N = (0, 0, \xi_N). \qquad (4.45)$$

Also, because of the Landau levels, the electrons have linear momentum only in the direction of the magnetic field,

$$\mathbf{p}_e = (0, 0, p_e). \qquad (4.46)$$

The matrix element is reduced to

$$\sum |M|^2 \simeq 8G_F^2 E_N E_P \left[(1 + 3C_A^2) E_\nu (E_e - p_e \xi_e) \right. \qquad (4.47)$$
$$\left. - (1 - C_A^2)|\mathbf{p}_\nu|(p_e - m_e s_e)\cos\theta \right],$$

where θ is the angle between the z-axis and the direction of the neutrino momentum.

The integrals up to the final electron integral are straight forward. We are left with

$$d\Gamma_n = A g_n dp_e (E_N - E_P - E_e)^2 \left[1 - \frac{p_e \xi_e}{E_e} \right] (1 - f_e), \qquad (4.48)$$

where

$$A = \frac{m_e^2 G_F^2 b}{(2\pi)^3} (1 - 3C_A^2)(1 - f_P(k_P)). \qquad (4.49)$$

The term $p_e \xi_e = \pm |p_e|$ gives us the helicity eigenstates. We can get the combinations required for finding the average helicity by evaluating

$$\Gamma_n(+) - \Gamma_n(-) = -4Ag_n \int_0^{p_0} dp_e (E_N - E_P - E_e)^2 \frac{|p_e|}{E_e} (1 - f_e), \quad (4.50)$$

$$\Gamma_n(+) + \Gamma_n(-) = 4Ag_n \int_0^{p_0} dp_e (E_N - E_P - E_e)^2 (1 - f_e). \quad (4.51)$$

In order to do the final integral over the Fermi distribution we appeal to the Sommerfeld expansion,

$$\int_0^{E_0} h(E)(1 - f(E)) dE = \int_\mu^{E_0} h(E) dE - \frac{T^2 \pi^2}{6} \frac{\partial}{\partial E} h(E) \Big|_{E=\mu}. \quad (4.52)$$

The particles in a neutron star are in chemical equilibrium. The maximum energy available for the electron is equal to its chemical potential, $E_0 = \mu$, leaving the integral part of the Sommerfeld expansion to vanish. Physically this makes sense because the equilibrium processes only occur thermally—the transition rate at zero temperature vanishes. Doing our integral has been reduced to taking a derivative,

$$\Gamma_n(+) - \Gamma_n(-) = \frac{2Ag_n T^2 \pi^2}{3} \frac{p_e}{E_e} \frac{\partial}{\partial p_e} (E_N - E_P - E_e)^2 \frac{p_e}{E_e} \Big|_{p_e = k_e} \quad (4.53)$$

$$\Gamma_n(+) + \Gamma_n(-) = -\frac{2Ag_n T^2 \pi^2}{3} \frac{p_e}{E_e} \frac{\partial}{\partial p_e} (E_N - E_P - E_e)^2 \Big|_{p_e = k_e}, \quad (4.54)$$

where remember that $E_e(p_e, n)$. We can sum over each of these to get the total decay rate, then take the ratio to get the average helicity. The important values are $E_N - E_P = \mu_e \sim k_e$ and the sum goes up to $n_{max} = k_e^2 / 2m_e^2 b$. The details after this are largely uninteresting and is computed by doing the sum numerically. As a check we find that the helicity at zero magnetic field is $\langle \Lambda \rangle = -1$ as we expect. Over the range of fields we are interested $B = 10^{12} - 10^{15}$ G the helicity is surprisingly constant. We arrive at

$$\langle \Lambda \rangle \simeq -0.84. \quad (4.55)$$

The helicity is close to -1, but not so close that it doesn't warrant a comment. With a large magnetic field the electron is forced into Landau levels. The single spin down state in the lowest level sometimes forces the electron into a right-handed configuration to conserve momentum. This occurs when the proton is created with the same spin as the initial neutron. In this case the electron and the neutrino must have opposite spins. If the electron is forced by the lowest Landau level to be spin down then the antineutrino must be spin up. Being right-handed, the antineutrino moves up in the direction of its spin. In order to conserve momentum the electron

must move down, forming a right-handed configuration. The electron is bullied into being right-handed by the antineutrino. The effect is not absolute though, and the intrinsic left-handedness of the weak interaction wins out.

4.2 Nuclear Matter: The Modified Urca Process

The direct Urca process is the simplest to consider, but it is unlikely to be the most common process in a star. It is much easier to conserve momentum if a nucleon is included to supplement momentum transfer. We will consider the mean free path of an electron scattering of a proton assisted by a neutron, equation (2.126). The inclusion of the nucleon-nucleon interaction into the matrix element is non-trivial and we will use the one pion exchange/Landau liquid method found in [119], the interaction illustrated in Figure 4.2.
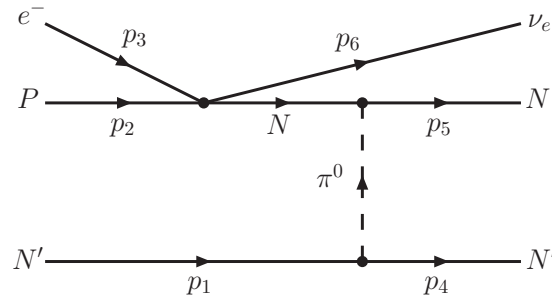
Figure 4.2: The modified Urca process.

There are many other diagrams similar to the one illustrated. They include all possibilities of pion exchange between protons and nucleons as well as crossing diagrams to account for the final neutrons being indistinguishable. Summing them all causes the vector contributions to cancel and we are left with the scattering matrix approximated to be

$$\sum_{spins} |\hat{S}|^2 = \frac{1}{\Omega^6} \frac{64 \, G_F^2}{(\mu_e)^2} C_A^2 \left(\frac{f}{m_\pi} \right)^4 \alpha_{\text{Urca}}, \tag{4.56}$$

where $f \sim 1$ is the p-wave πN coupling constant, $C_A = 1.26$ is the Gamow-Teller coupling, and $\alpha_{\text{Urca}} \sim (0.63 - 1.76)(n_0/n)^{2/3}$ is a factor that accounts for the pion propagator and the short range Landau liquid contributions. Following [119], but somewhat preempting the calculation, we approximate the propagator of the in-

ternal nucleon using the total lepton energy μ_e—remember that the energy the neutrino carries away is negligible.

To calculate the mean free path we will first calculate the transition rate

$$w = \frac{\Omega^6}{(2\pi)^{18}} \prod_{i=1}^{6} \int d^3 p_i \,\mathscr{S}\, (2\pi)^4 \Omega\, \delta^{(4)}(p_f - p_i) \sum_{spins} |\hat{S}|^2, \tag{4.57}$$

where S is the Pauli blocking factor.

We separate the transition rate into angular and radial parts leaving

$$w = \frac{\Omega}{(2\pi)^{14}} \sum_{spins} |\hat{S}|^2 \, P \, Q, \tag{4.58}$$

where

$$P = \prod_{i=1}^{6} \int p_i^2 dp_i \,\mathscr{S}\, \delta(E_f - E_i), \tag{4.59}$$

$$Q = \prod_{i=1}^{6} \int d\Omega_i \, \delta^{(3)}(\mathbf{p}_f - \mathbf{p}_i). \tag{4.60}$$

We start with the Q integral. The contribution from the momentum of the neutrino is negligible compared to the rest so we neglect it in the δ-function. This allows us to take an integral over all angles causing the term with angular dependence to vanish. As evaluated in Appendix B the angular integral is

$$Q = \frac{(4\pi)^5}{2 p_1 p_4 p_5}. \tag{4.61}$$

We can now do the PQ integral. Changing variables from momentum to energy and approximating the energy by the particle's fermi energy changes the measures to

$$p_1 dp_1 = m_N^* dE_1, \tag{4.62}$$
$$p_2^2 dp_2 = \mu_e m_P^* dE_2, \tag{4.63}$$
$$p_3^2 dp_3 = \mu_e^2 dE_3, \tag{4.64}$$
$$p_4 dp_4 = m_N^* dE_4, \tag{4.65}$$
$$p_5^2 dp_5 = m_N^* dE_5, \tag{4.66}$$
$$p_6^2 dp_6 = E_6^2 dE_6, \tag{4.67}$$

where we took $k_P \sim \mu_e$. Then we take the E_6 integral over the delta function and make substitutions $x_i = \pm\beta(E_i - \mu_i)$ to make the remaining integral dimensionless as in the direct Urca case. Compared to direct Urca, the two extra particles

contribute two more Fermi distributions to the statistical factor,

$$\mathscr{S} = \prod_{i=1}^{5} \frac{1}{1 + e^{x_i}} .$$
(4.68)

Using the beta equilibrium condition, $\mu_P + \mu_e = \mu_N$, all chemical potentials cancel, leaving

$$PQ = \frac{(4\pi)^5}{2} (m_P^*)^2 (m_N^*)^4 \mu_e T^7 I,$$
(4.69)

where I is the analytic integral evaluated in Appendix B,

$$
\begin{aligned}
I &= \prod_{i=1}^{5} \left(\int_{-\infty}^{\infty} \frac{dx_i}{1 + e^{x_i}} \right) \left(\sum_{j=1}^{5} x_j \right)^2 \Theta(x_1 + x_2 + x_3 + x_4 + x_5), && (4.70) \\
&= \prod_{i=1}^{4} \left(\int_{-\infty}^{\infty} dx_i \right) \int_{-(x_1+x_2+x_3+x_4)}^{\infty} dx_5 \left(\sum_{j=1}^{5} x_j \right)^2 \prod_{k=1}^{5} \frac{1}{1 + e^{x_k}}, && (4.71) \\
&\approx 192. && (4.72)
\end{aligned}
$$

Gathering all the terms together we get the transition rate per unit volume for an electron scattering off a proton assisted by a neutron,

$$
\begin{aligned}
\frac{w}{\Omega} &= \frac{G_F^2 C_A^2}{\pi^9} \frac{(m_N^*)^3 m_P^* \mu_e}{m_\pi^4} \alpha_{\text{Urca}} T^7 I, && (4.73) \\
&= 9.2 \times 10^{26} \left(\frac{\mu_e}{100 \text{ MeV}} \right) \left(\frac{m_N^*}{m_N} \right)^4 T_9^7 \ s^{-1} \ cm^{-3}, && (4.74)
\end{aligned}
$$

where as discussed earlier $m_N^* \sim m_P^* \sim 0.8 m_N$. The rate of this process is much smaller than we found earlier in the direct case (4.24) and the temperature dependence is now T^7 rather than T^5. Also, because of the density dependence of α_{Urca}, the transition rate is independent of density. Both of these differences result from this being a higher order calculation that involves two extra particles—the ingoing and outgoing neutron assisting in momentum conservation. This means that the transition rate is suppressed by a factor of α_{Urca} and that two extra factors of T to appear from the two extra measures of integration.

4.2.1 Estimate of the Current from Modified Beta Decay

We are interested in the mean free path of an electron. The volume occupied by a single electron is $\Omega_e \sim 10^{-36} \text{ cm}^3$, and the electron moves at the speed of light,

leaving the mean free path to be

$$\ell_e \sim 1.4 \times 10^{15} \, (T_9)^{-7} \left(\frac{n}{n_0} \right)^2 \text{ km.} \tag{4.75}$$

At the beginning of the star's life, when it is very hot $T \sim 10^{12}$ K, the electrons are trapped, then as the star cools the electrons are allowed to escape. Here we get a similar counterintuitive density dependance as (4.27) but the effect is stronger because there are two neutron Pauli blocking terms to contend with.

We now follow the same prescription as earlier to arrive at the value for the current,

$$J_v = 7.7 \times 10^{-14} \left(\frac{n}{n_0} \right)^{-4/3} T_9^7 \text{ MeV.} \tag{4.76}$$

This is by far the weakest current from any phase of matter. As before the current is strongest early in the star's life when it is hot, and though it is suppressed it can get quite large at high temperatures due to the T^7 dependence.

4.3 Kaon Condensate

As the density of the star gets above three times nuclear density is it possible that a charged kaon condensate will appear [66]. It is now energetically favourable for electrons to scatter off the condensate and turn into neutrinos. We are interested in calculating the transition rate of an electron decaying in the presence of a kaon condensate, equation (2.128). The effect of condensates on the scattering matrix was first used to describe pion condensates [68] and later for kaon condensates [70, 120] and involves evaluating the process given by the Feynman diagram in Figure 4.3.
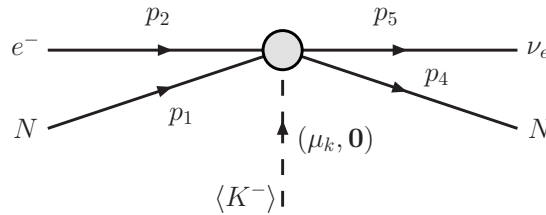
Figure 4.3: Electron decay in a kaon condensate.

The process needs the aid of a nucleon, similar to that of the modified beta decay, but the four-momentum from the kaon condensate does make it easier for energy-momentum to be conserved during the process. We start with the usual hadron and lepton currents and the kaon condensate is described by a chiral rotation in V-spin space, $U = e^{i\gamma^5\theta}$. For kaons a small rotation can have a large effect so only $\theta \ll 1$ must be considered. The matrix element, as found in [70], is given by

$$\sum_{\text{spins}} |\hat{S}|^2 = \frac{G_F^2\theta^2}{4\Omega^4}(1 + 3C_A^2)\sin^2\theta_c, \tag{4.77}$$

where $\theta^2 \sim 0.1$ is the kaon amplitude, $C_A = 1.26$ is the Gamow-Teller coupling, and $\theta_c \sim 13°$ is the Cabibbo angle.

We are interested in the regime where the kaon momentum $\mathbf{p}_3$ is zero. The transition rate is given by

$$w = \frac{\Omega^4}{(2\pi)^{12}} \int d^3p_1 d^3p_2 d^3p_4 d^3p_5 \,\mathscr{S}\,(2\pi)^4\Omega\delta(p_f - p_i)|\hat{S}|^2. \tag{4.78}$$

where S is the statistical factor containing Fermi blocking terms, Ω is the volume of the neutron star. The subscripts on p_1, p_2, p_4, and p_5, label the momentum of the ingoing neutron, the electron, the outgoing neutron, and the neutrino, respectively. Following the work done in [65] we can separate the angular and radial integrals so each can be evaluated independently,

$$w = \frac{\Omega^5}{(2\pi)^8} \sum_{\text{spins}} |\hat{S}|^2 PQ, \tag{4.79}$$

where

$$P = \int p_1^2 dp_1 \, p_2^2 dp_2 \, p_4^2 dp_4 \, p_5^2 dp_5 \,\mathscr{S}\,\delta(E_f - E_i), \tag{4.80}$$

$$Q = \int d\Omega_1 \, d\Omega_2 \, d\Omega_4 \, d\Omega_5 \,\delta^{(3)}(\mathbf{p}_f - \mathbf{p}_i). \tag{4.81}$$

We start by doing the angular integral Q is done in Appendix B and is the same as in earlier cases,

$$Q = \frac{(4\pi)^3}{2p_1p_2p_4}. \tag{4.82}$$

The PQ integral can now be started,

$$PQ = \frac{(4\pi)^3}{2p_1p_2p_4} \int p_1^2 dp_1 \, p_2^2 dp_2 \, p_4^2 dp_4 \, p_5 dp_5 \,\mathscr{S}\,\delta(E_1 + E_2 - E_3 - E_4 - E_5). \tag{4.83}$$

We first change the variables of integration from momentum to energy $p_i dp_i = E_i dE_i$ and perform the neutrino integral over the delta function. In an effort to make the final integral tractable, we follow [65] in approximating factors next to the measures as constant. The neutrons are non-relativistic so their energy is just their effective mass, m_N^*, and the electron is ultra relativistic, because of its large Fermi momentum, and the energy is just its chemical potential, μ_e. As before, these factors can then be moved outside the integral. It is also convenient to change variables to facilitate the final integral over the Pauli blocking factors. Changing variables takes $(E_1 + E_2 - E_3 - E_4)^2$ to $(x_1 + x_2 + x_4)^2 T^2$, where we used the equilibrium condition $\mu_k = \mu_e$. Upon changing variables the measure of integration gives us a factor T^3 and we are left with

$$PQ = \frac{(4\pi)^3}{2} (m_N^*)^2 \mu_e T^5 I, \tag{4.84}$$

where I is the same analytic integral that arises from the statistical factor $\mathscr{S}$ in the direct Urca process (4.21).

Putting everything together we get the transition rate per unit volume of an electron decaying into a kaon,

$$\begin{aligned}
\frac{w}{\Omega} &= \frac{G_F^2 \theta^2}{(2\pi)^5} (1 + 3C_A^2) \sin^2 \theta_c (m_N^*)^2 \mu_e T^5 I \tag{4.85} \\
&= 4.4 \times 10^{29} \left(\frac{\mu_e}{100 \text{ MeV}} \right) \left(\frac{m_N^*}{m_N} \right)^2 \left(\frac{n}{n_0} \right)^{2/3} (T_9)^5 \text{ s}^{-1} \text{ cm}^{-3}, \tag{4.86}
\end{aligned}$$

where $T_9 = T/(10^9 \text{ K})$ is the scaled temperature, and $m_N^* \sim 0.8 m_N$. The temperature dependance is the same as the direct Urca process (4.24), but we would expect it to be of higher order than direct Urca because it involves an extra particle, and thus smaller. The temperature dependence is the same because of the way we treat the kaons as a condensate, rather than an extra particle. The condensate picture is a rotation of the direct process, rather than a whole new particle interaction as in the modified Urca process.

4.3.1 Estimate of the Current in a Kaon Condensate

Because of the high chemical potential the electrons must be relativistic leaving the mean free path to be

$$\ell_e = 3.0 \times 10^{12} (T_9)^{-5} \left(\frac{n}{n_0} \right)^{4/3} \text{ km}. \tag{4.87}$$

Once again the mean free path larger than the radius of the neutron star and the electrons can escape. We also notice the counterintuitive, but now familiar, density

dependence discussed in the direct Urca case. This effective mean free path with the helicity intrinsic in the weak interaction creates a current given by equation (3.32),

$$J_{\mathrm{v}} \simeq 3.6 \times 10^{-11} \, (T_9)^5 \left(\frac{n}{n_0}\right)^{-2/3} \mathrm{MeV}. \tag{4.88}$$

Though the generation of the current in a kaon condensate happens though a wildly different process than direct Urca, and the numbers we use are quite different, we see that after the star has cooled the numbers conspire to give currents of similar magnitude (4.28).

4.4 Quark Matter

The last case we consider is what would occur if the hadrons separated into their constituent quarks. This is the case in quark stars, where degenerate quarks exist deconfined. In calculating the mean free path of electrons in quark matter there are two possible reactions we must consider, if we restrict ourselves to the lightest quarks, given in equation (2.129). Each is given by the Feynman diagram in Figure 4.4, where the d quark can be substituted out for the s quark.
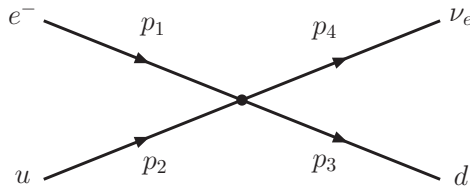
Figure 4.4: The direct Urca process for quarks.

Unlike nuclear beta decay, the lowest order quark beta processes do not require help from an external particle to to conserve momentum; they proceed unsuppressed [67]. Because they are deconfined, the Fermi momentum of the quarks are much closer to each other than the Fermi surfaces of the hadrons in neutron stars. We will first consider the transition into the down quark. The transition rate is given by

$$w = \frac{\Omega^4}{(2\pi)^{12}} \int d^3p_1 \, d^3p_2 \, d^3p_3 \, d^3p_4 \, S \, (2\pi)^4 \Omega \, \delta^{(4)}(p_f - p_i) \, |\hat{S}|^2, \tag{4.89}$$

where S is the statistical factor containing Fermi blocking terms, Ω is the volume of the phase space. The subscripts on p_1, p_2, p_3, and p_4, label the momentum of the ingoing electron, the up quark, the down quark, and the neutrino, respectively. The matrix element of this process is found in [67],

$$|\hat{S}|^2 = \frac{6}{\Omega^4} G_F^2 \cos^2\theta_c \frac{16\alpha_s}{3\pi}\left[1 - \frac{\mathbf{p}_3 \cdot \mathbf{p}_4}{E_3 E_4}\right], \tag{4.90}$$

which looks similar to the usual four Fermi matrix element but contains corrections due to the ability to relate the quark's momentum to the quark gluon coupling constant by $\alpha_s = \frac{g^2}{4\pi}$. We have also included the factor to account for the degrees of freedom of the quark here. The transition rate can be split into two integrals,

$$w = 64\frac{\Omega}{(2\pi)^9} G_F^2 \cos^2\theta_c \alpha_s PQ, \tag{4.91}$$

where

$$P = \prod_{i=1}^{4} \int p_i^2 dp_i \, S \, \delta E_f - E_i, \tag{4.92}$$

$$Q = \prod_{i=1}^{4} \int d\Omega_i \delta^{(3)}(\mathbf{p}_f - \mathbf{p}_i)\left[1 - \frac{\mathbf{p}_3 \cdot \mathbf{p}_4}{E_3 E_4}\right]. \tag{4.93}$$

These integrals are nearly identical to the kaon case. The Q integral is the same as in the direct Urca case (4.9). We make an approximation to the remaining PQ integral when we change variables from momentum to energy. As we have done in previous integrals, the momentum of the electron and quarks is replaced by their value at the fermi surface. Performing the neutrino integral, dE_4, over the delta function leaves us with the same integral as equation (4.15). We perform a similar change of variables as before to make the integral dimensionless. Following the same procedure as the direct Urca case, the quark beta equilibrium condition $\mu_e + \mu_u = \mu_d$ causes the chemical potentials to cancel, and the PQ integral becomes

$$PQ = \frac{(4\pi)^3}{2}\mu_e k_u k_d T^5 I, \tag{4.94}$$

where I is the same integral given in equation (4.21), which is the same as the direct Urca and kaon cases. An identical calculation can be done for the electron scattering into strange quarks. Putting everything together we get the transition rate for electrons in quark matter,

$$w_d = \Omega\frac{4}{\pi^6} G_F^2 \cos^2\theta_c \, \alpha_s k_e k_u k_d T^5 I, \tag{4.95}$$

$$w_s = \Omega\frac{4}{\pi^6} G_F^2 \sin^2\theta_c \, \alpha_s k_e k_u k_s T^5 I. \tag{4.96}$$

To estimate the magnitude of the transition we assume that $k_d \approx k_u \approx k_s$ as in the massless noninteracting case and use the relationship $k_e \approx \mu_e = (3Y_e)^{1/3}k_q$, where $Y_e = n_e/n_b$ is the ratio of electrons to baryons in the star. The Fermi momentum of the quarks is estimated using (5.7). We follow [67] in estimating $\alpha_s \approx 0.4$ and [60] for estimating $Y_e = 1 \times 10^{-3}$.

The total transition rate is the sum of w_s and w_d,

$$\frac{w}{\Omega} = 8.0 \times 10^{30} \left(\frac{n_b}{n_0} \right) (T_9)^5 \text{ s}^{-1} \text{ cm}^{-3}. \tag{4.97}$$

We see the T^5 temperature behaviour that has become a signature for the first order, four Fermi interaction.

4.4.1 Estimate of the Current in Quark Matter

As before, the first step in finding the current is estimating the mean free path of the electron in quark matter by assuming that the electron propagates at the speed of light. The same physics creates the current in quark matter and it is still non-dissipating. We now use the new definition of n_e to determine the volume occupied by a single electron, $\Omega = (Y_e n_b)^{-1}$, and we are left with

$$\ell_e = \frac{c}{w} = 1.2 \times 10^{10} (T_9)^{-5} \text{ km}. \tag{4.98}$$

The radius of the star, $R \sim 10$ km, is much smaller than this and the current will propagate. In quark matter the mean free path is not dependent on density; the Pauli suppression and enhancement cancel each other. When the electrons reach the crust they are removed from the system creating a new effective mean free path for the electron. This effective mean free path with the helicity intrinsic in the weak interaction creates a current

$$J_v = 7.0 \times 10^{-9} (T_9)^5 \left(\frac{n_b}{n_0} \right)^{1/3} \text{ MeV}. \tag{4.99}$$

The typical density for quark matter is $n_b \sim 10n_0$, but could easily be higher. Once again the numbers have conspired and the magnitude of the current is close to the value for both direct Urca (4.28) and kaon (4.88) processes. They are all first order processes, but we see a critical difference in the density dependence. Unlike the other currents the quark current actual gets larger with increasing density. This happens because quark stars remain charge neutral in a fundamentally different way than neutron stars, as discussed in Section 2.2.2 and the electron chemical potential is determined differently.

Table 4.1: A summary of the current per magnetic flux quantum calculated from each interaction. The value is for a single quantum of flux, such as that found in a type-II vortex. The appropriate density for the kaon and the direct Urca currents is $n = 3n_0$, for quarks is $n_b = 10n_0$, and for modified Urca is $n = n_0$.

	Current J_{V} (MeV)
Direct Beta Decay	$9.4 \times 10^{-10} \left(\frac{n}{n_0} \right)^{-2/3} (T_9)^5$
Modified Beta Decay	$7.7 \times 10^{-14} \left(\frac{n}{n_0} \right)^{-4/3} (T_9)^7$
Kaon Condensate	$3.6 \times 10^{-11} \left(\frac{n}{n_0} \right)^{-2/3} (T_9)^5$
Quark	$7.0 \times 10^{-9} \left(\frac{n_b}{n_0} \right)^{1/3} (T_9)^5$

4.5 Summary of Estimates

We have calculated the magnitude of the topological vector current in four types of nuclear matter and summarize them in Table 4.1. Direct beta decay, which is also the preferred reaction when hyperons are present, kaon condensates, and quark matter, all are radically different, but they all make a current about the same order. There is a stark difference in the modified Urca process, which occurs in ordinary nuclear matter where the proton fraction is below $1/9$. The current is four orders of magnitude smaller than the rest. This is because it is a higher order process involving more particles. It results in a more severe dependance on temperature which suppresses the process when the star cools.

The estimates of the current are relatively small in magnitude, but much larger currents exist on microscopic scales. The estimates represent a component of the current that produces a coherent effect in the entire region where matter is degenerate and the magnetic field all points in one direction. As a technical remark, the estimates of the current J_{V} are presented in MeV units. The current is defined as a number of particles crossing the surface equivalent to one quantum of magnetic flux per unit time. We can obtain the electromagnetic current in conventional units by multiplying by $e = \sqrt{4\pi\alpha}$ and converting the result into Amperes: $eJ_{\text{V}} \sim 10^2$ A for $J_{\text{V}} = 1$ MeV.

Chapter 5

Large Pulsar Kicks Generated by Topological Currents

We will discuss the application of topological currents to neutrons star kicks. The discussion follows that first presented in Charbonneau and Zhitnitsky [9] and Charbonneau, Hoffman, and Heyl [10]. We have spent the last chapter calculating the magnitude of the current for many different phases of matter. We will now directly use these values to discuss whether or not the current could be responsible for a kick, and if so, how big of a kick could the current possibly produce.

It is accepted that pulsars have much higher velocities than their progenitors, some moving as quickly as 1000 km/s [87, 93, 121–126]. There have been a number of studies that have compiled and modelled the velocities of pulsars. Although they disagree on whether the distribution is indeed bimodal, they agree that a significant number of pulsars are travelling faster than can be attributed to neutrino kicks. The analysis of [87] favours a bimodal velocity distribution with peaks at $90 \ \mathrm{km\,s^{-1}}$ and $500 \ \mathrm{km\,s^{-1}}$ with 15% of pulsars travelling at speeds greater than $1000 \ \mathrm{km\,s^{-1}}$. Alternatively [88] and [89] both argue for a single peaked distribution with an average velocity of $\sim 400 \ \mathrm{km\,s^{-1}}$, but point out that the faster pulsars B2011+38 and B2224+64 have speeds of $\sim 1600 \ \mathrm{km\,s^{-1}}$. Large velocities are unambiguously confirmed with the model independent measurement of pulsar B1508+55 moving at $1083^{+103}_{-90} \ \mathrm{km\,s^{-1}}$ [127]. Our goal is to explain these large kicks.

Currently no mechanism exists that can reliably kick the star hard enough. Explosions during collapse can only reliably kick a star 50 km/s [93], asymmetric explosions can only reach 200 km/s [126], and asymmetric neutrino emission is plagued by the problem that at temperatures high enough to produce the kick the neutrino is trapped inside the star [128, 129]. Recent hydrodynamic models that include neutrino luminosities to drive the explosions have been more successful [94, 95] in reaching the higher velocities observed. These models require maximum asymmetry due to instabilities and neutrino energy to be artificially introduced and fail to intrinsically predict the alignment of the spin and kick. The simulations also end before most of the kick is created and the actually kick velocity is an extrapolated result. However, they are very promising models. More

exotic mechanisms require exotic particles and more fine tuning. Alterations of the neutrino model that take into account only a thin shell of neutrinos require large temperatures and huge surface magnetic fields.

Another aspect of the kick we must account for is the apparent agreement between the direction of the kick and the rotation axis of the star [130]. With current models it is impossible to determine whether the kick direction and spin are aligned or anti-aligned or randomly distributed. But this alignment has lead to the hypothesis that kicks must be of long duration, much larger than the spin period [86].

The kick mechanism we will discuss relies on the existence of topological vector currents which have spent the last few chapters developing,

$$J_{\mathrm{v}} = (\mu_L - \mu_R)\frac{e\Phi}{(2\pi)^2}, \tag{5.1}$$

where μ_R and μ_L are the chemical potential of the right and left-handed electrons, and Φ is the magnetic flux. There are three requirements for topological vector currents to be present: an imbalance in left and right-handed particles $\mu_L \neq \mu_R$, degenerate matter $\mu \gg T$, and the presence of a background magnetic field $B \neq 0$. All of these are present in neutron and quark stars. The weak interaction, by which the star attains equilibrium, violates parity; particles created in this environment are primarily left-handed. The interior of the star is very dense, $\mu_e \sim 100$ MeV, and cold, $T \sim 1$ MeV, such that the degeneracy condition $\mu \gg T$ is met, and neutron stars are known to have huge surface magnetic fields, $B_{\mathrm{s}} \sim 10^{12}$ G.

If the electrons carried by the current can transfer their momentum into space—either by being ejected or by radiating photons—the current could push the star like a rocket. In typical neutron stars this is unlikely because the envelope (the region where $\mu \sim T$) is thought to be about 100 m thick. Once it reaches this thick crust, the current will likely travel along it and be reabsorbed into the bulk of the star. But if the crust is very thin, or nonexistent, the electrons may leave the system or emit photons that will carry their momentum to space. The electrosphere for bare quark stars is thought to be about 1000 fm [131][1]. With this in mind we conjecture that stars with very large kicks, $v \gg 200$ km s^{-1}, are quark stars and that slow moving stars, $v \leq 200$ km s^{-1}, are kicked by some other means, such as asymmetric explosions or neutrino emission, and are typical neutron stars. Confirmation of this would provide an elegant way to discriminate between neutron stars and quark stars. As is known, other criteria such as mass, size, cooling rate, etc. cannot

---

[1] It has been recently argued that a crust in quark stars could be much larger in size than previously thought due to development of a new heterogeneous mixed phase [132, 133]. As we mentioned above, it is not our goal to discuss the interaction of current with the crust, however, an intense current from the core of quark star may destroy the crust in this new mixed phase in few locations similar to volcanoes on earth.

easily discriminate between quark stars and neutron stars, see e.g. [64, 134] for review. This also naturally lends itself to a bimodal distribution for kick velocities as supported in [87].

The topological kicks we will discuss have a sustained nature that allows a rotation-kick correlation $\langle \vec{P} \cdot \vec{\Omega} \rangle$ to form regardless of the angle between the star's rotation and magnetic field. Neutron stars spin on the order of milliseconds, which is small compared to the kick duration. The force vectors from the kick form a cone aligned with the axis of rotation that average to produce a kick along the axis of rotation. Long duration kicks are supported by the analysis in [86].

Kicks caused by the topological current are very similar to neutrino kicks. The helicity of the electrons and the single spin state in the lowest Landau level allow electrons to travel with a preferred direction through the neutron star. The difference between the two mechanisms is the linear momentum that the particle transfers to the star. Neutrinos have an energy close to the temperature of the star, while the electrons, which are degenerate, have an energy close to their Fermi momentum. We will discuss this critical difference in Section 5.5.

A Rough Calculation

We will first provide a rough calculation demonstrating that topological kicks can provide the momentum required and do so because of the immense electron chemical potential, not because of the temperature of the star. Also, because of the correlation between the magnetic field and the spin axis, topological kicks naturally align with the spin axis of the star. Though it is unclear what will happen to the electrons when they reach the surface of the star, we can estimate the size of the kick if we assume the entire momentum carried by the topological current will be transferred into space by some means.

The first step in estimating the magnitude of a topological kick is determining the total momentum transferred to the star. There are $N_{\mathrm{v}} \sim 7 \cdot 10^{33}$ B/B_{c} quantum units of flux in a star that can be distributed in either superconducting domains or vortices, see eq. (2.142). The current is independent of the internal structure of the star. If all the electrons are shot out of the star or transfer their entire momentum, then the momentum is given by the total current (3.30), the number of electrons that leave the star per unit time. The momentum a single electron transfers out of the star is equal to its Fermi momentum, $k_e = 100$ MeV. The fuel for the kick is the chemical potential, not the temperature. Therefore the kick may continue even when star is already cool; the kick in our mechanism is not an instant event, but is rather a long, slow, steady process that pushes the star. Putting this all together, the current transfers $N_{\mathrm{v}} k_e \langle j \rangle$ units of momentum per unit of time.

The appropriate way to estimate the magnitude of the kick is to integrate the

rate of momentum transfer per unit time by taking into account the time evolution of the star. As Table 4.1 demonstrates, the current is very sensitive to temperature/time. We will account for this when we discuss the details of cooling later in this chapter. The rate of momentum transfer also changes as the star cools and the environment (density, phase) changes. We neglect all these complications for now and take a value for the current corresponding to $T \sim 10^9$ K.

The momentum transfer required for the star to reach a velocity of $v = 1000$ km/s is quite large. Per baryon, the momentum required is $m_n v \sim 3$ MeV. The total baryon number of a neutron star of one solar mass is $B_n \sim 10^{57}$. The momentum for the entire star is then $P \sim 3 \cdot 10^{57}$ MeV. If we choose a current $\langle j \rangle = 10^{-10} \, (T_9)^5$ MeV, corresponding to an average current in Table 4.1, the time required to attain this momentum is

$$
\begin{aligned}
t = \frac{P}{N_v k_e \langle j \rangle} &\approx 3 \cdot 10^{10} \left(\frac{v}{1000 \text{ km/s}} \right) \left(\frac{B_c}{B} \right) \left(\frac{10^{10} \text{ MeV}}{\langle j \rangle} \right) \left(\frac{10^9 \text{ K}}{T} \right)^5 \text{ s}, \\
&\approx 10{,}000 \text{ years},
\end{aligned}
\tag{5.2}
$$

We restore the canonical dimensionality of MeV^{-1} in seconds by multiplying $\hbar = 6.58 \cdot 10^{-22}$ MeV·s. This is a conservative estimate of the kick strength. The current is much larger at the star's birth (when it is hot) and kicks such as those seen in, for example, the Vela pulsar can be easily explained. If electrons actually leave the star, rather than transferring their momentum through radiation, the electron chemical potential will slowly decrease and the current may stop running. Charge neutrality will cause matter to accrete isotropically and possibly maintain some of the chemical potential.

The topological kick mechanism described here is similar to neutrino driven kicks in that both use P-odd effects and particles to carry momentum out of the star. The electron and neutrino have similar mean free paths, but the electrons leave much lower rate than the neutrinos. The fundamental difference in the two carriers in the energy they carry out of the star. At low temperatures, when the neutrinos can escape the star, they do not carry enough energy to explain the kick. In contrast, the electrons that make the non-dissipating current (or more precisely the quasi-particles which freely travel along the magnetic field) carry very large momentum $\sim \mu_e$. As a result the neutrino carries too little momentum when the mean free path becomes sufficiently long, while the momentum carried by the topological current remains very high even at very low temperatures $T \sim 10^8$ K. We will now discuss this in detail.

5.1   Simple Model of Quark Stars

As we focused mostly on neutron matter in the introduction we will review the model for quark stars used specifically for this calculation. The kick will likely only occur in quark stars that are bare or have very thin crusts. We will consider only the existence of light quarks in the star, which attain equilibrium through the quark direct Urca processes,

$$e^- + u\,(+\,\overline{\nu}_e) \quad \leftrightarrow \quad d\,(+\,\nu_e), \tag{5.3}$$

$$e^- + u\,(+\,\overline{\nu}_e) \quad \leftrightarrow \quad s\,(+\,\nu_e), \tag{5.4}$$

where the neutrino terms only appear in the final state of the interaction. The direct Urca processes in quark matter do not have the same Fermi momentum restrictions as in neutron matter and are thus not suppressed. These processes are at equilibrium when

$$\mu_u + \mu_e = \mu_d \quad \text{and} \quad \mu_u + \mu_e = \mu_s\,. \tag{5.5}$$

In this balance we ignore the neutrino chemical potential. In discussing the kick we will focus on temperatures where the star makes the transition from being opaque to neutrinos to being transparent. We will refer to this temperature range as the translucent regime. In the opaque regime the neutrino chemical potential is nonzero. As the star cools the mean free path of the neutrinos becomes large enough that all neutrinos created may freely leave the star. This is precisely the temperature at which the topological current begins to flow and creates a kick. In discussing these temperatures there is the concern that the neutrino chemical potential cannot be ignored. However, once in the transparent regime the neutrino chemical potential dissipates much faster than the time scale of the kick, thus we can safely ignore it.

The quark matter must also be electrically neutral,

$$\rho/e = \frac{2}{3}n_u - \frac{1}{3}n_d - \frac{1}{3}n_s - n_e = 0\,, \tag{5.6}$$

where ρ is the charge density and n_i are the number densities of the quarks and electrons. We will consider the simplest model where the quark masses are set to zero, thus their Fermi momenta are equal to their Fermi energies. Unfortunately, this approximation requires the electron density to be zero to satisfy equation (5.6), thus removing an essential element from the star: electrons. The strange quark mass is quite large and the number density should be described using nonrelativistic Fermi statistics, which readmits electrons into the mix to conserve charge. We will follow [67] by assuming that the quarks are all massless and an electron chemical potential is present to capture the contribution of the mass of the strange quark.

The Fermi momentum of the quark species can be written in terms of the baryon number density, denoted n_b, as

$$k_q = (\pi^2 n_b)^{1/3} \sim 235 \left(\frac{n_b}{n_0}\right)^{1/3} \text{MeV}. \tag{5.7}$$

For typical densities in the core of the neutron star the Fermi momentum is $k_q \sim 400$ MeV, which is greater than the strange quark mass. Neglecting the mass of the strange quark is a crude approximation but works well for this calculation. We can obtain the electron Fermi momentum using the fraction of electrons to baryons, $Y_e = n_e/n_b$, which yields

$$k_e = (3Y_e)^{1/3} k_q \sim 10 \left(\frac{n_b}{n_0}\right)^{1/3} \text{MeV}. \tag{5.8}$$

Because $k_e \gg m_e$, we find that $k_e \sim \mu_e$. [60] state a typical value for the electron fraction as $Y_e \lesssim 10^{-3}$, which is the value we will use. In the very core of the star the electron fraction may be lower $Y_e < 10^{-4}$[72]. This value is not critical in determining the strength of the kick because we will find that the dependance on k_e cancels. However, as we will discuss in Section 5.5, the value of the Fermi momentum k_e when compared to the core temperature of the star T_{core} is critical in understanding how topological currents generate large kicks.

5.2 The Cooling of Quark Stars

In order to properly determine the size of a kick we need to understand how the core temperature of the quark star evolves with time. Unfortunately, kicks are likely to occur right after the birth of the star during the most poorly understood stage of cooling. For insight into the cooling curve of a quark star we follow the work in two papers. The initial cooling of the star is described in [135], which focuses on neutrino diffusion through the star and thermal cooling. The star then cools until the neutrinos can escape the quark star and the cooling moves into a purely radiative regime as discussed in [136]. The part of the cooling curve between these two well defined mechanisms constitutes the translucent regime.

The quark direct Urca processes, which are weak interactions, create both the neutrinos responsible for cooling the star and the parity that drives the current. The topological current only flows when the mean free path of the electron with respect to the weak interaction is larger than the neutron star. As they take part in the same processes, this is also when neutrinos start to escape the star. The mean free path of the weak interaction for an electron in quark matter has been calculated in [9]
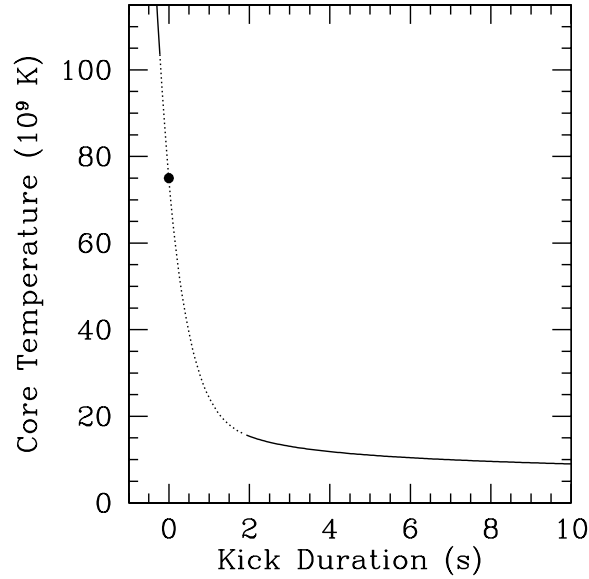
Figure 5.1: The dashed line indicates the translucent part of the cooling curve, modelled by exponential decay. The curve before the patch is taken from [135] and the curve after the patch is from [136]. The black dot marks the start of the kick at $t = 0$.

and is

$$\ell_e = 1.2 \times 10^{10} \left(\frac{T_{\text{core}}}{10^9 \text{ K}} \right)^{-5} \text{ km}. \tag{5.9}$$

Equation (5.9) tells us that for a star of radius $R \sim 10$ km the current starts to flow at $T_{\text{core}} \sim 8 \times 10^{10}$ K. At this point on the cooling curve the temperature changes on the scale of seconds.

   It is not clear how to model the short but critical cooling period that occurs in the translucent regime, as it is a very complicated process, but we assume it must make a smooth transition from the primarily thermal cooling of the core found in [135] to the neutrino cooling found in [136]. Because we are interested in an estimate of the kick and not the exact details of the cooling we will interpolate between these two cooling curves by assuming the transition is smooth and exponential. We will use the cooling curve from Figure 2a of [135] that models the cooling of the core of the star. We then piece it together using an exponential decay to cool the star to $10^{10.2}$ K and match the initialization of the cooling curve given in Figure

1 of [136]. By requiring that the first derivatives are equal it is possible to find a unique exponential decay that patches these cooling curves together. Figure 5.1 plots this patched region that describes the translucent region of the cooling curve.

It is possible that the cooling in the translucent regime is quite different from the exponential patch we propose. The severity of the exponential cooling provides us with a reasonable guess for the lower bound of the kick. Slower cooling in the translucent regime would result in larger kicks.

5.3 Estimating the Size of the Kick

The topological current runs along the magnetic field of the star and consists of electrons created in the core of the star travelling to the surface. Once at the surface these electrons transfer net momentum to the star. We assume that the absence of a crust on the quark star will allow all of the electron's momentum to be transferred. The electrons may be physically ejected from the star or the momentum may be transferred by some radiative process such as bremsstrahlung. The size of the kick is directly related to the strength of the current, which is related to the creation rate of left-handed electrons in the quark star and the population of electrons in the lowest Landau level. The calculations regarding the strength of the current in this paragraph are detailed in [9]. We provide only a brief illustrative overview here. The direct Urca processes for quarks create electrons at a rate per unit volume

$$
\frac{w}{\Omega} \;=\; \frac{G_F^2}{\pi^6}\,\alpha_s\,k_e\,k_q^2\,T^5\,I\,, \tag{5.10}
$$

$$
\;=\; 8.0 \times 10^{30}\left(\frac{n_b}{n_0}\right)\left(\frac{T_{\text{core}}}{10^9\ \text{K}}\right)^5\ \text{s}^{-1}\ \text{cm}^{-3}\,, \tag{5.11}
$$

where $\alpha_s = g^2/4\pi \approx 0.4$ and $I \approx 20.6$ is a dimensionless integral. The helicity of the electrons $\langle\Lambda\rangle = -0.84$ and the fraction of electrons in the lowest Landau level are contained in the parameter

$$
P_{\text{asym}}(\mu_e, T, B) \;\simeq\; -\langle\Lambda\rangle \cdot \left(\frac{m_e^2}{k_e^2}\frac{B}{B_c}\right)\,, \tag{5.12}
$$

$$
\;\simeq\; 2 \cdot 10^{-4}\left(\frac{B}{B_c}\right)\left(\frac{n_b}{n_0}\right)^{-2/3}. \tag{5.13}
$$

The total number current for electrons reaching the surface of the star is given

by

$$J_v = P_{asym} \frac{w}{\Omega} V_{star}, \tag{5.14}$$

$$= 2.6 \times 10^{26} \left(\frac{10 \, \text{MeV}}{k_e} \right) \left(\frac{B}{10 \, B_c} \right) \left(\frac{T_{core}}{10^9 \, \text{K}} \right)^5 \left(\frac{n_b}{n_0} \right)^{1/3} \text{MeV}, \tag{5.15}$$

where $B_c = 4.4 \times 10^{13}$ G is the critical magnetic field, T_{core} is the core temperature of the star, and n_0 is nuclear density. The typical density for quark matter is $n_b \sim 10 n_0$ but could easily be higher.

Because the current originates in the core of the star, we are interested in the strength of the internal magnetic field. Though many pulsars have a surface field of around 10^{12} G, the field in the bulk of the star is likely much stronger based on virial theorem arguments in [137]. The scalar virial theorem for the star states that

$$2T + W + 3\Pi + \mathcal{M} = 0, \tag{5.16}$$

where T is the total rotational kinetic energy, Π is the internal energy, W is the gravitational energy, and $\mathcal{M}$ is the magnetic energy. Because the kinetic energies are positive, the magnetic field energy can be at most equal to the gravitational energy, $(4\pi R^3/3)(B_{max}^2/8\pi) \sim GM^2/R$, which yield possible core fields of $B_{max} \sim 10^{18}$ G. This is an extremely large field and is unlikely as it is a strict upper bound. Based on this we choose a value of the core magnetic field to be $B_{core} = 10 B_c$.

The current, equation (5.14), gives a number rate of electrons reaching the surface of the star. To get the momentum transferred per second we simply multiply by the momentum each electron carries, k_e, which is large due to the degeneracy and is given by equation (5.8). The acceleration for a $1.4 M_\odot$ star is then

$$a = \frac{k_e \langle j(T_{core}) \rangle}{1.4 M_\odot}. \tag{5.17}$$

We see that all the factors of k_e cancel because $\langle j \rangle$ contains a factor of k_e^{-1} and the precise value of Y_e is not important. The kick is independent of the Fermi momentum of the electrons, but as we will discuss later this does not mean the Fermi momentum is unimportant.

As seen in Figure 5.2, the star quickly reaches a speed of

$$v_{max} \sim 1600 \, \text{km s}^{-1}, \tag{5.18}$$

which is big enough to account for the large kicks seen in many pulsars. This result relies on the internal magnetic field of the star being two orders of magnitude larger than what we observe on the surface of most pulsars. We have also neglected the
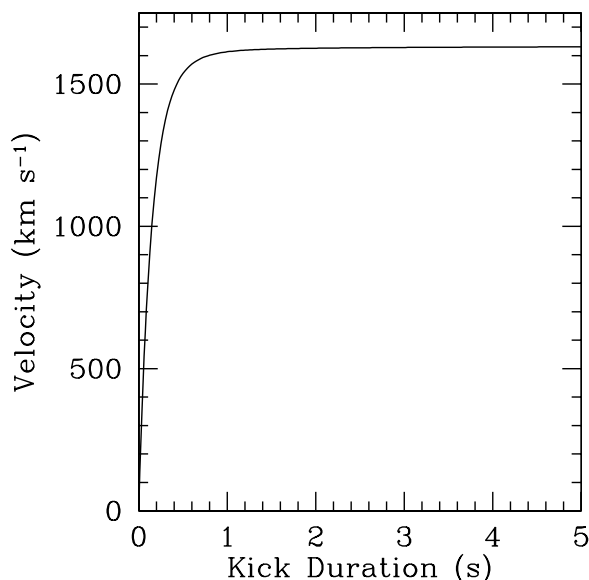
Figure 5.2: Time evolution of the kick for an internal magnetic field $B = 10\,B_c$.

dissipation of electrons in the electrosphere of the quark star. As plotted, the entire kick seems to happen very quickly, but the current keeps running throughout the star's life. With a large internal magnetic field the mechanism can account for kicks seen in young pulsars. But because the kick is constantly running, pulsars with smaller internal magnetic fields will eventually attain very large speeds very late in life.

5.4   The Effect of the Kick on Cooling

We want to ensure that the energy from the kick does not contribute significantly to the cooling of the star and that the neutrinos remain the dominant cooling mechanism during the kick. We find that at the beginning of the star's life the energy from the kick does not contribute to the cooling of the star, but later in life the current could become the dominant cooling mechanism.

The reason is that only a small fraction of the electrons created in the neutron star actually escape due to the low occupation of the lowest Landau levels. As discussed earlier the estimate for the neutrino kick has a similar suppression factor, but all of the neutrinos actually escape the star, even those that do not contribute

toward a neutrino kick. The electrons only propagate because the asymmetry in the lowest Landau level allows the helicity states to propagate out of the star. Those electrons that do not contribute toward the kick are trapped inside the star. The helicity states that reach the surface due to the current are the only electrons that contribute to the cooling of the star. The neutrinos cool the star with a luminosity $L_\nu \sim Tw$ where the electrons cool the star with an energy current (luminosity) of $L_e \sim k_e n_L w$. The ratio of electron cooling to neutrino cooling is

$$\frac{L_e}{L_\nu} \sim \frac{\mu_e n_L}{T} = \frac{m_e^2}{\mu_e T}\frac{B}{B_c}. \tag{5.19}$$

At first the electrons cool the star at about 1/100 the rate of neutrino cooling. As the star cools, eventually $L_e/L_\nu > 1$ and the more energy is lost due to the current than the neutrinos. This transition occurs at a temperature

$$T_t \sim 10^{-2}\left(\frac{B}{B_c}\right)\text{ MeV} \sim 10^8 \left(\frac{B}{B_c}\right)\text{ K}, \tag{5.20}$$

well after the kick has occurred. If electrons are escaping the star, new charged particles will accrete to maintain charge neutrality and add energy back to the star. But these will likely be much lower energy than those propelled from the star. The current may be an additional cooling mechanism to consider in stars that have cooled below 10^8 K.

5.5   The Difference Between Topological Kicks and Neutrino Kicks

It is important to understand the differences between neutrino kicks and topological kicks because superficially they seem very similar. In both cases a particle is created through the weak interaction with a favoured helicity (left-handed)[2] and the large magnetic field forces the electrons into Landau levels. The lowest Landau level only accepts a spin down electron, whereas all the rest allow both spin up and spin down states. Combining the preferred helicity of the particles with the spin state asymmetry in the lowest Landau level means that the neutrinos and electrons now travel with a preferred direction within the star. If the star is cool enough, these particles can escape the star without decaying. The neutrino does not participate in QED interactions and the electrons propagate due to the current, which is allowed because parity is a symmetry of QED. The particles that exit the star provide the linear momentum required to push the star.

---

[2]In a dense star the electrons are created with an average helicity $\langle \Lambda \rangle = -0.84$, but for simplicity we will assume in this section that they are all left-handed.

The electrons and neutrinos that contribute towards the kick are created at the same rate w, given by equation (5.10). We are only interested in interactions that create particles in the lowest Landau level so this rate is suppressed by a factor to account for the population of the lowest Landau level. The momentum transferred to provide the kick is simply the momentum per particle that escapes the star. On the surface of the star, where the chemical potential is low, Boltzmann statistics are used to model the occupation of the lowest Landau level. This is what is seen in many neutrino kick models. This is because neutrinos require such hot temperatures to produce kicks that only a thin shell near the edge of the star is considered to contribute to the kick. In the core of the star, where the electrons are very degenerate, we must use Fermi statistics. This predicts an occupation of

$$n_{\mathrm{L}} \sim \left(\frac{m_e^2}{k_e^2} \frac{B}{B_{\mathrm{c}}} \right) \tag{5.21}$$

in the lowest Landau level in the interior of the star.

At core temperatures below 7×10^{10} K the neutrinos can escape the star and the topological current is active. The flux of particles contributing to both the electron kick and the neutrino kick is about the same $\sim n_{\mathrm{L}} w$. The difference between the two mechanisms comes from the momentum that the relevant particle carries. The neutrinos are created thermally and the typical momentum of a neutrino is equal to the temperature of the star T. The momentum of the electrons comes from the large chemical potential, $\mu_e \sim 10$ MeV. The momentum transfer per unit time for neutrinos[3] is $F_\nu \sim T n_{\mathrm{L}} w$ and for electrons is $F_e \sim \mu_e n_{\mathrm{L}} w$. When the kick starts the star has a temperature of only $T \sim 1$ MeV. The electron kick is stronger than the neutrino kick by a factor of

$$\frac{F_e}{F_\nu} \sim \frac{\mu_e}{T} . \tag{5.22}$$

Initially, when the star is very hot, the electron kick is an order of magnitude stronger than the neutrino kick. Furthermore, as the star cools the neutrino kick gets even weaker, while the electrons continue to have a momentum dictated by their chemical potential. This why electrons generate larger kicks than neutrinos.

5.6   Modelling the Translucent Regime in Figure 5.1

In calculating the strength of the kick it is necessary to model the cooling of the star. The bulk of the kick happens in a rather difficult part of the cooling which we

---

[3]Notice energy per unit time has the T^6 dependance we expect for a calculation involving neutrino luminosity.

call the translucent regime. This regime is where the star transitions from being opaque to neutrinos to being transparent. Properly modelling the current in this regime would be difficult so we patch it instead. Cooling is an exponential process so we model this patch with an exponential decay,

$$y = ae^{-bt} + c. \tag{5.23}$$

For convenience we will make $t = 0$ the point where the dotted line in Figure 5.1 starts and $t = \tau$ the point where the dotted line ends. We have four boundary conditions available to us

$$y(0) = a + c, \tag{5.24}$$
$$y'(0) = -ab, \tag{5.25}$$
$$y(\tau) = ae^{-b\tau} + c, \tag{5.26}$$
$$y'(\tau) = -abe^{-b\tau}. \tag{5.27}$$

These correspond to the value and slope of the cooling curves derived from neutrino diffusion on the opaque side and free streaming neutrinos on the transparent side.

These can be rewritten to solve for the unknowns in our exponential,

$$a = (y(\tau) - y(0)) \left(\frac{y'(\tau)}{y'(0)} - 1 \right)^{-1}, \tag{5.28}$$
$$b = -\frac{y'(0)}{a}, \tag{5.29}$$
$$c = y(0) - a, \tag{5.30}$$
$$\tau = \frac{\ln|y'(\tau)| - \ln|ab|}{-b}. \tag{5.31}$$

The values from the opaque cooling curve taken from [135] are

$$y(0) = 10^{11} \text{ K and } y'(0) = -0.95 \times 10^{11} \text{ K s}^{-1}, \tag{5.32}$$

and the values from the transparent cooling curve taken from [136] are

$$y(\tau) = 10^{10.2} \text{ K and } y'(\tau) = -4.06 \times 10^{9} \text{ K s}^{-1}. \tag{5.33}$$

Plugging these is we see our patch has the form

$$T = (8.79 e^{-1.08t} + 1.21)10^{10} \text{ K for } t > 0 \text{ and } t < 2.91 \text{ s}, \tag{5.34}$$

where $t = 0$ denotes where the dotted line starts in Figure 5.1. This is a very crude way to determine the cooling of the star during the translucent regime, but

it allows for a realistic estimate of the kick caused by the current. Hydrodynamic models take this complex cooling into account as part of their simulation, but many neutrino kick models rely on a constant temperature on 10^{11} K for up to 10 seconds to produce their kicks.

5.7   Summary

The introduction of this model of pulsar kicks, which we refer to as topological kicks, is the cumulation of the last three chapters. We have worked from first principles to develop a kick model. We have found that these topological kicks can generate kicks greater than $1000 \, \mathrm{km\,s^{-1}}$. This may explain large pulsar kicks that are otherwise unattainable using traditional kick mechanisms. Topological kicks occur only if the electrons that make up the topological current can transfer their momentum through the star's crust. Because neutron stars have thick crusts, it is unlikely that they will be kicked due to this mechanism, but rather by mechanisms that generate weak kicks. In contrast, bare quark stars have no crust and they may allow the electrons to escape. Because of this distinction we conjecture that many of the fastest pulsars are quark stars.

In calculating the kick velocity we assumed that the cooling curve of the quarks star must make a smooth transition from the primarily thermal cooling of the core found in [135] to the neutrino cooling found in [136]. This patched cooling curve allowed us to integrate over time the momentum transferred from the topological current and obtain the strength of the kick. We have also demonstrated that the energy lost due to the current does not change the cooling of the star during the kick. But, after the star cools below 10^9 K the topological current becomes the dominant cooling mechanism rather than neutrino emission.

The magnitude of the kick also depends on the strength of the magnetic field inside the star. The virial theorem puts a limit on the internal field of the star that is much higher than the surface field. To generate the kick we used a field strength of $B_{\mathrm{core}} = 10B_{\mathrm{c}}$, which is a reasonable estimate for pulsars that have a surface magnetic field of $B_{\mathrm{s}} \sim 10^{12}$ G.

The observational evidence of this kick mechanism still needs to be developed. The fact that the kick mechanism is only expected to work with quark stars means that quark stars would generally be the faster moving pulsars. This would seem to favour a bimodal kick distribution, such as that discussed in [87] where the two peaks rested at 90 km/s and 500 km/s. One could conceive that the peak around 90 km/s is produced by hydrodynamic mechanisms and is populated by conventional neutron stars. The higher peak around 500 km/s would be populated by quark stars that have topological currents as a primary kick mechanism. If there

is indeed a bimodal kick distribution with neutron stars populating the lower peak and quark stars populating the higher peak, this would be observational evidence of the topological kick mechanism.

Chapter 6

Other Applications of Topological Currents in Dense Stars

In this section we briefly discuss four other applications of the topological vector current first introduced by Charbonneau and Zhitnitsky [9],

> Section 6.1: Toroidal Magnetic Fields
>
> Section 6.2: Magnetic Helicity
>
> Section 6.3: Pulsar Jets
>
> Section 6.4: Type-I vs. Type-II Superconductivity

These phenomena are observed in many neutron stars and appear to be unrelated to each other, but we will argue that they originate from the same source—non-dissipating topological currents.

6.1 Toroidal Magnetic Fields

There is a strong theoretical evidence for the existence of toroidal fields in neutron stars based on the instability of the poloidal magnetic field. References [24–26, 138, 139] argue that toroidal and poloidal fields of similar magnitudes must be necessary to stave off hydrodynamic instabilities—the toroidal field suppresses poloidal instabilities and vice versa. Much has been done to find the observational consequences of a toroidal field, for example [140].

Estimating the toroidal magnetic field is a very complicated problem that requires a self consistent solution of the equation of the magnetic hydrodynamics. Our induced, topological currents represent only a small part of the system. We are not attempting to solve this problem. Instead, we shall argue that the currents we estimated are more than sufficient to induce a toroidal magnetic field correlated on large scale of order 10 km.

A natural consequence of having a current running parallel to the poloidal magnetic field is that a toroidal component H_{tor} will be induced. The size of the field can be calculated naively using Ampere's law, but there is a subtlety because the

magnetic field is being induced inside a superconductor. The magnetic field observed in neutron stars $B \sim 10^{12}$ G is actually induced by a much larger field H. The suppression comes from the perfect diamagnetism of the proton superconductor (the Meissner effect). This perfect diamagnetism is ruined at a critical field $H_c \sim (\Phi_0/4\pi\lambda^2) \sim 10^{15}$ G where flux penetrates the star through small regions where superconductivity has been destroyed (vortices or domains). The supercurrents responsible for the perfect diamagnetism do not flow as easily and a small field is induced.

Regardless whether the flux penetrates the superconductor as single vortices or in flux domains, we can assume that the superconductor is type-II.[1] The relationship between the applied magnetic field H and induced magnetic field B in a type-II superconductor is very nonlinear. The details have been worked out in [141] and [142], where the latter is a direct application to neutron stars. The important points are that below the first critical field $H < H_{c1}$ there is no magnetic field B induced. Just above the critical field a magnetic field appears that is approximately $B \sim 10^{-3}H_{c1}$. As the applied magnetic field is increased above H_{c1} the induced field starts to approach the applied field.

We want to determine if the topological current produced by the poloidal field can induce a sufficient toroidal field by finding the length scale where $H_{tor} \sim H$. Following [142] we assume that $H \sim H_c$ and we get the relationship $B \sim 10^{-3}H$ for our magnetic field. We apply Ampere's law for a region of size L to get

$$H_{\text{tor}}2\pi L = ej \cdot \left(\frac{\pi L^2 B}{\Phi_0} \right), \tag{6.1}$$

where the expression in brackets describes the number of unit fluxes bundled in the area πL^2 such that we get the total current enclosed in our loop. We take $\Phi_0 = \pi/e$ and substitute use our relationship between H and B.

The naive estimate leads to the following expression for H_{tor} in terms of magnitude of poloidal magnetic field H,

$$\frac{H_{tor}}{H} \sim \alpha \langle j \rangle L \sim 4 \left(\frac{\langle j \rangle}{10^{-10} \text{ MeV}} \right) \left(\frac{L}{\text{km}} \right). \tag{6.2}$$

This shows that a typical current from Table 4.1 can induce a toroidal field the same magnitude as the poloidal field on scales the order $L \sim 1$ km, within the typical size of a neutron star. It is quite obvious that our estimate becomes unreliable when

---

[1]The mechanism for type-I like superconductivity discussed in [8] relies on the electromagnetic interaction between currents carrying vortices, not in altering the value of the Landau-Ginzburg parameter $\kappa = \lambda/\xi$. We then still use results from type-II superconductors (indicated by $\kappa > 1/\sqrt{2}$) but the vortices are now bunched together in large domains with higher winding numbers.

$H_{\text{tor}} \geq H$ and we can no longer ignore the current induced by the toroidal field. For $H_{\text{tor}} \geq H$ the problem requires a self consistent analysis which is beyond scope of the present paper. The point is that the toroidal field obviously develops as a result of topological currents and eq. (6.2) shows that its magnitude can easily become the same order as the poloidal magnetic field. If superconductivity is completely destroyed, which we will discuss the possibility of in Section 6.4, $B = H$ and the toroidal field can induced on a much smaller scale, $L \sim 1$ m.

6.2 A Source for Magnetic Helicity

Magnetic helicity, see e.g. [143], is defined as

$$\mathscr{H} \equiv \int d^3x \vec{A} \cdot \vec{B}. \tag{6.3}$$

The magnetic helicity is a topological object that can be expressed in terms of the linking number $n_{(\gamma_1, \gamma_2)}$ of two curves γ_1 and γ_2. The precise relation between $\mathscr{H}$ and interlinked flux Φ_1 and Φ_2 is given by

$$\mathscr{H} = 2\Phi_1\Phi_2 = 2\Phi_0^2 N_1 N_2 \,, \tag{6.4}$$

where $\Phi_1 = \Phi_0 N_1$ and $\Phi_2 = \Phi_0 N_2$ are expressed in terms of unit flux Φ_0 and the linking number is simply reduced to $n_{(\gamma_1, \gamma_2)} = N_1 N_2$. Therefore $\mathscr{H}$ takes integer values up to a normalization $2\Phi_0^2$. This linking number is preserved, $\frac{d\mathscr{H}}{dt} = 0$, in a magneto-fluid with zero resistivity, which is a very good approximation for neutron stars. This topological invariance provides the stability necessary for the poloidal field.

We want to emphasize that the magnetic helicity is the dot product of a vector and a pseudovector, making it a pseudoscalar. Under the parity transformation $\vec{x} \to -\vec{x}$ the magnetic helicity is $\mathscr{P}$-odd: $\mathscr{H} \to -\mathscr{H}$. This implies that the magnetic helicity can be only induced if there are parity violating processes producing a large coherent effect on macroscopic scales. Many attempts to generate helicity rely on instabilities in the magnetic field caused by the star's rotation. Such correlations $\vec{B} \cdot \vec{\Omega}$ are $\mathscr{P}$-even, and though they may generate toroidal fields they cannot be responsible for helicity.

Our observation here is that the non-dissipating topological current introduced in the present work has precisely this property: the topological current produces the $\mathscr{P}$-odd correlation $\langle \vec{P} \cdot \vec{B} \rangle$ and is capable of inducing magnetic helicity $\mathscr{H} \sim j$. In fact, our estimate for the induced toroidal field H_{tor} unambiguously implies that the magnetic helicity will be also induced, see eq. (6.2). The magnetic flux from the

toroidal and poloidal fields is always interlinked and contributes to the magnetic helicity,

$$\mathcal{H} = 2\Phi_{\text{torr}}\Phi, \tag{6.5}$$

where Φ and Φ_{torr} are the original poloidal and induced toroidal magnetic fluxes (6.2) correspondingly.

Strong observational evidence, see [140] and references therein, supporting the presence of the toroidal component unambiguously suggests that the magnetic helicity $\mathcal{H}$ must be non-zero in neutron stars. The $\mathcal{P}$-odd quality of the magnetic helicity may be strong, indirect evidence supporting our claim that $\mathcal{P}$-odd topological currents have been induced at some moment in the star's life. Otherwise, it is very difficult to understand how such a large, coherent $\mathcal{P}$-odd effect could be produced.

6.3 Pulsar Jets

A different but likely related phenomena is the recent observation of pulsar jets [144] that are apparently related to neutron star kicks [145, 146]. It has been argued that spin axes and proper motion directions of the Crab and Vela pulsars are aligned. Such a correlation would follow naturally if we suppose that the kick is caused by a non-dissipating current as we mentioned above. The current, and thus the proper motion, is aligned with the magnetic field, which itself is correlated with the axis of rotation. It would be very tempting to identify the observed inner jets [144] with the electrons/photons emitted as a result of the induced current.

It is possible that evidence of the topological current may be directly detected in these jets. An observational consequence of the current is that a component of the X-ray emission in the trail of the neutron star will be left circularly polarized. Because of the parity violation in the star, only left-handed electrons will contribute to the kick. When these left-handed electrons interact they will create mostly left-handed photons, which coherently will be seen as left circularly polarized X-rays. This signature of the current will be difficult to detect as measuring circular polarization is hard. There are also many other sources of X-rays and the contribution from the current is likely very small, but it further motivates the need for higher precision X-ray polarimetry [147].

6.4 Type-I vs. Type-II Superconductivity

The following discussion of type-I vs. type-II superconductivity came from the possibility that neutron stars may precess [148]. Recently, the timing noise has

been reinterpreted and what was thought to be precession is now thought to be fast changes in the emission state of the pulsar [149].

The problem with precession was that it conflicted with the commonly held belief that the protons form a type-II superconductor in the core [83, 84]. When a magnetic field is applied to a type-II superconductor the flux finds it energetically favourable to penetrate it by forming many vortices each carrying a unit of quantum flux. In a neutron star the large number of these get tangled with the superfluid neutron vortices that have formed to carry angular momentum. If the star precesses with a large enough angle the superfluid vortices must break through the superconducting vortices for rotation to continue. Incredibly large amounts of energy are dissipated in this process which would cause the star to stop rotating. It was shown that if the superconductor is type-I there is no conflict [150]. If the superconductor is type-I, where the flux bunches in large groups organizing macroscopically large domains, there is room for the neutron vortices to move around.

In [8] it was found that if a sufficiently large current runs along type-II vortices an attractive force arises that causes the vortices to bundle together like they would in a type-I superconductor even though the Landau-Ginzburg parameters indicate type-II behaviour. It was suggested that this was a potential solution for the precession problem. Even though the precession problem has disappeared with the reinterpretation of timing noise the result that a current along the vortex would cause a type-I superconductor still holds. The topological current discussed in this thesis is such a current that would run along the vortex and change the type of superconductivity.

Even if the current is not strong enough to make the vortices attract each other it has also been argued [8] that the mere presence of an induced, longitudinal current, arbitrarily small, would destroy superconductivity, thus resolving the problem. In many condensed matter systems such kind of instability has been experimentally tested (see [8] for relevant references). This instability can be delayed for small currents or even stabilized due to impurities. But the lesson from these condensed matter systems is that when a current aligns with the magnetic field creating the vortex the properties of the vortex lattice are completely changed or destroyed.

We expect similar behaviour in regions of the neutron star where both the Landau-Ginzburg parameter suggests type-II behaviour and longitudinal currents are induced. While many features of the system are still to be explored, the point is that that even small topological currents along the magnetic field could destroy the vortex lattice by replacing it with a new, unknown structure, similar to the condensed matter experiments mentioned above.

Chapter 7

Topological Currents in AdS/QCD

This chapter marks a departure from the previous program in which we developed the idea of topological currents in dense matter and then discussed the practical applications of the current in pulsar physics. We will now discuss the topological current in terms of its implications in string theory. As discussed in the background material (Section 2.3) the interest in string theory is not as a theory of everything but as a tool for doing calculations at strong coupling.

The motivation behind this work is simply that a potential theory of holographic QCD should contain all the results found in QCD. The initial investigations of topological currents using quantum field theory. These considerations only include the first order contribution to the anomaly through the triangle diagram and do not consider higher order corrections. The ensuing attempts to find evidence for these currents in string theory resulted in debate over whether or not these string models are complete [19, 20, 151]. These debates even went so far as to question the type of anomaly cancellation occurring in lattice calculations that confirm the presence of the topological current [152]. It was surmised that either the holographic model is somehow broken or that the topological currents do not exist at strong coupling. Evidence for the current has been seen at RHIC, which is believed to produce a strongly coupled quark-gluon plasma. It may be that the quark-gluon plasma is sufficiently weakly coupled for the current not to be completely suppressed. We will assume the holographic model is somehow deficient and aim to show how one might introduce the current into a holographic description.

It was pointed out [21] that that the source of the confusion lies in incorporating non-zero values of axial charge into these models. In previous derivations[19, 151], a temporal component of a static axial background field was used to mimic an axial chemical potential. This lead to the eventual cancellation of the current by Bardeen counter-terms. A possible solution to the problem, then, is that a chemical potential can only be introduced to a conserved quantum number, and so that a re-definition of axial charge is necessary [21].

We will begin with a brief introduction of a simple AdS/QCD model in Section 7.1, which is the model we will use to illustrate our point. In this section we

will solve the equations of motion and derive the expressions for the current using the holography. In Section 7.2 we will discuss how the introduction of Bardeen counter-terms restores the conservation of the vector current. In Section 7.3 we will show how this holographic model manages to reproduce the topological axial current,

$$J_A^3 = \frac{N_c}{2\pi^2} B\mu \,, \tag{7.1}$$

but fails to reproduce the topological vector current,

$$J_V^3 = \frac{N_c}{2\pi^2} B\mu_5 \,, \tag{7.2}$$

when using the standard boundary conditions. We will review a possible solution to this problem in Section 7.4 that involves reconsidering what the appropriate boundary conditions are. We will then introduce our solution to the problem in Section 7.5.

7.1 Soft-wall AdS/QCD

In the AdS/QCD model [153–155], the bottom-up approach is followed. The holographic dual lives on a 5D AdS space with the background metric

$$ds^2 = \frac{1}{z^2} \left(\eta_{\mu\nu} dx^\mu dx^\nu + dz^2 \right), \tag{7.3}$$

with $\eta_{\mu\nu} = \mathrm{diag}(-1,1,1,1)$. The well-known conformal symmetry of this space reflects the near-conformal behaviour of QCD in the UV ($z \to 0$ in the dual). To break this symmetry at low energies, a "hard wall" is introduced in the form of a brane in the IR ($z \to \infty$), effectively cutting off the space. In order to obtain the correct Regge behaviour, the "soft-wall" model was introduced by [156, 157], where the space is smoothly cut off by turning on the dilaton,

$$\Phi(z) = z^2. \tag{7.4}$$

In four-dimensions we are interested in calculating currents. These four-dimensional operators have five-dimensional fields as holographic counterparts. We are interested in axial and vector currents, so the five-dimensional fields are left and right-handed gauge fields L and R. The naïve global $SU(N_f)_L \times SU(N_f)_R$ flavour symmetry of the field theory becomes a local, gauge symmetry in the bulk, and the associated Noether currents J_L and J_R are dual to gauge fields L and R. We will focus on the case of a single flavour, as the extension to $N_f > 1$ is not relevant to

our discussion. The dynamics of the gauge fields in the bulk are described by the
action

$$S = S_{YM}[L] + S_{YM}[R] + S_{CS}[L] - S_{CS}[R], \tag{7.5}$$

where the components of the action are made from the quadratic expansion of the
Dirac-Born-Infeld (DBI) action and Chern-Simons (CS) terms,

$$S_{YM}[A] = -\frac{1}{8g_5^2} \int dz\, d^4x\, e^{-\Phi} \sqrt{-g}\, F_{MN} F^{MN}, \tag{7.6}$$

$$S_{CS}[A] = -\frac{N_c}{24\pi^2} \int dz\, d^4x\, \varepsilon^{MNQPR} A_M F_{NQ} F_{PR}. \tag{7.7}$$

The uppercase Latin indices run over all five coordinates $\{0,1,2,3,z\}$. The stan-
dard soft-wall model action has a scalar and pseudoscalar sector that we will ignore.

Here a Chern-Simons term has been included in order to reproduce the chiral
anomaly [158]. Note that the Chern-Simons action is not gauge invariant in that
its variation under a gauge transformation $A \to A + d\alpha$ is a surface term. Since
A is coupled to a chiral fermion on the boundary, one may think of this variation
as being cancelled by the variation of the boundary action, $\delta S = -\int d^4x\, \alpha \partial_\mu J^\mu$,
by virtue of the anomaly [159]. If we think of the holographic relationship be-
tween the bulk and boundary theories as arising from taking some limit of a larger
theory (D-branes, for example) then this is the statement that the larger theory is
completely anomaly free, but that the anomaly cancellation does not survive the de-
coupling limit. If we wish to study, for example, the boundary theory in isolation,
we must cancel the anomaly by hand (by renormalization). It is not possible to do
so for both left- and right-handed transformations (equivalently, vector and axial
transformations) by means of local counter-terms, but we can at least cancel the
vector anomaly, which is enough to keep the theory consistent. The counter-term,
given by Bardeen [160], and introduced in the holographic setting in [19–22, 159],
takes the form of a boundary term in the 5D bulk action,

$$S_{\text{Bardeen}} = -\frac{N_c}{12\pi^2} \int d^4x\, \varepsilon^{\mu\nu\rho\sigma} L_\mu R_\nu (L_{\rho\sigma} + R_{\rho\sigma}), \tag{7.8}$$

where $L_{\mu\nu}$ and $R_{\mu\nu}$ denote the left- and right-handed field tensors. This term is
introduced to ensure that the vector current is free of local anomalies. We will see
in Section 7.5.1 that the cancellation of the vector current due to these terms is not
complete if we allow for sources in the bulk. This source in the bulk introduces a
global anomaly responsible for the topological current.

7.1.1 Correlation Functions

Correlation functions involving the current operators $J^\mu \sim \bar{q}\gamma^\mu q$ in the 4D gauge theory are obtained by deforming the action by a small amount $\delta S \propto \int d^4 x\, j_\mu J^\mu$, and formally expanding the partition function order-by-order in j_μ. In the holographic correspondence such a deformation is dual to placing probes near the boundary in the 5D bulk theory. This amounts to deforming the boundary conditions for the gauge field A_a by a small amount j_a. Similarly, we can introduce a background field B_μ for the quarks by adding $\bar{q}\gamma^\mu b_\mu q$ to the Lagrangian of the 4D theory, deforming the boundary condition for A_a by a further amount b_a in the bulk. We will therefore require the following behaviour of the fields A^L and A^R near the boundary:

$$A^L_\mu(z \to 0) \to j^L_\mu + b^L_\mu,$$
$$A^R_\mu(z \to 0) \to j^R_\mu + b^R_\mu. \tag{7.9}$$

The electromagnetic currents are derived by taking derivatives of the action with respect to $j^{L/R}_\mu$ as these are dual to the current

$$\mathscr{J}^{L/R}_\mu = \frac{\delta S}{\delta j^{L/R}_\mu}, \tag{7.10}$$

where S is evaluated over a classical solution. Varying the action yields

$$\delta S = \int_M \left[\frac{\delta \mathscr{L}}{\delta A_a} - \partial_b \left(\frac{\delta \mathscr{L}}{\delta \partial_b A_a} \right) \right] \delta A_a + \int_{\partial M} n_b \left(\frac{\delta \mathscr{L}}{\delta \partial_b A_a} \delta A_a \right), \tag{7.11}$$

where n_b is normal to the boundary. This variation indicates we may evaluate Eqn. (7.10) using the equation

$$\mathscr{J}^{L/R}_\mu = \left. \frac{\delta \mathscr{L}}{\delta \partial_z A^{L/R}_\mu} \right|_{z=0} + \dots, \tag{7.12}$$

where $\dots$ represents the variation of the boundary contribution to the action. The symmetric combination of the boundary conditions we will use are

$$b^L_0 + b^R_0 = \mu, \tag{7.13a}$$
$$b^L_i + b^R_i = -x_j B_k, \tag{7.13b}$$

where we have chosen ijk to be the even permutations of 123.

7.1.2 The Equations of Motion

The first thing we will do is establish the equations of motion. We work in the $A_z = 0$ gauge which yields a Yang-Mills action

$$S_{YM}[A] = -\frac{1}{4g_5^2}\int dz\,d^4x\,\left\{\frac{e^{-\phi}}{z}A_\mu(\Box^{\mu\nu}-\partial^\mu\partial^\nu)A_\nu\right. \tag{7.14}$$

$$\left.+A_\mu\partial_z\frac{e^{-\phi}}{z}\partial_z A^\mu\right\} \tag{7.15}$$

$$+\frac{1}{4g_5^2}\int d^4x\,\frac{e^{-\phi}}{z}A_\mu\partial_z A^\mu\Big|_{z=0}^{z=\infty}. \tag{7.16}$$

Varying the Yang-Mills part of the action Eqn. (7.5) with respect to the left-handed potential yields

$$\frac{\delta S_{YM}[L]}{\delta L_\mu} = -\frac{R}{2g_5^2}\left[\frac{e^{-\phi}}{z}(\Box\eta^{\mu\nu}-\partial^\mu\partial^\nu)L_\nu+\partial_z\left(\frac{e^{-\phi}}{z}\partial_z L^\mu\right)\right]. \tag{7.17}$$

Varying with respect to the right-handed potential yields a similar result. The Chern-Simons term yields

$$\frac{\delta S_{CS}[L]}{\delta L_\mu} = \frac{kN_c}{2\pi^2}\varepsilon^{\mu\nu\rho\sigma}\partial_z L_\nu F_{\rho\sigma}. \tag{7.18}$$

Using the AdS/CFT relation $\frac{R}{g_5^2}=\frac{N_c}{12\pi^2}$ allows us to write the equations of motion as

$$\partial_z\left(\frac{e^{-\phi}}{z}\partial_z L^\mu\right)-24\varepsilon^{\mu\nu\rho\sigma}\partial_z L_\nu\partial_\rho L_\sigma=0, \tag{7.19}$$

$$\partial_z\left(\frac{e^{-\phi}}{z}\partial_z R^\mu\right)+24\varepsilon^{\mu\nu\rho\sigma}\partial_z R_\nu\partial_\rho R_\sigma=0. \tag{7.20}$$

We can also vary the system with respect to A_z and get an equation of motion that will later be used to write down the divergence of the current. This will be used solely to illustrate the role of the Bardeen counter-term in the preservation of the conservation of the vector current. The Yang-Mills portion gives us

$$\frac{\delta S_{YM}[L]}{\delta L_z} = -\frac{R}{2g_5^2}\frac{e^{\phi}}{z}\partial_z\partial_\mu L^\mu. \tag{7.21}$$

The contribution from the CS term is

$$\frac{\delta S_{CS}[L]}{\delta L_z} = \frac{N_c}{2\pi^2}\varepsilon^{\mu\nu\rho\sigma}\partial_\mu L_\nu\partial_\rho L_\sigma. \tag{7.22}$$

Rewriting the constants using the dictionary we get the equation of motion,

$$\frac{N_c}{24\pi^2}\frac{e^{\phi}}{z}\partial_z\partial_{\mu}L^{\mu} = \frac{N_c}{2\pi^2}\varepsilon^{\mu\nu\rho\sigma}\partial_{\mu}L_{\nu}\partial_{\rho}L_{\sigma}. \tag{7.23}$$

A similar equation of motion can be found for the right-handed field R_{μ} where the right hand side picks up a negative sign.

Specific Solutions

We are interested in a background magnetic field in the x^3 direction and choose $L_1(x_2) = R_1(x_2) = -\frac{1}{2}Bx_2$ such that they have only x_2 dependence. We can rewrite these fields in terms of the axial and vector fields A and V by using the relations $V = L + R$ and $A = L - R$. We should note that this convention differs from some papers that define the axial relation as $A = R - L$ and can result in sign differences when comparing equations involving axial components. Using our convention we arrive at the equations of motion

$$\partial_z\left(\frac{e^{-\phi}}{z}\partial_z V_0\right) + 12B\partial_z A_3 = 0, \tag{7.24}$$

$$\partial_z\left(\frac{e^{-\phi}}{z}\partial_z V_3\right) + 12B\partial_z A_0 = 0, \tag{7.25}$$

$$\partial_z\left(\frac{e^{-\phi}}{z}\partial_z A_0\right) + 12B\partial_z V_3 = 0, \tag{7.26}$$

$$\partial_z\left(\frac{e^{-\phi}}{z}\partial_z A_3\right) + 12B\partial_z V_0 = 0. \tag{7.27}$$

These can be solved by introducing a new coordinate w with

$$\partial_w = \frac{dz}{dw}\partial_z = \frac{e^{-\phi}}{z}\partial_z, \tag{7.28}$$

so that the appropriate solutions are

$$V_0(z) = v_{00} + a_{31}(e^{-\beta w(z)} - 1), \tag{7.29}$$

$$V_3(z) = v_{31} + a_{01}(e^{-\beta w(z)} - 1), \tag{7.30}$$

$$A_0(z) = (a_{00} + a_{01}) + a_{01}(e^{-\beta w(z)} - 1), \tag{7.31}$$

$$A_3(z) = (a_{30} + a_{31}) + a_{31}(e^{-\beta w(z)} - 1), \tag{7.32}$$

where $\beta = 12B$ and $w(z)$ has the property that $w(0) = 0$ and $w(\infty) = \infty$ such that we discard one set of solutions from the beginning. We must still apply appropriate boundary conditions to these solutions. We have grouped the constants in a way that will make the effect of these boundary conditions more transparent later in the paper.

7.1.3 Setting Up the Currents

We will now introduce the standard setup for holographic currents. As discussed earlier the 4-dimensional currents can be found using

$$J^{\mu} = \frac{\delta S}{\delta A_{\mu}(0)} = J_0^{\mu} + J_{\text{Bardeen}}^{\mu} = \left.\frac{\delta \mathscr{L}}{\delta \partial_z A_{\mu}}\right|_{z\to 0} + J_{\text{Bardeen}}^{\mu}. \qquad (7.33)$$

The Bardeen term is chosen to cancel nonconserved components in the vector current. This is the common procedure in quantum field theory as the vector current is the physical current. This process leaves the axial current anomalous.

The current receives contributions from both $F_{\mu z}F^{\mu z}$ and S_{CS}. The currents that arise from this are

$$J_{0,L}^{\mu} = -\frac{N_c}{24\pi^2}\frac{e^{-\phi}}{z}\partial_z L^{\mu} + \frac{N_c}{6\pi^2}\varepsilon^{\mu\nu\rho\sigma}L_{\nu}L_{\rho\sigma}, \qquad (7.34)$$

$$J_{0,R}^{\mu} = -\frac{N_c}{24\pi^2}\frac{e^{-\phi}}{z}\partial_z R^{\mu} - \frac{N_c}{6\pi^2}\varepsilon^{\mu\nu\rho\sigma}R_{\nu}R_{\rho\sigma}. \qquad (7.35)$$

And the Bardeen currents that come from the Bardeen action in Eqn. (7.8) are

$$J_{\text{Bardeen,L}}^{\mu} = -\frac{N_c}{6\pi^2}\varepsilon^{\mu\nu\rho\sigma}\left(R_{\nu}\partial_{\rho}R_{\sigma} + 2R_{\nu}\partial_{\rho}L_{\sigma} - L_{\nu}\partial_{\rho}R_{\sigma}\right), \qquad (7.36)$$

$$J_{\text{Bardeen,R}}^{\mu} = +\frac{N_c}{6\pi^2}\varepsilon^{\mu\nu\rho\sigma}\left(L_{\nu}\partial_{\rho}L_{\sigma} + 2L_{\nu}\partial_{\rho}R_{\sigma} - R_{\nu}\partial_{\rho}L_{\sigma}\right). \qquad (7.37)$$

As discussed earlier we can rewrite currents in terms of the axial and vector fields A and V by using the relations $V = L + R$ and $A = L - R$,

$$J_0^{\mu} = -\frac{N_c}{24\pi^2}\partial_w V^{\mu} + \frac{N_c}{12\pi^2}\varepsilon^{\mu\nu\rho\sigma}\left(V_{\nu}A_{\rho\sigma} + A_{\nu}V_{\rho\sigma}\right), \qquad (7.38)$$

$$J_{0,A}^{\mu} = -\frac{N_c}{24\pi^2}\partial_w A^{\mu} + \frac{N_c}{12\pi^2}\varepsilon^{\mu\nu\rho\sigma}\left(V_{\nu}V_{\rho\sigma} + A_{\nu}A_{\rho\sigma}\right), \qquad (7.39)$$

$$J_{\text{Bardeen}}^{\mu} = -\frac{N_c}{24\pi^2}\varepsilon^{\mu\nu\rho\sigma}\left(-4A_{\nu}V_{\rho\sigma} + 2V_{\nu}A_{\rho\sigma}\right), \qquad (7.40)$$

$$J_{\text{Bardeen,A}}^{\mu} = -\frac{N_c}{24\pi^2}\varepsilon^{\mu\nu\rho\sigma}2V_{\nu}V_{\rho\sigma}. \qquad (7.41)$$

We have used $V_{\mu\nu}$ and $A_{\mu\nu}$ to denote the field tensors composed of vector and axial fields respectively.

7.2 Cancellation of the Vector Anomaly

The first aspect of the problem that we will consider is the cancellation of the vector anomaly. The Bardeen terms are introduced to ensure that the vector current

is strictly conserved, even in the presence of an axial field. Consider the divergence of the vector current given by Eqn. (7.38),

$$\partial_\mu J_0^\mu = -\frac{N_c}{24\pi^2}\partial_w\partial_\mu V^\mu + \frac{N_c}{12\pi^2}\varepsilon^{\mu\nu\rho\sigma}\partial_\mu\left(V_\nu A_{\rho\sigma} + A_\nu V_{\rho\sigma}\right), \tag{7.42}$$

$$= -\frac{N_c}{2\pi^2}\varepsilon^{\mu\nu\rho\sigma}\partial_\mu V_\nu\partial_\rho A_\sigma + \frac{N_c}{3\pi^2}\varepsilon^{\mu\nu\rho\sigma}\left(\partial_\mu V_\nu\partial_\rho A_\sigma\right), \tag{7.43}$$

$$= -\frac{N_c}{6\pi^2}\varepsilon^{\mu\nu\rho\sigma}\partial_\mu V_\nu\partial_\rho A_\sigma, \tag{7.44}$$

where we used the right and left-handed version of Eqn. (7.23) to write

$$\frac{N_c}{24\pi^2}\frac{e^\phi}{z}\partial_z\partial_\mu V^\mu = \frac{N_c}{2\pi^2}\varepsilon^{\mu\nu\rho\sigma}\partial_\mu V_\nu\partial_\rho A_\sigma. \tag{7.45}$$

The divergence of the vector Bardeen current given by Eqn. (7.41) becomes

$$\partial_\mu J_{\text{Bardeen}}^\mu = -\frac{N_c}{24\pi^2}\varepsilon^{\mu\nu\rho\sigma}\partial_\mu\left(-4A_\nu V_{\rho\sigma} + 2V_\nu A_{\rho\sigma}\right), \tag{7.46}$$

$$= \frac{N_c}{6\pi^2}\varepsilon^{\mu\nu\rho\sigma}\partial_\mu V_\nu\partial_\rho A_\sigma. \tag{7.47}$$

The Bardeen terms also alter the divergence of the axial current. The divergence of the axial current given by Eqn. (7.39) is

$$\partial_\mu J_{0,A}^\mu = -\frac{N_c}{24\pi^2}\partial_w\partial_\mu A^\mu + \frac{N_c}{12\pi^2}\varepsilon^{\mu\nu\rho\sigma}\partial_\mu\left(V_\nu V_{\rho\sigma} + A_\nu A_{\rho\sigma}\right), \tag{7.48}$$

$$= -\frac{N_c}{12\pi^2}\left(\partial_\mu V_\nu\partial_\rho V_\sigma + A_\nu\partial_\rho A_\sigma\right), \tag{7.49}$$

where we used the left and right-handed versions of (7.23) to write

$$\frac{N_c}{24\pi^2}\frac{e^\phi}{z}\partial_z\partial_\mu A^\mu = \frac{N_c}{4\pi^2}\varepsilon^{\mu\nu\rho\sigma}\left(\partial_\mu V_\nu\partial_\rho V_\sigma + \partial_\mu A_\nu\partial_\rho A_\sigma\right). \tag{7.50}$$

The divergence of the axial Bardeen current given by Eqn. (7.41) is

$$\partial_\mu J_{\text{Bardeen,A}}^\mu = -\frac{N_c}{6\pi^2}\varepsilon^{\mu\nu\rho\sigma}\partial_\mu V_\nu\partial_\rho V_\sigma. \tag{7.51}$$

Without the counter-terms the anomaly appears in both the divergence of the vector and axial currents. This configuration where both currents are anomalous is known as the consistent anomaly. Adding the Bardeen counter-term shifts the anomaly from the vector current to axial current leaving us with the covariant anomaly,

$$\partial_\mu J^\mu = 0, \tag{7.52}$$

$$\partial_\mu J_A^\mu = -\frac{N_c}{12\pi^2}\varepsilon^{\mu\nu\rho\sigma}\left(3\partial_\mu V_\nu\partial_\rho V_\sigma + \partial_\mu A_\nu\partial_\rho A_\sigma\right). \tag{7.53}$$

The Bardeen terms do their job in conserving the vector current. The difference is that we have implemented the procedure of cancelling the anomaly from the holographic side.

7.3   The Problem

We have defined all the tools necessary to discuss the problem. We want to see how the definition of the axial chemical potential as the temporal component of the axial field fails to reproduce the topological vector current (7.2) when the Bardeen counter-terms are introduced. The standard technique is to apply the following boundary conditions to the holographic system.

At $z = \infty$ the boundary conditions are

$$V_0(\infty) = 0, \tag{7.54}$$
$$A_0(\infty) = 0. \tag{7.55}$$

Forcing the vector potential to vanish in the bulk at $z = \infty$ means that

$$v_{00} = a_{31} = \mu \tag{7.56}$$

as seen in Eqn. (7.29). This is how the vector chemical potential enters the derivation of the axial current. Forcing the axial field to go to zero in the bulk means that $a_{00} = 0$ in Eqn. (7.31).

In a related system, the confined phase of the Sakai-Sugimoto model, the condition $A_\mu(\infty) = 0$ is a natural choice for the following reason. In that model, the two gauge fields live on D-branes that join in the bulk, and thus are actually two branches of a single D-brane. Therefore $A_\mu(\infty) = 0$ reflects the continuity of the single gauge field. This continuity also reflects the breaking of chiral symmetry in the IR. Note that $A_\mu(\infty) = 0$ is not a gauge-dependent statement, as the theory is not gauge invariant under axial transformations. It is a statement about continuity.

At $z = 0$ (i.e., the holographic boundary) the vector combination is given by Eqn. (7.13a),

$$V_0(0) = v_{00} = \mu, \tag{7.57}$$
$$V_i(0) = -x_j B_k, \tag{7.58}$$

and we let the axial field be,

$$A_0(0) = a_{01} = \mu_5, \tag{7.59}$$
$$A_i(0) = 0. \tag{7.60}$$

We see that the zeroth component of the axial field is equated with the axial chemical potential. To take the temporal component of the axial field as the axial chemical potential is the common method of introducing and axial chemical potential into the holography. It mirrors the way the vector chemical potential is introduced by equating it with the temporal component of the vector field. By defining the chemical potentials outright we have approached the problem by using the grand canonical ensemble.

We assume no background axial field strength and take the background magnetic field to be in the x^3 direction,

$$A_{\mu\nu} = 0, \tag{7.61}$$

$$V_{21} = -B, \tag{7.62}$$

$$V_{12} = B. \tag{7.63}$$

We apply these conditions to find the vector current from Eqns. (7.38) and (7.40) and find that it vanishes,

$$J^3 = J_0^3 + J_{\text{Bardeen}}^3, \tag{7.64}$$

$$= -\frac{N_c}{24\pi^2}\partial_w V^3 + \frac{3N_c}{12\pi^2}\varepsilon^{3\nu\rho\sigma}A_\nu V_{\rho\sigma}, \tag{7.65}$$

$$= \frac{N_c}{2\pi^2}Ba_{01} + \frac{3N_c}{6\pi^2}\varepsilon^{3012}Ba_{01} = 0, \tag{7.66}$$

while the axial current from Eqns. (7.39) and (7.41) gives the result we would expect,

$$J_A^3 = J_{0,A}^3 + J_{\text{Bardeen},A}^3, \tag{7.67}$$

$$= -\frac{N_c}{24\pi^2}\partial_w A^3 + \frac{N_c}{12\pi^2}\varepsilon^{3\nu\rho\sigma}A_\nu A_{\rho\sigma}, \tag{7.68}$$

$$= \frac{N_c}{2\pi^2}B\mu, \tag{7.69}$$

where we used (7.56) to write this in terms of the chemical potential.

The contribution from the Bardeen counter-term that was introduced to ensure gauge invariance of the currents has made the contribution to the topological vector current from the axial chemical potential vanish. But, the axial current (7.1) that arises from a vector chemical potential still appears, even in the presence of the counter-terms. This demonstration of the counter-terms cancelling the vector current was originally done using the Sakai-Sugimoto model [19] and lead people to believe that maybe the topological vector current responsible for phenomena like the chiral magnetic effect did not exist in holographic QCD models. But the effect can be reproduced in many holographic models, like the one we present here. It became apparent that the problem was one of thermodynamics.

7.4 Rubakov's Solution

In the previous section, by choosing to set $V_0(z \to 0)$ equal to the chemical potential, μ, and $A_0(z \to 0)$ equal to the axial chemical potential, μ_5 we have chosen to work in the grand canonical ensemble with respect to both the vector fermion number $N_L + N_R$ and the axial fermion number $N_L - N_R$. However, the axial fermion number is not conserved, precisely because of the anomaly (7.53), and so the canonical and grand canonical ensembles do not represent equivalent pictures with regards to this operator. This was pointed out by Rubakov [21], among others. Working in the grand canonical ensemble requires us to replace the axial fermion number operator with one that is conserved [21].

Though Rubakov used a different holographic model than the one we employ, it is possible to demonstrate his solution. Rubakov stressed that the temporal component of the axial field is not the same thing as a chemical potential. The chemical potential must be introduced to the action conjugate to a conserved charge. The procedure is to shut off all axial fields A_μ and define a conserved charge to introduce a chemical potential μ_5. The charge is usually given by the temporal component of the current integrated over all space. With the anomaly present this definition of the charge is not conserved. To ensure the charge is conserved we use the part responsible for the nonconservation in Eqn. (7.53) to modify the charge,

$$Q^5_{\text{Rubakov}} = \int dx^3 J_0^5 + \frac{3N_c}{12\pi^2} \int dx^3 \varepsilon^{ijk} V_i \partial_j V_k. \tag{7.70}$$

Note that our axial current is defined as $L - R$ while Rubakov's is defined as $R - L$ giving a sign difference on our anomaly, as well as many of the other equations that follow. This charge is invariant under electromagnetic gauge transformations. We now add a chemical potential to the action,

$$S[\mu_5] = S + \mu_5 \int dx^0 Q^5_{\text{Rubakov}}, \tag{7.71}$$

$$= \left(S + \mu_5 \int dx^4 J_0^5 \right) + \mu_5 \frac{3N_c}{12\pi^2} \int dx^4 \varepsilon^{ijk} V_i \partial_j V_k, \tag{7.72}$$

where S is the original action of the system with the chemical potential introduced in such a way that we can find the current. As shown earlier, the Bardeen counter-terms cause all contributions to the current from S to vanish. The counter-terms also cancel the contributions of the vector field from the axial current J_0^5. The only contribution to the current is from the variation of the last term in Eq. (7.72). The variation produces

$$\frac{\delta S}{\delta V_i} = \mu_5 \frac{N_c}{4\pi^2} \varepsilon^{ijk} \partial_j V_k = \frac{N_c}{2\pi^2} \mu_5 B, \tag{7.73}$$

which is the vector current responsible for the chiral magnetic effect.

The axial chemical potential takes over the role of the temporal component of the axial field, but without the problems of getting cancelled by the counterterms. Though this arrives at the correct answer it is unappealing because we have to construct an effective action. The chemical potential is added in such a way it cannot be cancelled and then is used to derive the current. This is a solution, but it would be more desirable to see the current arise from the model itself. This is where our program starts.

7.5 A Solution Arising from Boundary Conditions

While Rubakov's method reproduced the accepted result, we would like to find a resolution that is contained within the holographic model. Working entirely in the grand canonical ensemble did not work. Working in the canonical ensemble, however, where one fixes the axial fermion number, is problematic on physical grounds. One imagines a state at some initial time, having some value $N_L - N_R$, evolving to a later time, and having a different value of $N_L - N_R$. Therefore, restricting the path integral to states with a fixed value of $N_L - N_R$ amounts to placing a *constraint* on the system. We will now address whether this constraint is physical.

We will discuss three physical systems in which a constraint fixes the value of $N_L - N_R$: induced topological currents in dense stars [9], the charge separation effect [11] and the chiral magnetic effect [12]. In each of these systems the constraint is due to the quasistatic nature of the system, particularly, they require a nontrivial boundary condition to induce and maintain an axial charge. For each example we will discuss the external mechanism responsible for introducing the axial charge and maintaining it such that the current can flow.

The first example is the appearance of topological currents in neutron stars, where the current was derived by considering the microscopic elements of the system [4, 6, 8, 9]. Given the complexity of neutron stars it is useful to think about the current in terms of numbers of particles. The current is given by

$$J_{\mathrm{V}} = (n_l - n_r)\frac{e\Phi}{2\pi}, \tag{7.74}$$

where $n_r(T, \mu)$ and $n_l(T, \mu)$ are the one-dimensional number densities of left and right-handed Dirac fermions and Φ is the magnetic flux. This formula tells us that to find the magnitude of the current one has to count the number of particles aligned with the magnetic field and subtract them against those aligned against the magnetic field. In a neutron star the equilibrium processes are given by beta and inverse beta decay, known collectively as the Urca processes. These are weak

interactions that act more on left-handed electrons than right-handed electrons. In an infinite system any difference in left and right-handed particles created by the weak interaction would be washed out due to detailed balance; the creation of a left-handed electron is as likely as the time-reversed process, the scattering of an electron and a proton to create a neutron and neutrino. The finite size of the star essentially breaks time-reversal symmetry and allows the electron to escape before it decays through the weak interaction. This causes a current to flow through the bulk of the star. The key is that electrons are constantly being added by beta decay to maintain the difference between left and right-handed electrons. These processes are like a pump that fixes the axial charge. This current may explain the anomalously large pulsar kicks that have been observed [10].

The second example is the charge separation effect [11], wherein a current appears in regions where there is a dynamical or spatially varying theta angle $\theta(\vec{x}, t)$. These regions may occur at RHIC where a collision creates a small bubble where $\theta(\vec{x}, t) \neq 0$ within a larger region (e.g., the rest of the world) where $\theta = 0$. The current takes the form

$$j_0 = N_c \sum_f \frac{e_f \mu_f}{2N_f \pi^2} \vec{\nabla}\theta \cdot \vec{\Omega}, \tag{7.75}$$

$$j_i = N_c \sum_f \frac{e_f \mu_f}{2N_f \pi^2} \partial_0 \theta \, \Omega_i, \tag{7.76}$$

where Ω is the angular velocity of the rotating coordinate frame, which mimics a magnetic field. The domain wall created as the theta angle transitions is the reason the current appears and draws charge to the surface of the theta bubble, which we can see if we integrate over the volume of the theta bubble. If the bubble was infinitely large or the gradient of the change was extremely small, the charge would not accumulate on the domain wall. The finiteness of the bubble has introduced a constraint in the parity violating aspect of the current. When the domain wall disappears, the parity violation in the system disappears and the charge separation vanishes with it.

The third example is the previously mentioned chiral magnetic effect [12]. The effect is often written as a statement of the current that causes the charge separation,

$$j_V = (\mu_l - \mu_r) \frac{e^2 B}{(2\pi)^2}, \tag{7.77}$$

but this current alone does not naturally appear in heavy ion collisions. What is required is an external source to introduce chirality into the system. In heavy ion collisions it may be possible for transitions to occur from one QCD vacuum to another. When this transition occurs, chirality is induced through a change in the

QCD winding number n_w, which can be written as the charge

$$Q_w = n_w(t = \infty) - n_w(t = -\infty).$$ (7.78)

If induced during a collision the charge will introduce a difference in the number of left and right-handed particles through the relation

$$N_L^f - N_R^f = 2Q_w.$$ (7.79)

The introduction of the topological charge Q_w allows the system to violate parity and induces a current. Only then can the charge separation occur.

We have seen three examples of how a constraint is used to hold the axial charge fixed during the life of the current. We should note that these are real systems. In particular the charge separation effect and the chiral magnetic effect explain the $\mathscr{P}$ and $\mathscr{CP}$ violation seen at RHIC [13–17]. We will not consider the physics behind the constraint, which often is poorly described in a formal field theory setting. We will only assume that one is necessary for the current to be nonzero.

7.5.1 New Boundary Conditions

As we have discussed, in previous derivations of the chiral magnetic effect using holography it was common to associate the axial field on the holographic boundary with the chemical potential. In light of the discussion in Section 7.1.1 the current does not appear in a system that is in true thermal equilibrium. As pointed out in [21] assigning the axial chemical potential to $A_0(0)$ is assigning a chemical potential to a quantity that is not conserved. In an effort to find the true conserved quantity we will derive the axial current without assigning a thermodynamic meaning to the boundary value of the axial field. We will then interpret the result afterwards by comparing it to the results found in QCD. We will find that there is a component of the axial field that survives the anomaly cancelation and that this component must be associated with the induced axial charge of the system.

By allowing the axial field in the bulk to take nonzero values, $A_0(\infty) \neq 0$, we allow the possibility for a source to add new charge into the system and contribute to the current. This is the exact source needed to provide the axial charge with the constraint required to keep it conserved as discussed in Section 7.5.

We now mirror the derivation in Section 7.3. As before we choose to use the grand canonical ensemble for the vector combination Eqn. (7.13a). At $z = 0$, on the holographic boundary we get

$$V_0(0) = v_{00} = \mu,$$ (7.80)
$$V_i(0) = -x_j B_k.$$ (7.81)

As discussed we choose not to assign the value of $A_\mu(0)$ any thermodynamic quantity. In the IR (i.e., $z = \infty$) we have more freedom in imposing boundary conditions.

In our model we wish to impose a nonzero axial charge on the boundary theory. As mentioned above, this is complicated by the fact that the axial charge is not conserved (equivalently, a lack of gauge invariance). Instead we suppose that there is an IR cut-off in the bulk, beyond which some source exists. In a string model like the Sakai-Sugimoto model, such a source would be provided by the endpoints of strings stretching between the flavour branes and D-branes playing the role of instantons. In a bottom-up model, the source must be inserted by hand. The value of A_μ at the cut-off depends on the magnitude of this source. Motivated by this observation, we allow for the possibility that $A^\mu(\infty) \neq 0$, reflecting the fact that we have a source of axial charge in the far IR. In the hard-wall model one could similarly impose a nonzero charge on the IR boundary by choosing the correct boundary conditions on the brane responsible for the hard IR cutoff. In the hard-wall model this boundary condition is not the result of a source, but is just a characteristic of the model.

This source beyond the IR represents the external source required to generate the vector current using the axial anomaly in field theory models. As discussed in Section 7.5 topological currents need an external source to manifest themselves. In neutron stars this source is the Urca processes constantly producing new left-handed electrons and in the chiral magnetic effect and charge separation effect this source is the topological charge induced by particle collisions. With this source we will be able to induce a topological vector current that survives the Bardeen cancelation.

We should note that this asymmetric treatment of the axial and vector field boundary conditions only arises because we cannot completely remove the anomaly. With the vector field there is no problem with assigning $V_0(0) = \mu$ because there is no anomaly associated with the current and the vector charge is conserved. The chemical potential can be assigned to the boundary value of the vector field. We could take the same approach with the vector field as we are with the axial field, but the boundary condition ends up still being $V_0(0) = \mu$. The special approach for the axial field is required because of the anomaly. If we had instead chosen a different Bardeen counter-term that made the axial current anomaly free and the vector current anomalous the story would be reversed.

By allowing the possibility for $A^\mu(\infty) \neq 0$ our boundary conditions at infinity given by the solutions to the equations of motion (7.29) and (7.31) are

$$V_0(\infty) = 0, \tag{7.82}$$

$$A_0(\infty) = a_{00}. \tag{7.83}$$

Forcing the vector current go to zero in the bulk means that $v_{00} = a_{31} = \mu$, which will contribute when we derive the axial current. The vector current is then found by using Eqns. (7.38) and (7.40). In our solution we assume no background axial field strength and a background magnetic field in the x^3 direction,

$$A_{\mu\nu} = 0, \tag{7.84}$$

$$V_{21} = -B, \tag{7.85}$$

$$V_{12} = B. \tag{7.86}$$

We apply these to the vector current from Eqns. (7.38) and (7.40), which is further simplified when we choose just the x_3 direction for the current along the magnetic field, to get

$$J_0^3 = -\frac{N_c}{24\pi^2}\partial_w V^3 + \frac{N_c}{6\pi^2}\varepsilon^{3012}A_0 B. \tag{7.87}$$

The Bardeen vector terms are similarly manipulated to give

$$J_{\text{Bardeen}}^3 = \frac{N_c}{3\pi^2}\varepsilon^{3012}A_0 B. \tag{7.88}$$

We now substitute in the solutions given in Eqns. (7.29)–(7.32). To calculate the true current we evaluate this on the boundary at $z = 0$. Using $\varepsilon^{3012} = -1$ the total current can now be written as

$$J^3 = J_0^3 + J_{\text{Bardeen}}^3. \tag{7.89}$$

$$= \frac{N_c}{2\pi^2}B(-a_{00}). \tag{7.90}$$

Recalling our solution for the axial field, $A_0(\infty) = a_{00}$, we see that not fixing the boundary condition in the bulk has yielded a connection between the UV and the IR. The current on the boundary depends on a boundary condition in the bulk,

$$J^3 = \frac{N_c}{2\pi^2}B(-A_0(\infty)). \tag{7.91}$$

The current vanishes if $A_0(\infty) = 0$ and a nonvanishing current depends on a discontinuity in the IR. Maintaining this field in the bulk acts as though a chiral charge is being fixed externally. However, without axial gauge invariance we do not have the equivalent of Gauss' law to relate $A(\infty) - A(0)$ to the magnitude of the source in the bulk. This would require treating the bulk and boundary in parallel, as discussed in Section 7.1. In our work we relax the interpretation of the value of the axial field in the bulk, since there is no equivalent Gauss' law available.

As a consistency check we can use equations (7.39) and (7.41) to find the axial current,

$$J_A^3 = \frac{N_c}{2\pi^2} B\mu \,. \tag{7.92}$$

This reproduces the standard result for anomalous axial currents first discussed in [6]. The procedure we have outlined to introduce the axial charge leaves the well-known result for the vector current unaffected. We would like to make a connection between this result and the result for the vector current. If we had not chosen $V(0) = \mu$ and $V(\infty) = 0$, but had taken an approach similar to that of the axial field in deriving the vector current, then Eqn. (7.92) would have a_{31} in it instead of μ. We would then compare Eqn. (7.92) with the result from [6] and find that $a_{31} = \mu$, an answer consistent with choosing $V(0) = \mu$ and $V(\infty) = 0$. Both methods, either setting the vector potential to zero in the bulk or leaving it free, achieve the same results for the axial current, unlike with the vector current.

If we had instead chosen to move the anomaly to the vector current instead of the axial current, we would still achieve the same results. With the vector current now anomalous, we would be free to define the axial chemical potential as the temporal component of the axial field on the holographic boundary, but we would have to redefine the vector chemical potential to be associated with a constraint in the bulk.

7.6 Discussion

In the spirit of the bottom-up approach we will now attempt to determine the physical meaning of the boundary condition in Eqn. (7.91) by comparing it to currents that arise in QCD. In an attempt to model the current we have chosen to make the boundary condition on the horizon nonzero. We do this because defining an axial chemical potential makes no sense when the axial charge is not conserved. This boundary condition occurs at an IR cutoff we imposed on the bulk. A nonzero boundary condition must be caused by a charge configuration (source) past this boundary further into the bulk (i.e., past the IR cutoff).

In quantum field theory one can describe the topological current in a very general way through the introduction of a dynamic theta angle $\theta(\vec{x},t) \neq 0$ that is induced by some nonequilibrium process. The existence of these processes in real systems is discussed at length in Section 7.5. The result of this is the induction of a term proportional to

$$\sim \theta(\vec{x},t) F_a^{\mu\nu} \widetilde{F}_{\mu\nu}^a. \tag{7.93}$$

After a chiral rotation this dynamic theta angle appears as a boundary term. This causes a current to be introduced that is proportional to the derivative of the theta angle. The current that arises from the portion of the current that varies with time is

$$\vec{J} = \dot{\theta}(\vec{x},t) \frac{N_c \vec{B}}{2\pi^2}. \tag{7.94}$$

Comparing this with Eqn. (7.91), we see that it is natural to identify the boundary condition in the bulk with the induced theta angle,

$$-A_0(\infty) = \dot{\theta}(\vec{x},t). \tag{7.95}$$

In field theory models $\dot{\theta}(\vec{x},t) \neq 0$ must be induced by some process. This is the constraint that violates parity and is responsible for a topological current. We have equated this induced $\dot{\theta}(\vec{x},t)$ to the boundary condition that survives Bardeen cancellation. By adding a source beyond the IR we have reproduced the current responsible for the chiral magnetic effect that does not get cancelled due to the Bardeen counter-terms.

It has been argued that a time-dependent theta angle is equivalent to an axial chemical potential $\dot{\theta} = \mu_5$ [114]. A change in the theta angle, an external process, induces a chemical potential in the system. A chemical potential must be associated with a conserved charge. This chemical potential must be conjugate to the conserved axial charge of the system. The conserved axial charge then must exist as a configuration in the bulk of the holography.

We can attempt to see what the charge configuration in the bulk looks like by using the definition for charge $Q = \frac{\partial S}{\partial \mu}$ and assuming that the axial chemical potential is defined as $\mu_5 = -A_0(\infty)$. The surface terms that contribute are those that contain A_0,

$$\frac{\partial S}{\partial \mu_5} = \frac{\partial}{\partial(-A_0(\infty))} \int d^4x \left\{ \frac{1}{4g_s^2} A_0 \frac{e^{-\phi}}{z} \partial_z A_0 \right. \tag{7.96}$$

$$- \frac{N_c}{24\pi^2} \varepsilon^{ijk} \left(\frac{2}{6} A_0 V_i V_{jk} + \frac{4}{6} V_i A_0 V_{jk} + \frac{12}{6} A_0 A_i A_{jk} \right) \tag{7.97}$$

$$\left. + \frac{N_c}{24\pi^2} \varepsilon^{ijk} A_0 A_i V_{jk} - \frac{N_c}{12\pi^2} \varepsilon^{ijk} A_0 V_i V_{jk} \right\} \bigg|_{z=\infty}, \tag{7.98}$$

where the first line is from the YM action, the second line is from the CS action, and the last line is from the Bardeen counter-term. Performing the derivative we

find that $A_0(\infty)$ is coupled to a charge,

$$Q^5_{\text{cutoff}} = \int d^4x \left(-\frac{N_c}{24\pi} \partial_w A_0 + \frac{2N_c}{24\pi^2} \varepsilon^{ijk} A_i A_{jk} \right. \tag{7.99}$$

$$\left. + \frac{3N_c}{24\pi^2} \varepsilon^{ijk} V_i V_{jk} - \frac{N_c}{24\pi^2} \varepsilon^{ijk} A_i V_{jk} \right) \Big|_{z=\infty}. \tag{7.100}$$

Let us look closer at the form of this charge.

One would expect the axial charge of the system to be given by integrating over the zeroth component of the axial current given by (7.39) and (7.41),

$$Q^5 = \int d^4x J_0^5, \tag{7.101}$$

$$= \int d^4x \left(-\frac{N_c}{24\pi} \partial_w A_0 + \frac{2N_c}{24\pi^2} \varepsilon^{ijk} A_i A_{jk} \right). \tag{7.102}$$

We see that the charge derived by assuming the boundary condition at infinity is an axial chemical potential (7.99) differs from the charge of the system found by looking at the zeroth component of the axial current (7.102). In fact, if we set $A_i = 0$, as Rubakov does, the two charges, Q^5 and Q^5_{cutoff}, differ by exactly the amount Rubakov used to define his conserved charge given by equation (7.70),

$$Q^5_{\text{Rubakov}} = \int d^4x \left(J_0^5 + \frac{3N_c}{24\pi^2} \varepsilon^{ijk} V_i V_{jk} \right). \tag{7.103}$$

The difference is that the charge we calculated for the boundary condition is evaluated at $z = \infty$, while Rubakov's rests on the holographic boundary. That the boundary value of the axial field $-A_0(\infty)$ is coupled to an object that matches the form of Rubakov's charge is evidence that $-A_0(\infty)$ is related to the axial chemical potential. What configuration past the IR would cause this boundary condition is unknown.

A similar definition of the axial chemical potential was necessitated in the work of [22][1], working in the context of linear response theory, where the horizon of an AdS-Schwarzschild black hole provides the screening of the IR physics. They define, based on the work of [161], the chemical potential as the difference in energy between the boundary and bulk. They then use the Kubo formula to derive their currents. A boundary condition from the bulk affects the current on the boundary.

7.7 Summary

We have introduced a new way of producing the topological current in holography. We see from Eqn. (7.95) that there is now an additional contribution to the current

---

[1]Thank you to Karl Landsteiner for pointing this out to us.

from allowing a non-zero boundary condition for the axial field in the bulk. When $A_0(\infty) = 0$ one expects the anomalous currents to fully cancel and, as discussed before, any contribution to the vector current to disappear. When $A_0(\infty) \neq 0$ we have introduced a boundary condition on the string theory side that achieves the well know result in the field theory side. This is a hint of how to introduce boundary conditions into AdS/CFT calculations that produce finite-volume sensitive results in QCD. We point out that the chiral magnetic effect is one application of this technique. We expect that it can be used to deal with all anomalous currents of the same nature.

Chapter 8

Conclusion

There are two goals of this thesis. The first is to argue that a persistent, topological current is induced in dense stars. This current is an unusual quantum phenomena that has no analogue in classical physics. The idea of the topological vector current introduced in Chapters 3 and 4 is fundamentally new. All the requirements for the current are present in dense stars: a large degeneracy $\mu_e \gg T$, an approximately chiral, Dirac-like spectrum at $\mu_e \gg m_e$, and a large magnetic field B. The second goal is to probe its existence at strong coupling using the AdS/CFT correspondence as a tool.

Confirmation of the existence of topological currents in neutron stars would have an effect on the physics of neutron stars. In Chapter 5 we discussed how the current may explain large pulsar kicks and give a way to discriminate between neutron stars and quark stars. In Chapter 6 we introduced many other ways the current could possible affect the physics of pulsars. Topological currents also provide a source of finite magnetic helicity, a $\mathscr{P}$-odd topological invariant that does not decay in a neutron star environment. This may shed some light on the origin of the strong, self-supporting system of toroidal and poloidal magnetic fields in neutron stars. We mention many apparently unrelated observational effects: neutron star kicks, toroidal fields, and magnetic helicity. These all have a $\mathscr{P}$-odd symmetry and it is likely that they all originate from the same $\mathscr{P}$-odd physics. The topological vector current introduced in this paper occurs because of parity violating effects. This current may be responsible for all of these $\mathscr{P}$-odd phenomena.

There is also a possibility that these types of currents will be observed terrestrially in the quark-gluon plasma created in gold-gold collisions at RHIC and thought to be created in lead-lead collisions at LHC [162, 163]. An analogue to the anomalous current has been used to predict a charge separation effect [11] and preliminary experimental results from RHIC are supporting it through the observation of parity violating interactions [13–17]. In this analogue each requirement for the current to exist in the neutron star has its complement: the role of the coherent magnetic field is played by the angular momentum $\vec{L}$, which occurs at non-central nuclei collisions, and the role of parity violating effects is played by the induced θ vacua. The observation of the charge separation indirectly supports our prediction of induced anomalous currents.

The work done in Chapter 7 on producing topological currents in a holographic model of QCD is related to the observation of the current at RHIC. The quark-gluon plasma at RHIC is likely in a regime that is still strongly interacting. One would like to be sure that the topological currents thought to be responsible for the parity violation seen at RHIC actually exist is a strongly coupled regime. This would mean that the very strong interactions in each nuclei-nuclei collision event cannot wash out the produced asymmetry. This parallels our argument in Chapter 3 that strong electromagnetic interactions do not wash out the $\mathscr{P}$-odd produced asymmetry and the relevant scale of the problem is the mean free path of the electron due to the weak interactions that are capable of washing out $\mathscr{P}$-odd effects. Our discovery of how to introduce currents into holographic models may help ensure that topological current phenomena, like the chiral magnetic and charge separation effects, are indeed the cause of the parity violation at RHIC.

In condensed matter laboratories low temperatures and strong magnetic fields present no technical difficulties. The key is finding a system of quasiparticles with a Dirac-like spectrum. There are such systems: superfluid He^3, high T_c superconductors with d-wave pairing, and graphene. Remarkably, in superfluid He^3 the current analogous to our anomalous current has been observed, see reviews [30] and [31].

There is still much to be done to refine the applications of topological currents in dense stars, which may advance the understanding of the phases of matter that exist inside quark and neutron stars. Having discussed how one can use topological currents to generate the large kicks observed in some pulsars, the next step is to study the current and magnetic fields interact outside the quark star. How exactly is the momentum transferred from the current to the kick? There is a possibility that the predominantly left-handed electrons that make up the topological currents could leave a polarization signature that could be observed.

There are also many questions to be answered about the nature of the poloidal and magnetic fields in neutron stars. A toroidal component is required for the stability of the poloidal component [25] and is responsible for the star's surface temperature distribution [140], but its source is undetermined. The configuration and strength of the topological current in the star suggests it is a candidate for the origin of this field. In addition, the cause of large glitches [73], discrete increases in the angular momentum of the neutron star's crust, is still unknown. It may be that macroscopic vortex sheets caused by currents are responsible for these.

The work done to topological currents in the framework of holographic QCD helped develop an new idea in holographic QCD. The realization made when introducing these currents is that a non-physical boundary condition in the bulk of the holography can contribute to physical results on the holographic boundary. It would be interesting to extend this usage of boundary conditions to calculations

in strongly coupled regimes that hinge on the existence of unphysical or abnormal boundary conditions. The most promising is the work done on ghost dynamics in curved space that may be the cause of dark energy [164].

Bibliography

[1] A. Vilenkin, *Macroscopic parity-violating effects: Neutrino fluxes from rotating black holes and in rotating thermal radiation*, *Phys. Rev. D* **20** (Oct, 1979) 1807–1812.

[2] A. Vilenkin, *Cancellation of equilibrium parity-violating currents*, *Phys. Rev. D* **22** (Dec, 1980) 3067–3079.

[3] A. Vilenkin, *Equilibrium parity-violating current in a magnetic field*, *Phys. Rev. D* **22** (Dec, 1980) 3080–3084.

[4] A. Y. Alekseev, V. V. Cheianov, and J. Fröhlich, *Universality of transport properties in equilibrium, the goldstone theorem, and chiral anomaly*, *Phys. Rev. Lett.* **81** (Oct, 1998) 3503–3506, [`arXiv:cond-mat/9803346`].

[5] D. T. Son and A. R. Zhitnitsky, *Quantum anomalies in dense matter*, *Phys. Rev.* **D70** (2004) 074018, [`hep-ph/0405216`].

[6] M. A. Metlitski and A. R. Zhitnitsky, *Anomalous axion interactions and topological currents in dense matter*, *Phys. Rev.* **D72** (2005) 045011, [`hep-ph/0505072`].

[7] M. A. Metlitski, *Currents on superconducting strings at finite chemical potential and temperature*, *Phys. Lett.* **B612** (2005) 137–146, [`hep-ph/0501144`].

[8] J. Charbonneau and A. Zhitnitsky, *A Novel Mechanism for Type-I Superconductivity in Neutron Stars*, *Phys. Rev.* **C76** (2007) 015801, [`astro-ph/0701308`].

[9] J. Charbonneau and A. Zhitnitsky, *Topological Currents in Neutron Stars: Kicks, Precession, Toroidal Fields, and Magnetic Helicity*, *JCAP* **1008** (2010) 010, [`arXiv:0903.4450`].

[10] J. Charbonneau, K. Hoffman, and J. Heyl, *Large Pulsar Kicks from Topological Currents*, *Mon. Not. Roy. Astron. Soc. Lett.* **404** (2010) L119–L123, [`arXiv:0912.3822`].

[11] D. Kharzeev and A. Zhitnitsky, *Charge separation induced by P-odd bubbles in QCD matter*, *Nucl. Phys.* **A797** (2007) 67–79, [`arXiv:0706.1026`].

[12] K. Fukushima, D. E. Kharzeev, and H. J. Warringa, *The Chiral Magnetic Effect*, *Phys. Rev.* **D78** (2008) 074033, [`arXiv:0808.3382`].

[13] S. A. Voloshin, *Parity violation in hot QCD: How to detect it*, *Phys. Rev.* **C70** (2004) 057901, [`hep-ph/0406311`].

[14] **STAR** Collaboration, I. V. Selyuzhenkov, *Global polarization and parity violation study in Au + Au collisions*, *Rom. Rep. Phys.* **58** (2006) 049–054, [`nucl-ex/0510069`].

[15] **STAR** Collaboration, S. A. Voloshin, *Experimental study of local strong parity violation in relativistic nuclear collisions*, *Nucl. Phys.* **A830** (2009) 377c–384c, [`arXiv:0907.2213`].

[16] **STAR** Collaboration, B. I. Abelev *et al.*, *Azimuthal Charged-Particle Correlations and Possible Local Strong Parity Violation*, *Phys. Rev. Lett.* **103** (2009) 251601, [`arXiv:0909.1739`].

[17] **STAR** Collaboration, B. I. Abelev *et al.*, *Observation of charge-dependent azimuthal correlations and possible local strong parity violation in heavy ion collisions*, *Phys. Rev.* **C81** (2010) 054908, [`arXiv:0909.1717`].

[18] O. Bergman, G. Lifschytz, and M. Lippert, *Magnetic properties of dense holographic QCD*, *Phys. Rev.* **D79** (2009) 105024, [`arXiv:0806.0366`].

[19] A. Rebhan, A. Schmitt, and S. A. Stricker, *Anomalies and the chiral magnetic effect in the Sakai- Sugimoto model*, *JHEP* **01** (2010) 026, [`arXiv:0909.4782`].

[20] A. Gorsky, P. N. Kopnin, and A. V. Zayakin, *On the Chiral Magnetic Effect in Soft-Wall AdS/QCD*, *Phys. Rev.* **D83** (2011) 014023, [`arXiv:1003.2293`].

[21] V. Rubakov, *On chiral magnetic effect and holography*, `arXiv:1005.1888`. * Temporary entry *.

[22] A. Gynther, K. Landsteiner, F. Pena-Benitez, and A. Rebhan, *Holographic Anomalous Conductivities and the Chiral Magnetic Effect*, `arXiv:1005.2587`.

[23] L. Brits and J. Charbonneau, *A Constraint-Based Approach to the Chiral Magnetic Effect*, `arXiv:1009.4230`.

[24] G. A. E. Wright, *Pinch instabilities in magnetic stars*, *MNRAS* **162** (1973) 339.

[25] P. Markey and R. Tayler, *The adiabatic stability of stars containing magnetic fields-ii*, *MNRAS* **163** (1973) 77.

[26] E. Flowers and M. A. Ruderman, *Evolution of pulsar magnetic fields*, *Astrophys. J.* **215** (1977) 302–310.

[27] H. C. Spruit, *Origin of neutron star magnetic fields*, *AIP Conf. Proc.* **983** (2008) 391–398, [`arXiv:0711.3650`].

[28] E. Witten, *Superconducting Strings*, *Nucl. Phys.* **B249** (1985) 557–592.

[29] A. J. Niemi and G. W. Semenoff, *Fermion Number Fractionization in Quantum Field Theory*, *Phys. Rept.* **135** (1986) 99.

[30] M. M. Salomaa and G. E. Volovik, *Quantized vortices in superfluid he*3, *Rev. Mod. Phys.* **59** (Jul, 1987) 533–613.

[31] G. E. Volovik, *Superfluid analogies of cosmological phenomena*, *Physics Reports* **351** (2001), no. 4 195 – 348.

[32] D. E. Kharzeev, L. D. McLerran, and H. J. Warringa, *The effects of topological charge change in heavy ion collisions: 'Event by event P and CP violation'*, *Nucl. Phys.* **A803** (2008) 227–253, [`arXiv:0711.0950`].

[33] D. T. Son and M. A. Stephanov, *Axial anomaly and magnetism of nuclear and quark matter*, *Phys. Rev.* **D77** (2008) 014021, [`arXiv:0710.1084`].

[34] J. A. Harvey, C. T. Hill, and R. J. Hill, *Anomaly mediated neutrino-photon interactions at finite baryon density*, *Phys. Rev. Lett.* **99** (2007) 261601, [`arXiv:0708.1281`].

[35] J. Steinberger, *On the use of subtraction fields and the lifetimes of some types of meson decay*, *Phys. Rev.* **76** (Oct, 1949) 1180–1186.

[36] J. Schwinger, *On gauge invariance and vacuum polarization*, *Phys. Rev.* **82** (Jun, 1951) 664–679.

[37] J. S. Bell and R. Jackiw, *A PCAC puzzle: pi0 → gamma gamma in the sigma model*, *Nuovo Cim.* **A60** (1969) 47–61.

[38] S. L. Adler, *Axial vector vertex in spinor electrodynamics*, *Phys. Rev.* **177** (1969) 2426–2438.

[39] P. H. Frampton, *Gauge Field Theories*. Wiley-VCH, October, 2008.

[40] M. E. Peskin and D. V. Schroeder, *An Introduction To Quantum Field Theory (Frontiers in Physics)*. Westview Press, October, 1995.

[41] L. H. Ryder, *Quantum Field Theory*. Cambridge University Press, 2 ed., June, 1996.

[42] S. L. Adler and W. A. Bardeen, *Absence of higher order corrections in the anomalous axial vector divergence equation*, *Phys. Rev.* **182** (1969) 1517–1536.

[43] K. Fujikawa, *Path Integral for Gauge Theories with Fermions*, *Phys. Rev.* **D21** (1980) 2848.

[44] K. Fujikawa and H. Suzuki, *Path Integrals and Quantum Anomalies*. Oxford University Press, USA, 2004.

[45] S. E. Thorsett and D. Chakrabarty, *Neutron star mass measurements. i. radio pulsars*, *The Astrophysical Journal* **512** (1999), no. 1 288.

[46] L. Landau, *On the theory of stars*, *Phys. Z. Sowjetunion* **1** (1932) 285.

[47] W. Baade and F. Zwicky, *On super-novae*, *Proc. of the Nat. Acad. of Sci.* **20** (1934) 254.

[48] J. R. Oppenheimer and G. M. Volkoff, *On massive neutron cores*, *Phys. Rev.* **55** (Feb, 1939) 374–381.

[49] R. C. Tolman, *Static solutions of einstein's field equations for spheres of fluid*, *Phys. Rev.* **55** (Feb, 1939) 364–373.

[50] A. Hewish, S. J. Bell, J. D. H. Pilkington, P. F. Scott, and R. A. Collins, *Observation of a rapidly pulsating radio source*, *Nature* **217** (1968) 709–713.

[51] F. Pacini, *Energy emission from a neutron star*, *Nature* **216** (Nov, 1967) 567–568. 10.1038/216567a0.

[52] T. Gold, *Rotating neutron stars as the origin of the pulsating radio sources*, *Nature* **218** (May, 1968) 731–732. 10.1038/218731a0.

[53] R. N. Manchester, G. B. Hobbs, A. Teoh, and M. Hobbs, *The atnf pulsar catalogue*, *Astronomical Journal* **129** (2005) [http://www.atnf.csiro.au/research/pulsar/psrcat].

[54] D. R. Lorimer and M. Kramer, *Handbook of Pulsar Astronomy*. Handbook of pulsar astronomy, by D.R. Lorimer and M. Kramer. Cambridge observing handbooks for research astronomers, Vol. 4. Cambridge, UK: Cambridge University Press, 2004, 2004.

[55] P. Ghosh, *Rotation and Accretion Powered Pulsars*, vol. 10. World Scientific, 2007.

[56] V. Kaspi and D. Helfand, *Constraining the birth events of neutron stars*, *Neutron Stars in Supernova Remnants (ASP Conference Proceedings)* **271** (2002) 3, [astro-ph/0201183].

[57] A. G. Lyne and F. Graham-Smith, *Pulsar astronomy / A.G. Lyne, F. Graham-Smith*. Cambridge University Press, Cambridge [England] ; New York :, 1990.

[58] P. Goldreich and W. H. Julian, *Pulsar electrodynamics*, *Astrophys. J.* **157** (1969) 869.

[59] V. Radhakrishnan and D. J. Cooke, *Magnetic Poles and the Polarization Structure of Pulsar Radiation*, *Astrophysical Letters* **3** (1969) 225.

[60] A. Y. P. P. Haensel and D. G. Yakovlev, *Neutron Stars 1: Equation of State and Structure*, vol. 326. Springer Science+Business Media, LCC, 2007.

[61] D. G. Yakovlev and C. J. Pethick, *Neutron star cooling*, *Ann. Rev. Astron. Astrophys.* **42** (2004) 169–210, [astro-ph/0402143].

[62] P. Demorest, T. Pennucci, S. Ransom, M. Roberts, and J. Hessels, *Shapiro delay measurement of a two solar mass neutron star*, *Nature* **467** (2010) 1081–1083, [arXiv:1010.5788].

[63] J. M. Lattimer, M. Prakash, C. J. Pethick, and P. Haensel, *Direct URCA process in neutron stars*, *Phys. Rev. Lett.* **66** (1991) 2701–2704.

[64] D. Page and S. Reddy, *Dense Matter in Compact Stars: Theoretical Developments and Observational Constraints*, *Ann. Rev. Nucl. Part. Sci.* **56** (2006) 327–374, [astro-ph/0608360].

[65] J. N. Bahcall and R. A. Wolf, *Neutron Stars. 2. Neutrino-Cooling and Observability*, *Phys. Rev.* **140** (1965) B1452–B1466.

[66] D. B. Kaplan and A. E. Nelson, *Strange Goings on in Dense Nucleonic Matter*, *Phys. Lett.* **B175** (1986) 57–63.

[67] N. Iwamoto, *Neutrino Emmisivities and Mean Free Paths of Degenerate Quark Matter*, *Ann. of Phys.* **141** (1982), no. 1 1.

[68] O. Maxwell, G. E. Brown, D. K. Campbell, R. F. Dashen, and J. T. Manassah, *Beta decay of pion condensates as a cooling mechanism for neutron stars*, *Astrophys. J.* **216** (1977) 77–85.

[69] J. N. Bahcall and R. A. Wolf, *Neutron Stars. 1. Properties at Absolute Zero Temperature*, *Phys. Rev.* **140** (1965) B1445–B1451.

[70] G. E. Brown, K. Kubodera, D. Page, and P. Pizzochero, *Strangeness Condensation and Cooling of Neutron Stars*, *Phys. Rev.* **D37** (1988) 2042–2046.

[71] A. Schmitt, *Dense matter in compact stars - A pedagogical introduction*, *Lect. Notes Phys.* **811** (2010) 1–111, [arXiv:1001.3294].

[72] E. Farhi and R. L. Jaffe, *Strange Matter*, *Phys. Rev.* **D30** (1984) 2379.

[73] R. E. Packard, *Pulsar speedups related to metastability of the superfluid neutron-star core*, *Phys. Rev. Lett.* **28** (Apr, 1972) 1080–1082.

[74] D. Page, M. Prakash, J. M. Lattimer, and A. W. Steiner, *Rapid cooling of the neutron star in cassiopeia a triggered by neutron superfluidity in dense matter*, *Phys. Rev. Lett.* **106** (Feb, 2011) 081101.

[75] P. S. Shternin, D. G. Yakovlev, C. O. Heinke, W. C. G. Ho, and D. J. Patnaude, *Cooling neutron star in the Cassiopeia A supernova remnant: Evidence for superfluidity in the core*, arXiv:1012.0045.

[76] J. Sauls, *Superfluidity in the interiors of neutron stars*, *NATo ASI Series C* **262** (1989) 457.

[77] N. W. Ashcroft and D. N. Mermin, *Solid State Physics*. Thomson Learning, Toronto, 1 ed., Jan., 1976.

[78] R. Tamagaki, *Superfluid state in neutron star matter. i*, *Progress of Theoretical Physics* **44** (1970), no. 4 905–928.

[79] A. Sedrakian, *Type-i superconductivity and neutron star precession*, *Phys. Rev. D* **71** (Apr, 2005) 083003.

[80] D. Pines and M. Alpar, *Superfluidity in neutron stars*, *Nature* **316** (Jul, 1985) 27–32. 10.1038/316027a0.

[81] D. Page, J. M. Lattimer, M. Prakash, and A. W. Steiner, *Minimal cooling of neutron stars: A new paradigm*, *The Astrophysical Journal Supplement Series* **155** (2004), no. 2 623.

[82] M. G. Alford, A. Schmitt, K. Rajagopal, and T. Schäfer, *Color superconductivity in dense quark matter*, *Rev. Mod. Phys.* **80** (Nov, 2008) 1455–1515.

[83] B. Link, *Constraining Hadronic Superfluidity with Neutron Star Precession*, *Phys. Rev. Lett.* **91** (2003) 101101, [astro-ph/0302441].

[84] B. Link, *Incompatibility of long-period neutron star precession with creeping neutron vortices*, astro-ph/0608319.

[85] K. B. W. Buckley, M. A. Metlitski, and A. R. Zhitnitsky, *Neutron Stars as Type I Superconductors*, *Phys. Rev. Lett.* **92** (2004) 151102, [astro-ph/0308148].

[86] H. Spruit and E. S. Phinney, *Why pulsars rotate and move: kicks at birth*, *Nature* **393** (1998) 139–141, [astro-ph/9803201].

[87] Z. Arzoumanian, D. F. Chernoffs, and J. M. Cordes, *The Velocity Distribution of Isolated Radio Pulsars s*, *Astrophys. J.* **568** (2002) 289–301, [astro-ph/0106159].

[88] G. Hobbs, D. R. Lorimer, A. G. Lyne, and M. Kramer, *A statistical study of 233 pulsar proper motions*, *Mon. Not. Roy. Astron. Soc.* **360** (2005) 974–992, [astro-ph/0504584].

[89] C.-A. Faucher-Giguere and V. M. Kaspi, *Birth and evolution of isolated radio pulsars*, *The Astrophysical Journal* **643** (2006), no. 1 332–355.

[90] C.-Y. Ng and R. W. Romani, *Fitting pulsar wind tori*, *The Astrophysical Journal* **601** (2004), no. 1 479.

[91] S. Johnston, G. Hobbs, S. Vigeland, M. Kramer, J. M. Weisberg, and A. G. Lyne, *Evidence for alignment of the rotation and velocity vectors in pulsars*, *Monthly Notices of the Royal Astronomical Society* **364** (2005), no. 4 1397–1412.

[92] D. Lai, C. Wang, and J. Han, *Neutron star kicks: Mechanisms and observational constraints*, *Chinese Journal of Astronomy and Astrophysics* **6** (2006), no. S2 241–247.

[93] D. Lai, *Neutron Star Kicks and Supernova Asymmetry*. Cambridge University Press, 2003.

[94] L. Scheck, T. Plewa, H.-T. Janka, K. Kifonidis, and E. Mueller, *Pulsar Recoil by Large-Scale Anisotropies in Supernova Explosions*, *Phys. Rev. Lett.* **92** (2004) 011103, [`astro-ph/0307352`].

[95] J. Nordhaus, T. D. Brandt, A. Burrows, E. Livne, and C. D. Ott, *Theoretical Support for the Hydrodynamic Mechanism of Pulsar Kicks*, *Phys. Rev.* **D82** (2010) 103016, [`arXiv:1010.0674`].

[96] E. R. Harrison and E. Tademaru, *Acceleration of pulsars by asymmetric radiation*, *Astrophys. J.* **201** (Oct., 1975) 447–461.

[97] D. Lai, D. F. Chernoff, and J. M. Cordes, *Pulsar jets: Implications for neutron star kicks and initial spins*, *The Astrophysical Journal* **549** (2001), no. 2 1111–1118, [`http://www.journals.uchicago.edu/doi/pdf/10.1086/319455`].

[98] J. M. Maldacena, *The large N limit of superconformal field theories and supergravity*, *Adv. Theor. Math. Phys.* **2** (1998) 231–252, [`hep-th/9711200`].

[99] G. Policastro, D. T. Son, and A. O. Starinets, *The shear viscosity of strongly coupled N = 4 supersymmetric Yang-Mills plasma*, *Phys. Rev. Lett.* **87** (2001) 081601, [`hep-th/0104066`].

[100] D. T. Son and A. O. Starinets, *Viscosity, Black Holes, and Quantum Field Theory*, *Ann. Rev. Nucl. Part. Sci.* **57** (2007) 95–118, [`arXiv:0704.0240`].

[101] O. Aharony, S. S. Gubser, J. M. Maldacena, H. Ooguri, and Y. Oz, *Large N field theories, string theory and gravity*, *Phys. Rept.* **323** (2000) 183–386, [`hep-th/9905111`].

[102] G. T. Horowitz and A. Strominger, *Black strings and P-branes*, *Nucl. Phys.* **B360** (1991) 197–209.

[103] S. S. Gubser, I. R. Klebanov, and A. W. Peet, *Entropy and Temperature of Black 3-Branes*, *Phys. Rev.* **D54** (1996) 3915–3919, [`hep-th/9602135`].

[104] E. D'Hoker and D. H. Phong, *Lectures on supersymmetric Yang-Mills theory and integrable systems*, `hep-th/9912271`.

[105] D. Young, *The AdS/CFT Correspondence: Classical, Quantum, and Thermodynamical Aspects*, `arXiv:0706.3751`.

[106] S. S. Gubser, I. R. Klebanov, and A. M. Polyakov, *Gauge theory correlators from non-critical string theory*, *Phys. Lett.* **B428** (1998) 105–114, [`hep-th/9802109`].

[107] E. Witten, *Anti-de Sitter space and holography*, *Adv. Theor. Math. Phys.* **2** (1998) 253–291, [`hep-th/9802150`].

[108] G. Policastro, D. T. Son, and A. O. Starinets, *From AdS/CFT correspondence to hydrodynamics*, *JHEP* **09** (2002) 043, [`hep-th/0205052`].

[109] D. T. Son and A. O. Starinets, *Minkowski-space correlators in AdS/CFT correspondence: Recipe and applications*, *JHEP* **09** (2002) 042, [`hep-th/0205051`].

[110] S. S. Gubser, I. R. Klebanov, and A. A. Tseytlin, *Coupling constant dependence in the thermodynamics of N = 4 supersymmetric Yang-Mills theory*, *Nucl. Phys.* **B534** (1998) 202–222, [`hep-th/9805156`].

[111] A. Buchel, J. T. Liu, and A. O. Starinets, *Coupling constant dependence of the shear viscosity in N=4 supersymmetric Yang-Mills theory*, *Nucl. Phys.* **B707** (2005) 56–68, [`hep-th/0406264`].

[112] D. Mateos, *String Theory and Quantum Chromodynamics*, *Class. Quant. Grav.* **24** (2007) S713–S740, [`arXiv:0709.1523`].

[113] A. Buchel, *On universality of stress-energy tensor correlation functions in supergravity*, *Phys. Lett.* **B609** (2005) 392–401, [`hep-th/0408095`].

[114] D. E. Kharzeev, *Topologically induced local P and CP violation in QCD x QED*, *Annals Phys.* **325** (2010) 205–218, [`arXiv:0911.3715`].

[115] A. Kusenko, G. Segre, and A. Vilenkin, *Neutrino transport: No asymmetry in equilibrium*, *Phys. Lett.* **B437** (1998) 359–361, [`astro-ph/9806205`].

[116] I. Sagert and J. Schaffner-Bielich, *Pulsar kicks by anisotropic neutrino emission from quark matter in strong magnetic fields*, `arXiv:0708.2352`.

[117] J. J. Matese and R. F. O'Connell, *Neutron Beta Decay in a Uniform Constant Magnetic Field*, *Phys. Rev.* **180** (1969) 1289–1292.

[118] O. F. Dorofeev, V. N. Rodionov, and I. M. Ternov, *Anisotropic neutrino emission in beta processes induced by an intense magnetic field*, *JETP Lett.* **40** (1984) 917–920.

[119] B. L. Friman and O. V. Maxwell, *Neutron Star Neutrino Emissivities*, *Astrophys. J.* **232** (1979) 541.

[120] G. E. Brown, V. Thorsson, K. Kubodera, and M. Rho, *A Novel mechanism for kaon condensation in neutron star matter*, *Phys. Lett.* **B291** (1992) 355–362.

[121] J. E. Gunn and J. P. Ostriker, *On the nature of pulsars. iii. analysis of observations*, *Astrophys. J.* **160** (1970) 979.

[122] A. G. Lyne and D. R. Lorimer, *High birth velocities of radio pulsars*, *Nature* **369** (1994) 127.

[123] B. M. S. Hansen and E. S. Phinney, *The Pulsar kick velocity distribution*, *Mon. Not. Roy. Astron. Soc.* **291** (1997) 569, [`astro-ph/9708071`].

[124] J. M. Cordes and D. F. Chernoff, *Neutron Star Population Dynamics.II: 3D Space Velocities of Young Pulsars*, *Astrophys. J.* **505** (1998) 315–338, [`astro-ph/9707308`].

[125] C. Fryer, A. Burrows, and W. Benz, *Population Synthesis for Neutron Star Systems with Intrinsic Kicks*, *Astrophys. J.* **496** (1998) 333, [`astro-ph/9710333`].

[126] C. L. Fryer, *Neutron star kicks from asymmetric collapse*, *Astrophys. J.* **601** (2004) L175–L178, [`astro-ph/0312265`].

[127] S. Chatterjee *et al.*, *Getting Its Kicks: A VLBA Parallax for the Hyperfast Pulsar B1508+55*, *Astrophys. J.* **630** (2005) L61–L64, [`astro-ph/0509031`].

[128] I. Sagert and J. Schaffner-Bielich, *Asymmetric neutrino emission in quark matter and pulsar kicks*, `astro-ph/0612776`.

[129] I. Sagert and J. Schaffner-Bielich, *Pulsar kicks by anisotropic neutrino emission from quark matter*, *J. Phys.* **G35** (2008) 014062, [`arXiv:0707.0577`].

[130] C. Wang, D. Lai, and J. Han, *Spin-Kick Correlation in Neutron Stars: Alignment Conditions and Implications*, *Astrophys. J.* **656** (2007) 399–407, [astro-ph/0607666].

[131] C. Alcock, E. Farhi, and A. Olinto, *Strange stars*, *Astrophys. J.* **310** (1986) 261–272.

[132] P. Jaikumar, S. Reddy, and A. W. Steiner, *The strange star surface: A crust with nuggets*, *Phys. Rev. Lett.* **96** (2006) 041101, [nucl-th/0507055].

[133] M. G. Alford, K. Rajagopal, S. Reddy, and A. W. Steiner, *The stability of strange star crusts and strangelets*, *Phys. Rev.* **D73** (2006) 114016, [hep-ph/0604134].

[134] S. Reddy, *Novel phases at high density and their roles in the structure and evolution of neutron stars*, *Acta Phys. Polon.* **B33** (2002) 4101–4140, [nucl-th/0211045].

[135] P. Haensel, B. B. Paczynski, and P. P. Amsterdamski, *Gamma-ray bursts from colliding strange stars*, *Astrophys. J.* **375** (1991) 209–215.

[136] D. Page and V. V. Usov, *Thermal Evolution and Light Curves of Young Bare Strange Stars*, *Phys. Rev. Lett.* **89** (2002) 131101, [astro-ph/0204275].

[137] D. Lai and S. L. Shapiro, *Cold equation of state in a strong magnetic field - Effects of inverse beta-decay*, *Astrophys. J.* **383** (1991) 745–751.

[138] K. H. Prendergast, *The equilibrium of a self-gravitating incompressible fluid sphere with a magnetic field. i.*, *Astrophys. J.* **123** (1956) 498.

[139] R. J. Tayler, *The adiabatic stability of stars containing magnetic fields-i.toroidal fields*, *MNRAS* **161** (1973) 365.

[140] D. Page, U. Geppert, and M. Kueker, *Cooling of Neutron Stars with Strong Toroidal Magnetic Fields*, *Astrophys. Space Sci.* **308** (2007) 403–412, [astro-ph/0701442].

[141] M. Tinkham, *Introduction to Superconductivity*. McGraw-Hill Inc., 2nd ed., 1996.

[142] I. Easson and C. J. Pethick, *Stress tensor of cosmic and laboratory type-ii superconductors*, *Phys. Rev. D* **16** (Jul, 1977) 275–280.

[143] A. R. Choudhuri, *The Physics of Fluids and Plasmas: An Introduction for Astrophysicists*. Cambridge University Press, 1998.

[144] G. G. Pavlov, O. Y. Kargaltsev, D. Sanwal, , and G. P. Garmire, *Variability of the vela pulsar wind nebula observed with chandra*, *The Astrophysical Journal Letters* **554** (2001), no. 2 L189–L192.

[145] C. Wang, D. Lai, and J. Han, *Neutron Star Kicks in Isolated and Binary Pulsars: Observational Constraints and Implications for Kick Mechanisms*, *Astrophys. J.* **639** (2006) 1007–1017, [`astro-ph/0509484`].

[146] D. Lai, D. F. Chernoff, and J. M. Cordes, *Pulsar jets: Implications for neutron star kicks and initial spins*, *The Astrophysical Journal* **549** (2001), no. 2 1111.

[147] M. C. Weisskopf *et al.*, *The prospects for X-ray polarimetry and its potential use for understanding neutron stars*, `astro-ph/0611483`.

[148] I. H. Stairs, A. G. Lyne, and S. L. Shemar, *Evidence for free precession in a pulsar*, *Nature* **406** (2000) 484–486.

[149] A. Lyne, G. Hobbs, M. Kramer, I. Stairs, and B. Stappers, *Switched magnetospheric regulation of pulsar spin-down*, *Science* **329** (2010), no. 5990 408–412, [`http://www.sciencemag.org/content/329/5990/408.full.pdf`].

[150] A. Sedrakian, *Type-I superconductivity and neutron star precession*, *Phys. Rev.* **D71** (2005) 083003, [`astro-ph/0408467`].

[151] H.-U. Yee, *Holographic Chiral Magnetic Conductivity*, *JHEP* **11** (2009) 085, [`arXiv:0908.4189`].

[152] P. V. Buividovich, M. N. Chernodub, E. V. Luschevskaya, and M. I. Polikarpov, *Numerical evidence of chiral magnetic effect in lattice gauge theory*, *Phys. Rev.* **D80** (2009) 054503, [`arXiv:0907.0494`].

[153] J. Polchinski and M. J. Strassler, *Hard scattering and gauge / string duality*, *Phys. Rev. Lett.* **88** (2002) 031601, [`hep-th/0109174`].

[154] J. Erlich, E. Katz, D. T. Son, and M. A. Stephanov, *QCD and a Holographic Model of Hadrons*, *Phys. Rev. Lett.* **95** (2005) 261602, [`hep-ph/0501128`].

[155] L. Da Rold and A. Pomarol, *Chiral symmetry breaking from five dimensional spaces*, *Nucl. Phys.* **B721** (2005) 79–97, [hep-ph/0501218].

[156] O. Andreev, $1/q^2$ *corrections and gauge / string duality*, *Phys. Rev.* **D73** (2006) 107901, [hep-th/0603170].

[157] A. Karch, E. Katz, D. T. Son, and M. A. Stephanov, *Linear Confinement and AdS/QCD*, *Phys. Rev.* **D74** (2006) 015005, [hep-ph/0602229].

[158] S. K. Domokos and J. A. Harvey, *Baryon number-induced Chern-Simons couplings of vector and axial-vector mesons in holographic QCD*, *Phys. Rev. Lett.* **99** (2007) 141602, [arXiv:0704.1604].

[159] C. T. Hill, *Anomalies, Chern-Simons terms and chiral delocalization in extra dimensions*, *Phys. Rev.* **D73** (2006) 085001, [hep-th/0601154].

[160] W. A. Bardeen, *Anomalous Ward identities in spinor field theories*, *Phys.Rev.* **184** (1969) 1848–1857.

[161] K. Ghoroku, M. Ishihara, and A. Nakamura, *D3/D7 holographic Gauge theory and Chemical potential*, *Phys. Rev.* **D76** (2007) 124006, [arXiv:0708.3706].

[162] **The ALICE** Collaboration, K. Aamodt *et al.*, *Elliptic flow of charged particles in Pb-Pb collisions at 2.76 TeV*, arXiv:1011.3914.

[163] **The ALICE** Collaboration, K. Aamodt *et al.*, *Charged-particle multiplicity density at mid-rapidity in central Pb-Pb collisions at sqrt(sNN) = 2.76 TeV*, *Phys. Rev. Lett.* **105** (2010) 252301, [arXiv:1011.3916].

[164] A. R. Zhitnitsky, *The Gauge Fields and Ghosts in Rindler Space*, arXiv:1004.2040.

Appendix A

Details for Calculating Thermal Properties from Gravity

A.1 Minkowski Correlation Functions

One more piece of the AdS/CFT dictionary is required before we go ahead. There is a connection between operators and fields. Since we want to find properties of the Maxwell field our operator is $O = -\mathscr{L} = \frac{1}{4}F_{\mu\nu}^2$ which corresponds to the scalar dilaton field ϕ on the gravity side. So when we calculate correlation functions for the Maxwell field we will always take derivatives with respect to the boundary of the dilaton field ϕ_0.

We will follow the discussion from [100, 109]. Let's consider the action of a scalar field in the background that has a metric of the form

$$ds^2 = g_{rr}dr^2 + g_{\mu\nu}(r)dx^\mu dx^\nu \,. \tag{A.1}$$

A more general metric may be chosen but we are interested in this one as the AdS$_5$ metric conforms to it. Up to second order in ϕ the action is

$$S = K \int d^4x \int dr \sqrt{-g}[g^{rr}\partial_r\phi\partial_r\phi + g^{\mu\nu}\partial_\mu\phi\partial_\nu\phi - m^2\phi^2]\,, \tag{A.2}$$

where $K = -\pi^3 R^5/4\kappa_{10}^2$. The Euler-Lagrange equations of motion follow easily,

$$\partial_r(\sqrt{-g}\,g^{rr}\partial_r\phi) + \sqrt{-g}(g^{\mu\nu}\partial_\mu\partial_\nu + m^2)\phi = 0\,. \tag{A.3}$$

In order to take functional derivatives of this we need to write it in terms of the boundary fields ϕ_0. We assume that ϕ has the solution

$$\phi(r,x) = \int \frac{d^4k}{(2\pi)^4}e^{ik\cdot x}f_k(r)\phi_0(k)\,, \tag{A.4}$$

and plug it in to the action

$$
\begin{aligned}
S &= K \int d^4x \int dr \int \frac{d^4k}{(2\pi)^4} \int \frac{d^4k'}{(2\pi)^4} \sqrt{-g}\, e^{i(k+k')\cdot x} \big[g^{rr} \partial_r f_k(r) \partial_r f_{k'}(r) \\
&\quad - (g^{\mu\nu} k_\mu k'_\nu + m^2) f_k(r) f_{k'}(r) \big] \phi_0(k) \phi_0(k')\,, \\
&= K \int dr \int \frac{d^4k}{(2\pi)^4} \sqrt{-g}\, \big[g^{rr} \partial_r f_k(r) \partial_r f_{-k}(r) \\
&\quad - (g^{\mu\nu} k_\mu k_\nu + m^2) f_k(r) f_{-k}(r) \big] \phi_0(k) \phi_0(-k)\,.
\end{aligned}
\tag{A.5}
$$

Substituting the solution for $\phi(r,x)$ in to the equation of motion gives the equation of motion for $f_k(r)$,

$$
-\sqrt{-g}(g^{\mu\nu} k_\mu k_\nu + m^2) f_{-k} = \partial_r(\sqrt{-g}\, g^{rr} \partial_r f_{-k})\,.
\tag{A.6}
$$

Performing integration by parts on the first term of (A.5) and substituting in the equation of motion for the second term yields

$$
\begin{aligned}
S &= K \int dr \int \frac{d^4k}{(2\pi)^4} \big[\partial_r(\sqrt{-g} g^{rr} f_k(r) \partial_r f_{-k}(r)) - f_k(r) \partial_r(\sqrt{-g}\, g^{rr} \partial_r f_{-k}) \\
&\quad + f_k(r) \partial_r(\sqrt{-g}\, g^{rr} \partial_r f_{-k}) \big] \phi_0(k) \phi_0(-k)\,, \\
&= K \int dr \int \frac{d^4k}{(2\pi)^4} \partial_r(\sqrt{-g} g^{rr} f_k(r) \partial_r f_{-k}(r)) \phi_0(k) \phi_0(-k)\,, \\
&= K \int \frac{d^4k}{(2\pi)^4} \sqrt{-g} g^{rr} f_k(r) \partial_r f_{-k}(r) \phi_0(k) \phi_0(-k) \Big|_{r_B}^{r_H}\,, \\
&= \int \frac{d^4k}{(2\pi)^4} \phi_0(-k) [F(r_H,k) - F(r_B,k)] \phi_0(k)\,,
\end{aligned}
\tag{A.7}
$$

where r_B and r_H are respectively the values for the boundary of the space and the horizon and

$$
F(r,k) = K\sqrt{-g} g^{rr} f_{-k}(r) \partial_r f_k(r)
\tag{A.8}
$$

is the kernel. This is our candidate for the two-point retarded Green's function.

To calculate the correlation function on the gravity side we follow the same prescription we would on the field theory side. To find a two-point function we take two functional derivatives, but now with respect to $\phi_0(x)$ instead of $J(x)$.

The fist thing we want to do is rewrite the action in position space. To do so

we define

$$\phi_0(k) = \int d^4 x e^{ikx} \phi_0(x), \tag{A.9}$$

$$\phi_0(-k) = \int d^4 y e^{-ikx} \phi_0(y), \tag{A.10}$$

$$F(x-y) = \int \frac{d^4 k}{(2\pi)^4} F(k) e^{ik(x-y)}. \tag{A.11}$$

The action then becomes

$$S(x-y) = \int d^4 x \int d^4 y \phi_0(x) [F(r_H, x-y) - F(r_B, x-y)] \phi_0(y). \tag{A.12}$$

We place this into the partition function and we can now take functional derivatives of it. The two-point correlation function is given by

$$
\begin{aligned}
&< 0|TO(x_1)O(x_2)|0 > \\
&= \frac{1}{Z_0} \frac{-i\delta}{\delta\phi_0(x_1)} \frac{-i\delta}{\delta\phi_0(x_2)} e^{iS[\phi_0(x),\phi_0(y)]}, \\
&= \frac{1}{Z_0} \frac{-i\delta}{\delta\phi_0(x_1)} \left[\int d^4 y [F(r_H, x_1-y) - F(r_B, x_1-y)] \phi_0(y) \right. \\
&\quad \left. + \int d^4 x \phi_0(x) [F(r_H, x-x_1) - F(r_B, x-x_1)] e^{iS[\phi_0(x),\phi_0(y)]} \right] \Bigg|_{\phi_0=0}, \\
&= i[F(r_B, x_1-x_2) + F(r_B, x_2-x_1)] - i[F(r_H, x_1-x_2) + F(r_H, x_2-x_1)] \tag{A.13}
\end{aligned}
$$

Taking the Fourier transform of this, the propagator in momentum space is

$$< 0|TO(k)O(0)|0 > = i[F(r_B, k) + F(r_B, -k)] - i[F(r_H, k) + F(r_H, -k)]. \tag{A.14}$$

The retarded Green's function in momentum space is defined as

$$G^R(k) = -i < 0|TO(k)O(0)|0 >, \tag{A.15}$$

which means that

$$G^R(k) = [F(r_B, k) + F(r_B, -k)] - [F(r_H, k) + F(r_H, -k)], \tag{A.16}$$

which is great. The problem is that retarded Green's functions are supposed to be imaginary, and this is real. We can prove it by first noticing that $f_k(r)$ is the Fourier transform of a real function. It then has the property $f_k(r)^* = f_{-k}(r)$. Then $F(r, k)$ can be written as

$$
\begin{aligned}
F(r, k) &= K\sqrt{-g} g^{rr} f_k^*(r) \partial_r f_k(r), \\
&= F(r, -k)^*, \tag{A.17}
\end{aligned}
$$

then the Green's function can be written as

$$
\begin{aligned}
G^{\mathrm{R}}(k) &= [F(r_{\mathrm{B}},k)^* + F(r_{\mathrm{B}},k)] - [F(r_{\mathrm{H}},k)^* + F(r_{\mathrm{H}},k)], \\
&= Re[F(r_{\mathrm{B}},k)] - Re[F(r_{\mathrm{H}},k)],
\end{aligned}
\tag{A.18}
$$

as a real function. Apparently blindly following the program laid out for Euclidean AdS/CFT does not work. In order to get a sensible retarded Green's function it is necessary to make a new conjecture for the relation between Minkowski correlation functions on the CFT side and the correlation functions on the gravity side. Throwing out the contributions from the horizon does not help because the result is still real.

These difficulties can be avoided if we conjecture that the Green's function is defined similarly to the zero temperature case,

$$
G^{\mathrm{R}}(k) = -2F(k,r)\Big|_{r_{\mathrm{B}}}.
\tag{A.19}
$$

This is where the real conjecture for calculating Minkowski correlation functions occurs. It doesn't follow strictly by following the Euclidean AdS/CFT correspondence but it does seem natural. The justification for it is that has worked in all testable cases. The contribution from the horizon is discarded because we don't want solutions that are emitted from the horizon. This will be done consistently throughout the calculation.

A.2   Hydrodynamics and the Kubo Formula

We are interested in how to think of hydrodynamics as an effective field theory that describes the dynamics of a system at large distance and time scales. However, unlike most effective field theories, hydrodynamics must be described in terms of its equations of motion rather than its Lagrangian. Dissipative terms are very difficult to encode in a Lagrangian formalism. It should still be possible to use the equations of motion to extract low-energy Green's functions.

We will follow the discussion on the Kubo formula found in [100]. The method of finding a two point correlation function in field theory starts by coupling a source $J(x)$ to an operator $O(x)$ and adding it to the existing action,

$$
S = S_0 + \int dk J(x) O(x).
\tag{A.20}
$$

This source perturbs the system and the average value of $O(x)$ will differ from its equilibrium value. When the source $J(x)$ is tiny the perturbations are given by

linear response theory,

$$\langle O(x) \rangle = i \int dx' G^{\mathrm{R}}(x - x') J(x), \tag{A.21}$$

in terms of the retarded Green's function $G^{\mathrm{R}}(x - x')$.

The hydrodynamic equations of motion are just the conservation laws of energy and momentum,

$$\partial_\mu T^\mu_\nu = 0. \tag{A.22}$$

To make this a solvable system the number of independent equations must be reduced. This is done through the assumption of local thermal equilibrium. The energy momentum tensor must also be expanded enough that the dissipative terms appear. The elements of the dissipative terms are then found by use of rotational symmetry. The energy momentum tensor can be written as

$$T^{\mu\nu} = (\varepsilon + P) u^\mu u^\nu + P g^{\mu\nu} - \sigma^{\mu\nu}, \tag{A.23}$$

where ε is the energy density, P is the pressure, u^μ is the local fluid velocity, and σ is the dissipative term. The first two terms comprise the familiar equations for ideal fluids. The dissipative term, which only has non-zero spatial components, is given by

$$\sigma_{ij} = \eta \left(\partial_i u_j + \partial_j u_i - \frac{2}{3} \delta_{ij} \partial_k u_k \right) + \zeta \delta_{ij} \partial_k u_k, \tag{A.24}$$

where η is the shear viscosity and ζ is the bulk viscosity.

In order to use our effective field theory formulation a perturbative source must be introduced. For an energy momentum tensor this is naturally the metric. So, the hydrodynamic equations must be generalized to curved space. We can then find the response of a tiny perturbation of the flat metric. We're primarily concerned with calculating dissipative properties so we will only consider $\sigma^{\mu\nu}$ in curved space,

$$\sigma^{\mu\nu} = P^{\mu\alpha} P^{\nu\beta} \left[\eta \left(\nabla_\alpha u_\beta + \nabla_\beta u_\alpha - \frac{2}{3} g_{\alpha\beta} \nabla_\rho u^\rho \right) + \zeta g_{\alpha\beta} \nabla_\rho u^\rho \right], \tag{A.25}$$

where $P^{\mu\nu} = g^{\mu\nu} + u^\mu u^\nu$ is a projection operator.

We choose our metric to be of the form

$$g_{ij}(t, \mathbf{x}) = \delta_{ij} + h_{ij}(t), \quad h_{ij}(t) \ll 1, \tag{A.26}$$

$$g_{00}(t, \mathbf{x}) = -1, \tag{A.27}$$

$$g_{0i}(t, \mathbf{x}) = 0. \tag{A.28}$$

The perturbation is assumed to be traceless $h_{ii}(t) = 0$ and because it is spatially homogeneous if the fluid moves the fluid is only allowed to move uniformly $u^i = u^i(t)$. But because of parity the fluid can't all go in one direction, so it must be stationary $u^\mu = (1, 0, 0, 0)$. The metric is chosen such that the only non-zero components of $P^{\mu\nu}$ are spatial. Substituting this and $g_{\mu\nu}$ into the dissipative term of the curved space energy momentum tensor gives,

$$\sigma^{\mu\nu} = P^{\mu\alpha}P^{\nu\beta}\left[\eta\left(\partial_\alpha u_\beta - \Gamma^\gamma_{\alpha\beta}u_\gamma + \partial_\beta u_\alpha - \Gamma^\gamma_{\beta\alpha}u_\gamma\right)\right. \tag{A.29}$$

$$\left. + \left(\zeta - \frac{2}{3}\eta\right)g_{\alpha\beta}g^{\gamma\rho}\left(\partial_\gamma u_\rho - \Gamma^\sigma_{\gamma\rho}u_\sigma\right)\right] \tag{A.30}$$

$$= -P^{im}P^{jn}\left[\eta 2\Gamma^0_{mn} + \left(\zeta - \frac{2}{3}\eta\right)g_{mn}g^{pq}\Gamma^0_{pq}\right]. \tag{A.31}$$

Components of this give either the shear or bulk viscosity. Consider an off diagonal component of the dissipation tensor - we will find that this corresponds to a shear viscosity. The second term can be neglected as it is a higher order in h_{ij} than the first term leaving us with

$$\sigma^{xy} \approx P^{xm}P^{yn}[\eta\partial_0 h_{mn}], \tag{A.32}$$

$$= -\eta\partial_0 h_{xy} - \eta h^{xm}h^{yn}\partial_0 h_{mn}, \tag{A.33}$$

$$\approx -\eta\partial_0 h_{xy}, \tag{A.34}$$

where we have thrown out the second term due to $h_{ij} \ll 1$.

We can compare the Fourier transform of this result to the linear response (A.21), remembering that h_{ij} is our source, and notice that to lowest order in ω we have

$$G^{\text{R}}(k) = -i\eta\omega + \mathcal{O}(\omega^2). \tag{A.35}$$

Rearranging we see that we have derived the Kubo relation for the shear viscosity it terms of a Green's function,

$$\eta = -\lim_{\omega\to 0}\frac{1}{\omega}\text{Im}\, G^{\text{R}}(k, \omega). \tag{A.36}$$

Appendix B

Evaluating Integrals

Two particularly interesting integrals are required to calculate the magnitude of the current. Both appear because we need to calculate the rate at which electrons are created in dense matter.

B.1 Angular Integrals

B.1.1 The Integral to Get Equation (4.61)

In calculating the diagram for the modified Urca process we are interested in the angular integral

$$Q = \int d\Omega_1 \, d\Omega_2 \, d\Omega_3 \, d\Omega_4 \, d\Omega_5 \, d\Omega_6 \, \delta^{(3)}(\mathbf{p}_f - \mathbf{p}_i), \tag{B.1}$$

where $\mathbf{p}_i - \mathbf{p}_f = \mathbf{p}_1 - \mathbf{p}_4 - \mathbf{p}_5 + \mathbf{p}_s$ and $\mathbf{p}_s = \mathbf{p}_2 + \mathbf{p}_3 - \mathbf{p}_6$. The first step is to break the δ-function down into

$$\frac{\delta(p_5 - |\mathbf{p}_1 + \mathbf{p}_s - \mathbf{p}_4|)}{p_5^2} \delta(\Omega_5 - \Omega_{1-4+s}), \tag{B.2}$$

and take the Ω_5 integral to get

$$Q = \int d\Omega_1 \, d\Omega_2 \, d\Omega_3 \, d\Omega_4 \, d\Omega_6 \, \frac{\delta(p_5 - |\mathbf{p}_1 + \mathbf{p}_s - \mathbf{p}_4|)}{p_5^2}. \tag{B.3}$$

We can use the δ-function identity

$$\delta(f(x)) = \prod_i \frac{\delta(x - a_i)}{|f'(a_i)|}, \tag{B.4}$$

where a_i are the roots of $f(x)$, to further write the δ-function as

$$\delta(p_5 - |\mathbf{p}_1 + \mathbf{p}_s - \mathbf{p}_4|), \tag{B.5}$$

$$= \delta(p_3 - (p_1^2 + (\mathbf{p}_4 - \mathbf{p}_s)^2 - 2p_1|\mathbf{p}_4 - \mathbf{p}_s|\cos(\theta_1))^{1/2}), \tag{B.6}$$

$$= \delta\left(\cos(\theta_1) - \frac{(p_3^2 - (p_1^2 + (p_1^2 + (\mathbf{p}_4 - \mathbf{p}_s)^2)^{1/2})}{2p_1|\mathbf{p}_4 - \mathbf{p}_s|}\right) \frac{p_3}{p_1|\mathbf{p}_4 - \mathbf{p}_s|}. \tag{B.7}$$

Taking the $d\Omega_1$ integral yields

$$Q = \frac{2\pi}{p_1 p_3} \int d\Omega_2 \, d\Omega_4 \, d\Omega_5 \, d\Omega_6 \, \frac{1}{|\mathbf{p}_4 - \mathbf{p}_s|}. \tag{B.8}$$

The physics of the problems helps us the rest of the way. We restrict the momentum of the particles to lie close within their Fermi momentum as seen in Section 2.2.2 the neutron Fermi momentum is much larger than the proton and electron Fermi momentum. We make the approximation $p_4 \gg p_s$ so we can move p_2 out of the integral. We are left with four solid angle integrals that contribute 4π each leaving us with

$$Q = \frac{2\pi(4\pi)^4}{p_1 p_2 p_3}. \tag{B.9}$$

This is used in the calculation of the transition rate of the modified Urca process.

B.1.2   The Integral to Get Equation (4.9)

The rest of diagrams (direct Urca, kaon, and quark) have only four angular integrals. Consider the diagram above with no assisting neutron N'. We have the integral

$$Q = \int d\Omega_2 \, d\Omega_3 \, d\Omega_5 \, d\Omega_6 \, \delta^{(3)}(\mathbf{p}_f - \mathbf{p}_i), \tag{B.10}$$

where $\mathbf{p}_i - \mathbf{p}_f = \mathbf{p}_2 + \mathbf{p}_3 - \mathbf{p}_5 - \mathbf{p}_6$. Using the same steps as above we can write the integral as

$$Q = \frac{2\pi}{p_2 p_5} \int d\Omega_3 \, d\Omega_6 \, \frac{1}{|\mathbf{p}_3 - \mathbf{p}_6|}. \tag{B.11}$$

The neutrino actually has no Fermi surface so we let $p_6 = 0$ and the integral evaluates to

$$Q = \frac{2\pi(4\pi)^2}{p_2 p_3 p_5}. \tag{B.12}$$

This is used in calculating the direct Urca, kaon, and quark transition rates.

B.2   Radial Integrals

The Pauli blocking factors

$$\mathscr{S} = \prod_{i=1}^{5} \frac{1}{1 + e^{x_i}} \quad \text{and} \quad \mathscr{S} = \prod_{i=1}^{3} \frac{1}{1 + e^{x_i}} \tag{B.13}$$

add a complex dimension to otherwise simple integrals. In the main text the radial integrals for the modified and direct processes arise for these statistical factors are reduced to two dimensionless integrals.

B.2.1 Evaluating the Integral in Equation (4.70)

This radial integral must be evaluated to find the transition rate of the modified Urca processes. First consider the integral (4.70) which we write in the more transparent way,

$$I \;=\; \int_0^\infty dy\, y^2 K, \tag{B.14}$$

$$K \;=\; \int \prod_{j=1}^5 dx_j \,(1+e^{x_i})^{-1}\, \delta\!\left(\sum_{i=1}^5 x_i - y\right). \tag{B.15}$$

Though I is restricted on the bottom, we will extend the integration boundaries from $-\infty$ to ∞. This introduces a small amount of error in the calculation on the order $e^{-\beta E_P}$.

Our fist step in evaluating these integrals is to rewrite the δ-function as its Fourier transform,

$$\delta(z) = \frac{1}{2\pi} \int_{-\infty}^\infty e^{izy} dz. \tag{B.16}$$

This allows us to rearrange the integral such that

$$K \;=\; \frac{1}{2\pi} \int_{-\infty}^\infty dz\, e^{-izy} f(z)^5, \tag{B.17}$$

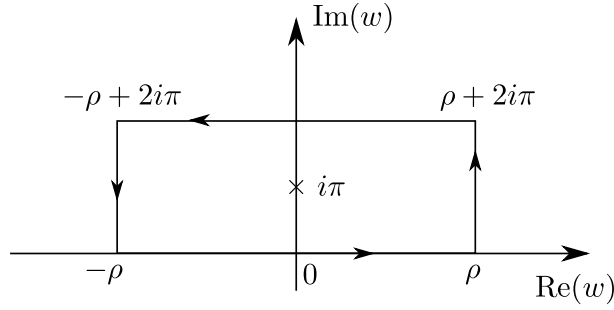$$f(z) \;=\; \int_{-\infty}^\infty dx\, e^{izx} (e^x + 1)^{-1}. \tag{B.18}$$

We are now ready to tackle our first integral. We evaluate $f(z)$ by considering the integral

$$F \;=\; \oint dw\, e^{izw} (e^w + 1)^{-1}. \tag{B.19}$$

evaluated around the contour shown in Figure B.1,

The vertical parts of the path give no contribution to the integral. We can see this using the path $w = \rho + it$ which we can bound the absolute value of using

$$\left| \int_0^{2\pi} i\, dt\, e^{iz(\rho+it)} \left(e^{\rho+it} + 1\right)^{-1} \right| \le \int_0^{2\pi} dt\, e^{-zt} (e^\rho - 1)^{-1}, \tag{B.20}$$

Figure B.1: Contour for the integral F given by (B.19).

of which the R.H.S. goes to zero as $\rho \to \infty$.

The contribution along $2\pi i$ only shifts the value of the integral of the path along zero such that

$$\int_{c=2\pi i} dw\, e^{izw} (e^w + 1)^{-1} = -e^{-2\pi z} \int_{c=0} dw\, e^{izw} (e^w + 1)^{-1}. \tag{B.21}$$

The only pole enclosed by this contour is at $w = i\pi$ where the residue is

$$\left. \frac{e^{izw}}{\frac{d}{dw}(e^w + 1)} \right|_{w=i\pi} = -e^{-\pi z}. \tag{B.22}$$

The integral F is given by

$$F = f(z) - e^{-2\pi z} f(z) = -2\pi i e^{-\pi z}, \tag{B.23}$$

for which we can solve to get

$$f(z) = \frac{-2\pi i}{e^{\pi z} - e^{-\pi z}} = \frac{\pi}{i \sinh(\pi z)}. \tag{B.24}$$

We can now substitute this back into our integral K,

$$K = \frac{1}{2\pi} \int_{-\infty}^{\infty} dz\, e^{-izy} \left(\frac{\pi}{i \sinh(\pi z)} \right)^5, \tag{B.25}$$

and attempt to evaluate it. Because there is a pole at $w = 0$ the proper way to evaluate this would be to use the fractional reside theorem and evaluate the integral over a contour that passes along the real axis. Unfortunately the pole is of order 5

and the fractional residue theorem fails. So instead we will shift contour down by a small amount ε such that the integral becomes

$$K = \lim_{\rho \to \infty} \frac{1}{2\pi} \int_{-\rho-i\varepsilon}^{\rho-i\varepsilon} dz\, e^{-izy} \left(\frac{\pi}{i \sinh(\pi z)} \right)^5 . \tag{B.26}$$

We then close the contour back along $z = i$ as shown in Figure B.2. Along the top of the contour where $z' \to z + i$ our integral becomes

$$K' = \lim_{\rho \to \infty} \frac{-e^y}{2\pi} \int_{\rho+i-i\varepsilon}^{-\rho+i-i\varepsilon} dz'\, e^{-iz'y} \left(\frac{\pi}{i \sinh(\pi z')} \right)^5 , \tag{B.27}$$
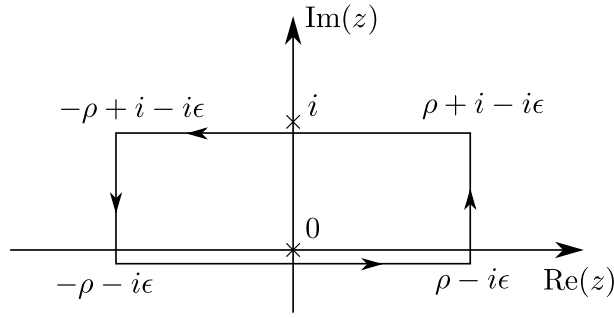
$$= e^y K. \tag{B.28}$$

Figure B.2: Contour for the integral K given by (B.26)

With this shift the contour then neatly encompasses a single pole. This integral is evaluated much the same way the previous one was. As in the previous contour integral the vertical components contribute nothing as $\rho \to \infty$ and we can write the integral around the entire contour as

$$(1+e^y)K = 2\pi i \, \mathrm{Res} \left(\frac{e^{-izy}}{2\pi} \left(\frac{\pi}{i \sinh(\pi z)} \right)^5 , z = 0 \right) . \tag{B.29}$$

The series expansion reveals the residue to be

$$\frac{1}{2\pi i} \left(\frac{3}{8}\pi^4 + \frac{5}{12}\pi^2 y^2 + \frac{1}{24}y^4 \right) , \tag{B.30}$$

which means that

$$K = \left(\frac{3}{8}\pi^4 + \frac{5}{12}\pi^2 y^2 + \frac{1}{24}y^4 \right) \frac{1}{1+e^y} . \tag{B.31}$$

We are now able to evaluate the integral we set out to evaluate,

$$I \ = \ \int_0^\infty dy \left(\frac{3}{8}\pi^4 y^2 + \frac{5}{12}\pi^2 y^4 + \frac{1}{24}y^6 \right) \frac{1}{1+e^y}, \tag{B.32}$$

$$= \ \frac{945}{32}\zeta(7) + \frac{75}{8}\pi^2\zeta(5) + \frac{9}{16}\pi^4\zeta(3), \tag{B.33}$$

$$\approx \ 192. \tag{B.34}$$

This value is used to calculate the transition rate of the modified Urca process.

B.2.2   Evaluating the Integral in Equation (4.21)

The integral for the direct Urca, kaon, and quark processes is nearly identical to the one just presented for the modified Urca process. The only difference comes from the factors of $f(z)$. We start with

$$I \ = \ \int_0^\infty dy\, y^2 K, \tag{B.35}$$

$$K \ = \ \int \prod_{j=1}^3 dx_j\,(1+e^{x_i})^{-1}\, \delta\left(\sum_{i=1}^3 x_i - y \right). \tag{B.36}$$

Just as before we can use $f(z)$ given by equation (B.24) to write J as

$$K = \frac{1}{2\pi} \int_{-\infty}^\infty dz\, e^{-izy} \left(\frac{\pi}{i\sinh(\pi z)} \right)^3. \tag{B.37}$$

This is evaluated using the contour given in Figure B.2. The only difference is the residue

$$(1+e^y)K = 2\pi i \operatorname{Res}\left(\frac{e^{-izy}}{2\pi} \left(\frac{\pi}{i\sinh(\pi z)} \right)^3, z=0 \right). \tag{B.38}$$

which is evaluated by looking at the coefficient of the $1/z$ term in the series expansion to yield

$$K = \frac{y^2 + \pi^2}{2(1+e^y)}. \tag{B.39}$$

The integral I is then

$$I \ = \ \int_0^\infty dy\, \frac{y^4 + \pi^2 y^2}{2(1+e^y)}, \tag{B.40}$$

$$= \ \frac{45}{4}\zeta(5) + \frac{3}{14}\pi^2\zeta(3). \tag{B.41}$$

$$\approx \ 20.6. \tag{B.42}$$

This result is used to calculate the transition rate of the direct Urca, kaon, and quark processes.